Ph.D. Thesis, s010132

Magnetic Separation and Hydrodynamic Interactions in Microfluidic Systems

Christian Ingemann Mikkelsen

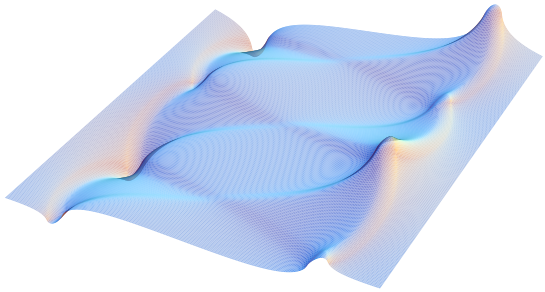

Main Supervisor: Henrik Bruus, Co-supervisor: Mikkel Fougt Hansen

MIC — Department of Micro and Nanotechnology
Technical University of Denmark

May 18, 2005

Abstract

Magnetic bead manipulation, in particular separation, in microfluidic systems is a technique which offers to simplify and integrate separation and rinsing procedures for minute samples of biological material. We study the physics of magnetic bead motion in such systems.

The force on a body in a magnetic field is determined from principles of thermodynamics. From that result, the force between two spherical linearly paramagnetic particles immersed in an external magnetic field is derived provided that they are well separated. Furthermore, we find the magnetic dipole moments that two linearly paramagnetic spherical particles induce in one another; both being immersed in an external magnetic field. The leading magnetic interaction force decays as particle separation to the power -3.

The hydrodynamic interaction, which stems from the fluid motion set about by particles moving in a viscous fluid, is shown to decay with separation to the power -1 by means of hydrodynamic Green's functions. The magnetic interaction decays much faster with separation. This significantly influences the dynamics of magnetic bead motion which is illustrated through numerical simulations that study individual beads.

Instead of adding more and more beads on an individual basis, we go on to treat the beads as a continuum described by a distribution that is coupled to the problem of fluid flow in a model microfluidic channel. This shows that hydrodynamic interactions help the capturing of magnetic beads and that this depends on the concentration of beads. An effort is underway to test this prediction in experiments.

Finally, we have derived an analytic framework for the description of the slow motion of spherical particles in a viscous fluid in confined geometries. This enables us to derive a first approximation to the mobility of a spherical particle at the centre of a cube filled with viscous fluid.

Resumé

Manipulation af magnetiske partikler, i særdeleshed separation, i mikrovæskesystemer er en teknik, som tillader simplifikation og integration af separations- og oprensningsprocedurer for små mængder af biologisk materiale. Vi studerer her fysikken bag magnetiske kuglers bevægelse i sådanne systemer.

Vi udleder kraften på et legeme i et magnetfelt udfra termodynamiske principper og fra dette udledt kraften mellem to sfæriske, lineært paramagnetiske partikler i et eksternt magnetfelt under antagelse af, at de ikke er for tæt sammen. Derudover finder vi de magnetiske dipolemomenter, som to sfæriske, lineært paramagnetiske partikler inducerer i hinanden, når de er påtrykt et eksternt magnetfelt. Den førende magnetiske vekselvirking aftager med partikelafstanden i tredie potens.

Den hydrodynamiske vekselvirkning, der skyldes væskebevægelse, der opstår når partiklerne bevæger sig gennem væsken, vises ved hjælp af hydrodynamiske Greensfunktioner at aftage med partikelafstanden i første potense. Den magnetiske vekselvirkning aftager altså meget hurtigere med afstanden. Dette påvirker afgørende de magnetiske kuglers bevægelse, hvilket vi illustrerer ved numeriske simulationer, hvor vi behandler kuglerne særskilt.

I stedet for at tilføre flere kugler en ad gangen går vi videre og behandler kuglerne som et kontinuum, som beskrives ved en fordeling, som er koblet sammen med væskestrømningsproblemet i en modelmikrovæskekanal. Dette viser, at hydrodynamiske vekselvirkninger hjælper indfangningen af magnetiske kugler, og at dette afhænger af koncentrationen af kugler. Der bliver arbejdet på at undersøge denne forudsigelse eksperimentelt.

Endeligt har vi udledt et analytisk redskab til beskrivelse af langsomtbevægende sfæriske partikler i viskøs væske indesluttet i en beholder. Dette gør det muligt at udlede en førstetilnærmelse til mobiliteten for en kugleformet partikel placeret i centrum af en terningformet kasse fyldt med viskøs væske.

Preface

The present dissertation is the result of the work I have undertaken over the last 18 months under the supervision of professor Henrik Bruus and associate professor Mikkel Fougt Hansen both at MIC who both kindly took me under their scientific wings after I had to terminate the PhD-project that I had hitherto pursued.

I happily seized the opportunity to work in a, to me, completely new field and going through the quandary phase. A year and a half is not a long time to contribute to the advancement of knowledge and a comparably large part of my effort has gone into computer simulations which are forgiving in the sense that one can be rather certain of obtaining something for the effort. To my own taste, simulation may lack some of the technical appeal of analytical arguments so it is a great joy to be able to present some original theoretical work reaching something quintessential.

Over the course of my PhD-work, I have published two papers in international scientific journals [9, 36], submitted one [37] and contributed three times to research conferences [10, 38, 36].

This thesis submitted for my PhD degree at the DTU is wholly my work but I have relied on the guidance and help of many. Firstly, my thanks go to my two supervisors for their guidance and to the Dean of Research professor Kristian Stubkjær for letting me change projects however implausible it may have seemed so that I would be able to hand in a thesis a year and a half later. Secondly, my thanks are extended to my very good friends Thoa Nguyen, Karin Nordström Andersen, Haiyan Ou, Jacob Sparre Andersen and Rasmus Kousholt Sandberg for their never failing encouragements. Especially, I acknowledge the care and patience that Thoa and Jacob have had to mount after hours of careful proof-reading of my ever changing manuscript just having me vehemently defend every single convoluted and awkward sentence or attack the use of the gerund. In honesty, I can say that I meant every single misprint at the time I wrote them.

Lastly, I wish to thank my family for extending patience to cover everything from food and lodging to the pieces of graphics that were beyond my own skills to produce.

Christian Ingemann Mikkelsen
MIC — Department of Micro and Nanotechnology
Technical University of Denmark
15 May 2005

Contents

List of figures **xiii**

List of symbols **xv**

1 Introduction **1**
1.1 Dielectrophoresis . . . 2
1.2 Magnetophoresis . . . 3
1.3 Hydrodynamics . . . 4
1.4 Outline of the Thesis . . . 5
1.5 Finished and published papers . . . 6

2 Force on a magnetized object **9**
2.1 Magnetic force on a body . . . 10
2.1.1 Thermodynamics . . . 10
2.1.2 The magnetic force from the free energy . . . 13
2.2 Magnetic forces between two particles . . . 14
2.3 Magnetic particle in pure dipole field . . . 15
2.4 Two magnetic spheres in an external magnetic field . . . 19
2.5 Discussion . . . 20

3 Motion of few beads **21**
3.1 Hydrodynamic interactions between beads . . . 21
3.1.1 Motion in a viscous fluid . . . 22
3.1.2 Motion in fluid flow and external magnetic field . . . 23
3.1.3 Hydrodynamic Green's functions . . . 24
3.2 Simulations . . . 27
3.2.1 Two-bead simulations . . . 29
3.2.2 Few-bead simulations . . . 29
3.3 Discussion . . . 33

4 Motion of many beads **35**
4.1 Introduction . . . 35
4.2 The physical problem . . . 35
4.3 Continuum model . . . 36

4.3.1 Fluid flow . . . 36
4.3.2 Bead motion . . . 37
4.3.3 Magnetic force . . . 38
4.3.4 Boundary conditions . . . 39
4.3.5 Simulations . . . 40
4.4 Results . . . 40
4.4.1 Qualitative picture . . . 40
4.4.2 Quantitative measures . . . 42
4.4.3 Concentration dependence . . . 44
4.4.4 Influence of diffusion constant . . . 46
4.4.5 Other force laws . . . 47
4.5 Bead current for finite size beads . . . 48
4.6 Simplified view . . . 51
4.7 Discussion . . . 52

5 Experimental test **55**
5.1 Principle . . . 55
5.2 Implementation and design . . . 56
5.3 Simulations . . . 59
5.4 Discussion . . . 59

6 The induced force method **61**
6.1 Principle . . . 61
6.2 Expansions of forces and velocities . . . 64
6.2.1 At the spherical particles . . . 64
6.2.2 At the walls . . . 65
6.3 Equation hierarchy . . . 66
6.3.1 Translational velocity . . . 66
6.3.2 Rotational velocity . . . 68
6.3.3 Higher order velocity moments . . . 68
6.3.4 Walls . . . 69
6.4 Solution procedure . . . 71
6.4.1 An application . . . 72
6.5 Outlook . . . 74

7 Summary and outlook **75**

A Field from sphere in pure dipole fields: x and y-dipoles **77**
A.1 Dipole along the x-direction . . . 77
A.2 Dipole along the y-direction . . . 78

B Implementation in Matlab **81**

C Paper published in J. Magn. Magn. Mater. **85**

D Conference Proceedings from μTAS 2004 **93**

E Paper submitted to Lab-on-a-Chip **97**

List of Figures

2.1 Magnetizable sphere and point dipole. 16

3.1 Capturing of two magnetic beads in the presence of hydrodynamic interactions. 30
3.2 Capturing of two magnetic beads in the absence of hydrodynamic interactions. 31
3.3 Speed-up of capturing as function of bead number. 32

4.1 Sketch of microfluidic system used in simulations. 37
4.2 Steady state bead distribution at low concentrations. 41
4.3 The flow roll set up in capturing of magnetic beads. 42
4.4 Beads settling at the upper wall. 42
4.5 Steady state bead distribution at high concentrations. 43
4.6 Fraction of beads caught as function of magnetic field and fluid flow. 44
4.7 Fraction of beads caught collapsed at low concentration. 45
4.8 Fraction of beads caught collapsed at high concentration. 46
4.9 Fraction of beads caught as function of initial concentration. 47
4.10 Influence of hydrodynamic interactions. 48
4.11 Influence of the diffusion constant. 49
4.12 Influence of a different force law. 50
4.13 Simple single bead model as for different magnetic field strengths. 53

5.1 Picture of experimental device. 56
5.2 Sketch of experimental device. 58

6.1 A single spherical particle at the centre of a cubic box. 63

List of symbols

Symbol	Description	Unit
$\mathbf{u}$	Fluid velocity	$\mathrm{m\,s^{-1}}$
$\mathbf{v}$	Rigid body translational velocity	$\mathrm{m\,s^{-1}}$
$\boldsymbol{\omega}$	Rigid body rotational velocity	$\mathrm{rad\,s^{-1}}$
$\mathbf{F}$	Force	$\mathrm{N} = \mathrm{kg\,m\,s^{-2}}$
$\mathbf{f}$	Point force	$\mathrm{N\,m^{-3}}$
$\boldsymbol{\sigma}$	Stress tensor	$\mathrm{N\,m^{-2}}$
η	Viscosity, dynamic	$\mathrm{kg\,m^{-1}\,s^{-1}} = \mathrm{Pa\,s}$
p	Pressure	$\mathrm{N\,m^{-2}} = \mathrm{Pa}$
$\mathbf{H}$	Magnetic field, induction	$\mathrm{A\,m^{-1}}$
$\mathbf{B}$	Magnetic field, flux density	T
$\mathbf{A}$	Magnetic vector potential	$\mathrm{T\,m}$
ψ	Magnetic scalar potential	A
$\mathbf{M}$	Magnetization, volumetric	$\mathrm{A\,m^{-1}}$
$\mathbf{m}$	Magnetic moment, (dipole)	$\mathrm{A\,m^2}$
μ	Permeability	$\mathrm{N\,A^{-2}}$
μ_o	Vacuum permeability	$\mathrm{N\,A^{-2}}$
χ	Susceptibility	1
$\mathbf{E}$	Electric field	$\mathrm{V\,m^{-1}}$
$\mathbf{J}$	Electric current density	$\mathrm{A\,m^{-2}}$
I	Electric current	A
q	Electric charge	C
$\mathbf{r}$	Position vector	m
$\mathbf{s}$	Separation vector	m
a	Particle radius	m
m	Particle mass	kg
ρ	Mass density	$\mathrm{kg\,m^{-3}}$
b	Mobility	$\mathrm{s\,kg^{-1}}$
τ	Time constant	s
d	Wire separation	m
h	Height	m
$\mathbf{k}$	Reciprocal space vector	$\mathrm{m^{-1}}$

Symbol	Description	Unit
T	Temperature	K
k_B	Boltzmann's constant	$\mathrm{J\,K^{-1}}$
S	Entropy density	$\mathrm{J\,K^{-1}}$
F	Free energy	J
ζ	Chemical potential per unit mass	$\mathrm{J\,kg^{-1}}$
c	Bead concentration	$\mathrm{m^{-3}}$
$\mathbf{j}$	Bead current density	$\mathrm{m^{-2}\,s^{-1}}$
D	Diffusion constant	$\mathrm{m^2\,s^{-1}}$
γ	Rate of capture	$\mathrm{m^{-1}\,s^{-1}}$
β	Fraction captured	1
$\mathrm{P}_n(x)$	Legendre polynomial	
$\mathrm{j}_n(x)$	Spherical Bessel function	

Chapter 1

Introduction

In the following we study the physics of the motion of magnetic beads in microfluidic systems. We study several of different aspects: the forces on single beads and between a number of beads, the influence of having a few beads together and the effect of having so many beads that they are best described as a continuum. We describe experiments which are under way to test some of the ideas and finally provide a general theoretical framework that can treat not just the motion of several beads but also their interactions with walls.

As we consider beads in microchannels distances are very short and Reynolds numbers are low as well. Drag dominates bead motion and inertia plays no rôle. However, this is also on a scale where classical physics rules. All beads considered are spherical and hard; the fluid is Newtonian and very much like water. It is remarkable that there is anything to discuss with such an orthodox physical system, however, the collective motion of spherical beads in a small channel is not so simple to describe.

There is an on-going effort to miniaturize a variety of traditional laboratory functions under the label 'lab-on-a-chip' such that they can be made automatic and integrated onto a chip. Such processes, typically, rely on the physical manipulation of fluids, filtering, separation, mixing, and transport, and these operations need to be translated into a format compatible with integration onto a chip and with the physics of fluids on a submillimetre scale.

Two phenomena that find application are the manipulation of small objects by means of electric or magnetic fields. In particular electric manipulation of polarizable objects, dielectrophoresis, has been popular as it is easy and convenient to generate electric fields. The oft ignored baby brother of dielectrophoresis is magnetophoresis — the manipulation of objects (particles) by means of magnetic fields.

Recently, there has been an increasing interest in using magnetic beads in separation of, say, biochemical species in microfluidic systems [13, 54]. The principle is to have biochemically functionalized polymer beads with inclusions of superparamagnetic nanometre-size particles of, for example, magnetite or maghemite. With appropriately treated bead surfaces, the beads will have specific affinity to particular biochemical or biological species. Because of their strong paramagnetism they can be separated out of solution by means of magnetic fields. As most biological material is either diamagnetic or only very weakly

paramagnetic this separation is specific.

A number of designs have appeared in the literature either on the basis of external permanent [14, 29], integrated electromagnets [3, 11, 12, 47] or a combination [41]. They are all based on a microchannel in which fluid passes through carrying the magnetic beads which may have bound to the species for which the beads have specific affinity. In the case of external permanent magnets, there are often either mechanically structured magnetizable material such as pillars integrated to provide suitable gradients or electrical leads run through that can do the same. Permanent magnets have the advantage that they provide currentless performance and strong fields whereas electromagnets provide easily controllable magnetic fields but at the price of heat dissipation or weaker fields.

Magnetophoresis finds its application in separation processes where some entity of interest is either magnetic itself or attached to, for example, a magnetic bead. The entity can then be retained at will with the aid of magnetic fields. Since most materials show negligible para- or diamagnetism, it is usually necessary to introduce a magnetic 'handle' such as the mentioned magnetic beads. This is in contrast to dielectrophoresis as dielectric constants of common substances generally are more varied.

For the experimentalist this is both a blessing and a curse. Consider analysing a blood sample: The sample contains literally thousands of different chemical and biological species which are essentially all indifferent to the application of a magnetic field. By the introduction of magnetic beads that bind specifically to one of these species — something which is possible in biology — one can single out only the bound species. However, it *is* necessary to introduce these beads. One cannot rely on the intrinsic magnetic properties of the system at hand.

A nice feature of magnetophoresis with beads is that it lends itself easily to use in microsystems. The magnetic field can easily come from an external permanent or an integrated electromagnet. There need not be heat dissipation or electrolysis as there would be with dielectrophoresis. There is no need for a mechanical filter for retention which complicates rinsing and flushing steps.

Having lined up benefits of magnetophoresis as an introduction, we can briefly look upon the close relative dielectrophoresis that hinges on similar ideas. Since most people are more familiar with electrostatics than magnetostatics and since there exist electric charges it makes an easier starting point.

1.1 Dielectrophoresis

Before restricting attention exclusively to magnetophoresis, it is fruitful to point out some of the merits of the analogous technique using electric fields.

A physical object that is subject to an electrical field will in general be polarized; the centres of the negative charge and the positive charge will not coincide and a net electric moment will in general result. Clearly, it is possible to dream up fields and geometries where no net *dipole* moment will be induced but we'll leave that aside. If the electric field is inhomogeneous then the centre of negative charge will feel one field strength and direction while the positive another. This means that there will be a net force acting on

the object as a whole. This is what we call dielectrophoresis.

The essence of the phenomenon is the action of a field upon a field induced electric polarization. It is similar to optical trapping as in an optical tweezer but the term dielectrophoresis is applied to the case of fields much more slowly varying than optical frequencies.

A little hand-waving lets us derive the expression for the force on the induced dipole. Later we are going to derive the analogous expression for the magnetic force rigorously. We imagine the dipole as two charges $+q$ and $-q$ separated by a distance s. The total force on the dipole will then be

$$\mathbf{F} = +q\mathbf{E}(\mathbf{r}+\mathbf{s}) - q\mathbf{E}(\mathbf{r}) \approx q\big(\mathbf{s}\cdot\boldsymbol{\nabla}\big)\mathbf{E}(\mathbf{r}). \tag{1.1}$$

The vector $q\mathbf{s}$ can be identified with the electric dipole moment.

If the dipole moment is induced by the presence of the same electric field, as is the assumption inherent in dielectrophoresis, and the dipole moment is proportional to the applied field then the force becomes proportional to the gradient of the field squared. For a sphere of radius a the result is particularly simple

$$\mathbf{F} = 2\pi\varepsilon_1 a^3 \frac{\varepsilon_2-\varepsilon_1}{\varepsilon_2+2\varepsilon_1}\boldsymbol{\nabla}E_{\text{ext}}^2 \tag{1.2}$$

where the surrounding medium and the sphere are assumed to have permittivities ε_1 and ε_2 respectively [25]. The combination $(\varepsilon_2-\varepsilon_1)/(\varepsilon_2+2\varepsilon_1)$ is called the Clausius-Mossotti-factor and depends on the specific geometry through depolarization effects [25]. This result should be compared with the analogous expression in the magnetic case which we derive later, Eq. (2.21). Depending on the relative magnitudes of the permittivities, the force can either be in the direction of field maxima or field minima. In the former case, one speaks of *positive* dielectrophoresis and in the latter of *negative* dielectrophoresis.

The strong selling point about dielectrophoresis is that many entities will show it of and by themselves. What is necessary is that the entity has a permittivity that differs appreciably from that of the surrounding medium. For biological applications the medium will often be aqueous and as pure water is polar and has a high permittivity many, less polar for example, substances will show an appreciable (negative) dielectrophoretic effect.

Furthermore, entities with an internal structure such as cells can display a varied spectral response that enables sorting by applying fields with different frequencies to catch and release entities selectively. The frequency dependence comes about because of loss mechanisms such as conduction or intrinsic dielectric loss that sets a time scale for the response. If the entity has some internal structure such as that of a lipid double membrane then there can be spectral windows of positive or negative dielectrophoresis.

1.2 Magnetophoresis

The magnetic analogue of dielectrophoresis is magnetophoresis where a net force results on a para- or diamagnetic body from the application of an inhomogeneous magnetic field.

Here there are no magnetic charges to separate but microscopic dipole moments are aligned so that a net magnetic moment $\mathbf{m}$ results and we can guess a net force $\mathbf{F}$ proportional to

$$\mathbf{F} = \big(\mathbf{m} \cdot \boldsymbol{\nabla}\big)\mathbf{H}(\mathbf{r}) \tag{1.3}$$

in analogy with the electrostatic case. Later on, we will derive the force on a magnetizable body with a lot more care but this will do for the present. The net force on the body depends on the gradient of the field; a homogeneous magnetic field only gives rise to a torque.

Until now, the analogy with dielectrophoresis carries through, however, the differences lie in the magnetic and electric properties of matter. We already pointed out that the dielectric properties of matter varies greatly at least if one considers the range of dielectric constants for household materials from plastics ($\varepsilon \approx 2\varepsilon_{\mathrm{o}}$) to water ($\varepsilon \approx 80\varepsilon_{\mathrm{o}}$). The situation is different with the magnetic properties as most common substances are either very weakly paramagnetic or diamagnetic with well-known exceptions, iron and lodestone for example, that have *permanent* magnetizations.

Doing magnetophoresis experiments with bead that are permanently magnetic would rather impractical as the beads would attract one another and agglomerate together so it would only really work properly for beads that are superparamagnetic as those mentioned above. In itself, superparamagnetism is an interesting phenomenon that is worthy of a brief introduction. If we consider a nanometre-size particle of a ferromagnetic substance then the energy barrier to reverse the direction of magnetization can become comparable with thermal energies leading to frequent flipping of the net magnetic moment [45]. We can thus see the net magnetic moment as a single spin in classical Langevin theory and from that calculate the resulting magnetization in an external magnetic field at finite temperature [15]. In this way, a superparamagnetic particle appears to be strongly paramagnetic in that it is the ordered response from millions of atoms at a time and the response is very nearly linear for moderate applied fields as the response is Langevinian [15].

It is really the availability of biochemically functionalized polymer beads with superparamagnetic inclusions that makes this enterprise of magnetophoresis interesting from an application point of view. It is fortuitous that magnetic fields generally do not interfere with biological material, that they can easily be generated with electromagnets and that specific entities can be targeted with suitably functionalized magnetic beads.

1.3 Hydrodynamics

The usual path of study of magnetic bead manipulation is to concentrate on the magnetic side of the problem but in this work we will see that the hydrodynamics of it is very important. The fact that magnetic beads move in a viscous fluid sets up a sort of interaction which is due to the fact that the motion of beads leads to a flow of the fluid. When focusing exclusively on the motion of beads, this comes up in the guise of an effective interaction between the beads.

The fluid mechanics and hydrodynamics of bead motion in microchannels are quite forgiving subjects as hydrodynamics comes (compare with turbulence) as the flows involved

are laminar but even then the mathematical treatment based on the Stokes equation can be challenging but a lot can still be said and done.

In the absence of moving beads, the hydrodynamics of a microchannel in the limit of laminar flow is standard textbook material. The Poiseuille flow as it is called of a channel of rectangular or circular cross section is the staple of introductory hydrodynamics and can be done analytically with all its glory. The flow due motion of even a spherical particle is somewhat more complicated and did pose a paradox in its time but was eventually resolved through the work of the Swede C.W. Oseen.

1.4 Outline of the Thesis

The bulk of this thesis is the chapters 2 to 6 where we cover a range of topics pertaining to the motion of magnetic beads in microfluidics. The first direction in which we set out is the magnetic aspects of bead motion which we treat in Chapter 2. First of all, the force on a magnetic object is derived from thermodynamic principles and examined in detail. This was necessary to settle a dispute that had appeared in the literature. Its value lies not in novelty but in care. From that we derive the force between two spherical beads under assumptions that amount to the beads being well apart. Going further, we derive a framework that is capable of treating the case of beads that are so close that they are able to magnetize one another significantly.

From that we proceed to what is to become the main theme in the present work; the influence of hydrodynamic interactions. We start out in Chapter 3 by deriving in a straightforward manner the stokeslet which is a hydrodynamic Green's function corresponding to the action of a point force. This simple tool enables us to make the observation crucial herein that hydrodynamic interactions dominate over the magnetic ones. To support this observation, we provide simulations that employs Green's functions to take into account hydrodynamic interactions in bead capturing.

To make a complementary argument and to take the effect of having beads moving under the influence of an external force more fully into account, we model and simulate the beads as a continuous distribution which is coupled to the fluid flow. This reveals a strong influence of the number of beads on capturing through hydrodynamics interactions which we see in Chapter 4. Briefly in Chapter 5, we touch upon experiments that are underway to test whether the influence of the concentration of beads can be seen in a device. This is very much work in progress being carried out at MIC in collaboration with Kristian Smistrup, Anders Brask and my supervisors.

The theoretical approaches described so far have all left something to be desired if in no other aspects then in elegance and systematics. Their final applications have rested on numerical simulations that limit certain types of insight that analytical methods can provide. In Chapter 6, we extend an analytical framework originally devised to study particle diffusion and sedimentation of dense dispersions to provide an avenue into the study of bead motion in constricted geometries such as in a microchannel. The framework is systematic and analytical and, in our view, promises a whole new approach to particle motion in microfludic systems that relies less on brute force numerical simulations. The

method is applied to the rather modest problem of a bead placed at the centre of a cubical box but this should only be taken as an illustration of its application.

1.5 Finished and published papers

Paper submitted to Lab-on-a-Chip
Title
Microfluidic capturing-dynamics of paramagnetic bead suspension
Authors
Christian Mikkelsen and Henrik Bruus

Paper published in J. Magn. Magn. Mater.
Title
Theoretical comparison of magnetic and hydrodynamic interactions between magnetically tagged particles in microfluidic systems
Authors
Christian Mikkelsen, Mikkel Fougt Hansen and Henrik Bruus
Reference
J. Magn. Magn. Mater. **293**, 578–83, (2005).

Conference Proceedings from μTAS 2004
Title
Magnetic separation in microsystems: effects of hydrodynamic interaction
Authors
Christian Mikkelsen, Mikkel Fougt Hansen and Henrik Bruus
Reference
Micro Total Analysis Systems 2004—Proceedings of μTAS 2004, Volume 1, 587–9, (2004).

Conference Proceedings from OFC 2004
Title
Orthogonal optical labeling based on a 40 Gbit/s DPSK payload and a 2.5 Gbit/s IM label
Authors
Nan Chi, Lin Xu, Jianfeng Zhang, Pablo V. Holm-Nielsen, Christophe Peucheret, Christian Mikkelsen, Haiyan Ou, Jorge Seoane and Palle Jeppesen **Reference**
Optical Fiber Communication Conference 2004, FO6.

Paper published in Electronics Letters
Title
Transmission and label encoding/erasure of orthogonally labelled signal using 40 Gbit/s RZ-DPSK payload and 2.5 Gbit/s IM label
Authors
Nan Chi, C. Mikkelsen, Lin Xu, Jianfeng Zhang, P.V. Holm-Nielsen, Haiyan Ou, J. Seoane,

C. Peucheret and P. Jeppesen
Reference
Electronics Letters **39**, 1335–6, (2003).

Chapter 2

Force on a magnetized object

In this chapter we investigate and derive the force on a magnetic object from the most general considerations available to us. We do this and derive the force expression anew because of a dispute as recent as 2001 in Physical Review Letters over the exact expression for the force on a magnetizable body — a question with a distinct 1873 character about it [39, 16, 17]. In the literature there are a bewildering multitude of slightly different expressions for the magnetic force all hinging on various different assumptions and approximations. For example [40]

$$\mathbf{F} = \frac{V\Delta\chi}{\mu_\mathrm{o}}(\mathbf{B}\cdot\boldsymbol{\nabla})\mathbf{B} \tag{2.1}$$

where V is the volume, $\Delta\chi$ is the magnetic susceptibility relative to the surrounding medium and $\mathbf{B}$ is the magnetic flux density. Or [11]

$$\mathbf{F} = V\chi(\mathbf{H}\cdot\boldsymbol{\nabla})\mathbf{B} \tag{2.2}$$

where χ is the magnetic susceptibility "by volume" and $\mathbf{H}$ is the magnetic field. Odenbach and Liu [39] even suggests the validity of two different force expressions,

$$\mathbf{F}_K = \int \mu_\mathrm{o} M_i \boldsymbol{\nabla} H_i \, d\mathbf{r} \tag{2.3}$$

and

$$\mathbf{F}_v = \int M_i \boldsymbol{\nabla} B_i \, d\mathbf{r} \tag{2.4}$$

in slightly different situations. In these expressions, summation over the repeated i-indices is implied.

A lot of the confusion stems from not distinguishing between the conceptually separate $\mathbf{H}$ and $\mathbf{B}$-fields and not properly specifying whether the fields are those in the presence or absence of the object upon which the force is acting. As we will see below, there is considerable subtlety involved in this question, and this warrants careful and methodical derivation from first principles.

We will not use the terms magnetic induction or flux density but refer to the two magnetic fields as the magnetic **H**- and **B**-fields which are related to the permeability μ and magnetization through

$$\mathbf{B} = \mu_{\mathrm{o}}(\mathbf{H} + \mathbf{M}) = \mu\mathbf{H}. \tag{2.5}$$

Everywhere, permeabilities and susceptibilities χ refer to the properties of materials not objects. The **H**- and **B**-fields are governed by two Maxwell's equations which in the static case in the presence of a stationary current distribution **J** read

$$\boldsymbol{\nabla} \cdot \mathbf{B} = 0 \quad \text{and} \quad \boldsymbol{\nabla} \times \mathbf{H} = \mathbf{J}. \tag{2.6}$$

We will use the fact that **B** being divergence-free can be written as the curl of a vector potential **A**

$$\mathbf{B} = \boldsymbol{\nabla} \times \mathbf{A} \tag{2.7}$$

and that **H** being irrotational in the absence of currents can be written as the gradient of some scalar potential.

2.1 Magnetic force on a body

The starting point is the magnetophoretic effect itself. We consider the force upon a spherical, linearly paramagnetic particle of radius a with permeability $\mu = \mu_{\mathrm{o}}(1 + \chi)$ immersed in a magnetic field $\mathbf{H}_{\mathrm{ext}}$ which, in general, will not be assumed homogeneous. We picture the particle being placed in a medium which is essentially non-magnetic, i.e. the permeability does not deviate appreciably from that of vacuum, μ_{o}. This assumption is almost always justified.

The external magnetic field will magnetize the particle, inducing a magnetic moment. Two things happen to a magnetic moment in a field. Firstly, it is subject to a torque, however, as we have assumed the particle to be linearly (para-)magnetic the moment will be aligned with the field so the net torque vanishes. Secondly, if the field is inhomogeneous, the particle will feel a net force as the "one end" of the magnetic moment will be subject to a different magnetic field strength than the other. This is the essence of the magnetophoretic effect.

2.1.1 Thermodynamics

A material body immersed in a magnetic field undergoes changes in its thermodynamic state and thus its thermodynamic potentials. However, this is a subtle point as a body in general will be magnetized and thus modify the field in which it is immersed making it necessary to specify whether one is refering to fields before introducing the body and thus measured or calculated in its absence or to fields including the body and thus taking full account of changes in the sources of the magnetic field. It turns out, fortunately, that it is possible to sidestep such problems partially and express quantities in terms of the field in the absence of the body, i.e. the applied field. We need not (always) calculate a self-consistent solution for the field and the physical properties of the sources and the body.

Our point of departure is the free energy expressed in terms of the magnetic H-field for all of space including the body. We then subtract the free energy that would exist in vacuum in the absence of the body and interpret the remainder as pertaining to the material body.

Now, to fix attention on something a little more concrete, picture a current distribution over some conductors in a region of space which gives rise to a magnetic H-field $\mathbf{H}_{\text{ext}}$. The currents are being maintained by electromotive forces, if necessary work can be done to maintain the currents. This field $\mathbf{H}_{\text{ext}}$ is taken to be in the absence of our material body. In the presence of the body things happen: the body is magnetized and changes occur to the state of the body, spins and circulating currents are ordered. This cannot, of course, be neglected and gives rise to the fields denoted $\mathbf{B}$ and $\mathbf{H}$.

The thermodynamic differential for the free energy density in terms of H-fields $\widetilde{F}$ is

$$d\widetilde{F} = -SdT + \zeta d\varrho - \mathbf{B} \cdot d\mathbf{H}. \tag{2.8}$$

Here and in the following, we are proceeding along lines laid out in Landau & Lifshitz [28] and there is little use in deviating from their notation: S is the entropy density, T the temperature, ζ the chemical potential per unit mass, ϱ is the mass density, and the tilde in $\widetilde{F}$ indicates that this free energy is a function of H rather than B-fields.

Now our choice of free energy with tilde as thermodynamic potential can be justified. We will only consider processes taking place at constant temperature and at constant mass density, further, we have already decided that our 'handle' on magnetism is currents and thus H-fields. As a sidenote, it is not really possible to get a similar handle on B-fields, as Callen [7] puts it, "There exist no walls restrictive with respect to magnetic moment."

In vacuo, the relation between H and B is simple; with the choice of SI-units — a proportionality, $\mathbf{B} = \mu_{\text{o}}\mathbf{H}$. The vacuum contribution to the free energy density is thus $\widetilde{F}_{\text{vac}} = -\frac{1}{2}\mu_{\text{o}}H_{\text{ext}}^2$. The total free energy, $\widetilde{\mathcal{F}}$, attributable to the material body we define as

$$\widetilde{\mathcal{F}} = \int (\widetilde{F} - \widetilde{F}_{\text{vac}})\, dV = \int (\widetilde{F} + \tfrac{1}{2}\mu_{\text{o}}H_{\text{ext}}^2)\, dV, \tag{2.9}$$

where $\widetilde{F}$ is the 'conventional' free energy density defined all over space.

Thus, the free energy has been redefined by subtracting the vacuum free energy density — a quantity that makes no reference whatsoever to the thermodynamics of the body. Differentials valid for the conventional free energy are precisely the same for the new total free energy, and, when doing thermodynamic processes, what we really care about are the differentials rather than the thermodynamic potentials in themselves. The redefined free energy is just as good as the old one for describing physical processes. This is the first crucial observation.

The second observation is that, on physical grounds, the differential of the total free energy can be greatly simplified compared to the the form above. As it stands, the problem needs to be specified in terms of the unmodified free energy including calculation of the actual B- and H-fields before we subtract a contribution from the vacuum; not much in the way of a simplification.

The way to proceed is to write down the differential of the modified free energy Eq. (2.9) using the expression for the unmodified one Eq. (2.8),

$$\delta\widetilde{\mathcal{F}} = \int (\delta\widetilde{F} - \delta\widetilde{F}_{\rm vac})\, dV = -\int (\mathbf{B}\cdot\delta\mathbf{H} - \mu_{\rm o}\mathbf{H}_{\rm ext}\cdot\delta\mathbf{H}_{\rm ext})\, dV, \tag{2.10}$$

and then to add and subtract $(\mathbf{B}-\mu_{\rm o}\mathbf{H})\cdot\delta\mathbf{H}$ from the integrand. After regrouping the terms, we get the following,

$$\delta\widetilde{\mathcal{F}} = -\int \mu_{\rm o}(\mathbf{H}-\mathbf{H}_{\rm ext})\cdot\delta\mathbf{H}_{\rm ext}\, dV - \int (\delta\mathbf{H}-\delta\mathbf{H}_{\rm ext})\cdot\mathbf{B}\, dV - \int (\mathbf{B}-\mu_{\rm o}\mathbf{H})\cdot\delta\mathbf{H}_{\rm ext}\, dV. \tag{2.11}$$

Now, let us just step back to ponder this. The way to look at this is that we have some physical setup with an arrangement of currents and some material body. To this we attribute some free energy — a thermodynamic potential. Physical processes change this free energy. We are considering the implications of some otherwise unspecified small step in an isothermal process which keeps the mass density fixed. There is no restriction as to whether what is being changed is the body or the current distributions. We allow for both, not just a change in $\mathbf{H}$ but also in $\mathbf{H}_{\rm ext}$.

The next steps are showing that the first and second integrals vanish: this is done by writing fields in terms of potentials, transforming the integrals, and arguing that these integrals vanish. The third integral is then the prescription for calculating changes in free energy.

We now show that the first integral vanishes. To this end we write the varied field in the absence of the material body, $\delta\mathbf{H}_{\rm ext}$, as the curl of a vector potential, $\mu_{\rm o}\,\delta\mathbf{H}_{\rm ext} = \boldsymbol{\nabla}\times\delta\mathbf{A}_{\rm ext}$. With the aid of an identity for the divergence of a cross product, the integrand

$$\mu_{\rm o}(\mathbf{H}-\mathbf{H}_{\rm ext})\cdot\delta\mathbf{H}_{\rm ext} = \nabla\cdot\big(\delta\mathbf{A}_{\rm ext}\times(\mathbf{H}-\mathbf{H}_{\rm ext})\big) + \delta\mathbf{A}_{\rm ext}\cdot\boldsymbol{\nabla}\times(\mathbf{H}-\mathbf{H}_{\rm ext}). \tag{2.12}$$

With the aid of the divergence or Gauss theorem, the first integral transforms into a surface integral over the surface at infinity, in all,

$$-\int \mu_{\rm o}(\mathbf{H}-\mathbf{H}_{\rm ext})\cdot\delta\mathbf{H}_{\rm ext}\, dV = \oint \delta\mathbf{A}_{\rm ext}\times(\mathbf{H}-\mathbf{H}_{\rm ext})da + \int \delta\mathbf{A}_{\rm ext}\cdot\boldsymbol{\nabla}\times(\mathbf{H}-\mathbf{H}_{\rm ext})\, dV. \tag{2.13}$$

The surface integral at infinity vanishes, so we are left with the second integral. Reasoning based on thermodynamics presupposes equilibrium and thus that transients have died out. The total currents across the conductors that generate $\mathbf{H}$ and $\mathbf{H}_{\rm ext}$ are assumed to be the same; this is how the fields before and after are constructed. What might be different is the spatial distribution over the cross sections of the conductors, however, stationary currents are unaffected by static magnetic fields: a time-varying magnetic field *can* influence the current distribution but stationary currents are only affected by the electric fields, in particular those fields driving the current. Thus even the current *distributions* must be the same before and after placing the body in the magnetic field so the *curls* of $\mathbf{H}_{\rm ext}$ and $\mathbf{H}$ must be identical: the integrand vanishes.

Having showed, carefully, the first integral of Eq. (2.11) to vanish, we proceed with the second. In lieu of $\mathbf{B}$, we can have a vector potential $\mathbf{A}$ so that $\mathbf{B} = \boldsymbol{\nabla}\times\mathbf{A}$. This enters

the integrand and we write it as a divergence of a cross product and a term containing the curl of some H-field,

$$(\delta\mathbf{H} - \delta\mathbf{H}_{\text{ext}}) \cdot \mathbf{B} = \boldsymbol{\nabla} \cdot \big(\mathbf{A} \times (\delta\mathbf{H} - \mathbf{H}_{\text{ext}})\big) + \mathbf{A} \cdot \boldsymbol{\nabla} \times (\delta\mathbf{H} - \delta\mathbf{H}_{\text{ext}}). \tag{2.14}$$

The divergence term is converted into a surface integral at infinity by virtue of the divergence theorem and thus vanishes. The δ-terms appearing in the curl are changes in the fields with and without the body due to the process we are studying. Because of linearity of electromagnetism these are actually legitimate physical fields just as the fields before and after the process step, and we can ascribe them current distributions $\delta\mathbf{j}$ and $\delta\mathbf{j}_{\text{ext}}$. More over, the current distributions are the same with and without body by arguments as above. The curls are thus the same and the second term of the integrand vanishes. Left is the third term of Eq. (2.11),

$$\delta\widetilde{\mathcal{F}} = -\int (\mathbf{B} - \mu_{\text{o}}\mathbf{H}) \cdot \delta\mathbf{H}_{\text{ext}}\, dV \tag{2.15}$$

or

$$\delta\widetilde{\mathcal{F}} = -\int_{\text{body}} \mu_{\text{o}}\mathbf{M} \cdot \delta\mathbf{H}_{\text{ext}}\, dV. \tag{2.16}$$

As the body in question is the only volume over which $\mathbf{M}$ does not vanish identically, we restrict the integration to the volume of the body. If the material is linear with respect to magnetic fields, calculations are straight-forward.

2.1.2 The magnetic force from the free energy

Leaving Landau & Lifshitz, the result can be used simply to calculate the force on a magnetized object. Firstly, a force $\mathbf{F}$ due to the *field* performing work upon the *body* over some distance $\delta\mathbf{s}$ changes the free energy of the *field* by

$$\delta\widetilde{\mathcal{F}} = -\mathbf{F} \cdot \delta\mathbf{s}. \tag{2.17}$$

By considering the free energy change during a small (virtual) displacement $\delta\mathbf{s}$ we find the force stemming from the magnetic field. A displacement of the body in the field means that the field *sans* body appears to have changed by $(\delta\mathbf{s}\cdot\nabla)\mathbf{H}_{\text{ext}}$. This is exactly the $\delta\mathbf{H}_{\text{ext}}$ we are after. Inserting this into Eq. (2.16) gives

$$\delta\widetilde{\mathcal{F}} = \delta s_j \int_{\text{body}} \mu_{\text{o}} M_i \partial_j (H_{\text{ext}})_i\, dV, \tag{2.18}$$

where we conveniently interpret the integral as the force from the magnetic field $\mathbf{H}_{\text{ext}}$ on the magnetic moment distribution $\mathbf{M}(\mathbf{r})$.

If the body is non-conducting and the fields are static then $\boldsymbol{\nabla} \times \mathbf{H}_{\text{ext}} = 0$ and the force in an external magnetic field on a magnetized object can be written

$$\mathbf{F} = \mu_{\text{o}} \int (\mathbf{M} \cdot \boldsymbol{\nabla})\mathbf{H}_{\text{ext}}\, dV, \tag{2.19}$$

where the integration is, again, understood to be carried out over the volume of the object, i.e. where the magnetization is non-vanishing.

Now, if the field is not *too* inhomogeneous, i.e. $a|\boldsymbol{\nabla}\mathbf{H}| \ll |\mathbf{H}|$, we calculate the magnetization as the magnetization of a spherical particle in a homogeneous field which is known to be,

$$\mathbf{M} = \frac{3\chi}{\chi+3}\mathbf{H}_{\text{ext}} = 3\frac{\mu-\mu_{\text{o}}}{\mu+2\mu_{\text{o}}}\mathbf{H}_{\text{ext}}, \tag{2.20}$$

assuming non-magnetic surroundings and, conveniently, is constant over the volume of the particle [24]. This is an exceptional case; the magnetization will usually vary over the volume and is generally not known in closed form.

The resulting total force is then found simply by carrying out the integration over the volume of the particle,

$$\mathbf{F} = 2\pi\mu_{\text{o}}\, a^3 \frac{\mu-\mu_{\text{o}}}{\mu+2\mu_{\text{o}}}\, \boldsymbol{\nabla} H_{\text{ext}}^2. \tag{2.21}$$

The validity of this expression depends on the proportionality of the magnetization with the field and on the field inhomogeneity not being too great so that the magnetization can be taken as constant.

Some quick observations are in order: If the particle is paramagnetic, $\mu > \mu_{\text{o}}$, as we have assumed then it will be attracted toward higher magnetic fields. This is called *positive magnetophoresis*, conversely, diamagnetic particles which are repelled by high magnetic fields exhibit *negative* magnetophoresis. The total force quickly saturates for susceptibilities larger than unity — and equivalently for permeabilities larger than that of vacuum.

As for the dispute in the literature on the form of the correct expression for the force on a magnetic body [39, 16, 17] where Odenbach & Liu argued for the validity of two different force expressions, we can rule in favour of Engel [16, 17]. The core of the matter is imprecision in specifying which fields one is referring to. As we have seen one obtains the correct force when one calculates the gradient of the magnetic H-field in the absence of the body. In the experiment of Odenbach & Liu, they had arranged the experiment that the difference between the correct expression Eq. (2.19) and the incorrect ones Eqs. (2.3) and (2.4) used with the magnetic B-field calculated in the presence of the body was on the order of a few per cent and thus indistinguishable experimentally.

2.2 Magnetic forces between two particles

In the preceding, we looked at the force on a single body or particle; now we turn to the case of more than one in an external magnetic field. The magnetic field is changed by the presence of additional magnetic particles and this gives rise to an effective interaction. This is the first step into considering interactions of many particles.

We look at the case of just two particles. The interaction comes about in different ways: (a) The field due to the magnetization of the one particle induces an additional magnetic moment in the other particle; (b) the field due to the magnetization of the one particle gives rise to an inhomogeneity of the field at the position of the other particle

and thus a force; (c) the additional magnetic moment interacts with the dipole field of the neighbouring particle. Symbolically, we write

$$\mathbf{F}_{\text{total}} = \mu_{\text{o}} \int \Big((\mathbf{M}_{\text{ext}} + \mathbf{M}_{\text{ind}}) \cdot \boldsymbol{\nabla} \Big) (\mathbf{H}_{\text{ext}} + \mathbf{H}_{\text{ind}})\, dV \tag{2.22}$$

where $\mathbf{M}_{\text{ext}}$ is the magnetization caused by the applied field $\mathbf{H}_{\text{ext}}$, and $\mathbf{H}_{\text{ind}}$ is the field from the induced magnetization in a particle. The magnetization caused by the induced field from the other particle is $\mathbf{M}_{\text{ind}}$.

Different contributions are identified by expanding the product in the integrand: The applied field and the magnetization created by it are independent of the interparticle separation s. The induced field, $\mathbf{H}_{\text{ind}}$, is predominantly a dipole field. For a spherical particle in a homogeneous magnetic field this is true exactly, in general this will only be an approximation. The field from a dipole falls off as separation cubed and we generally assume that the fields are so small that the magnetizations are proportional to the external fields so that

$$\mathbf{H}_{\text{ind}} \propto \frac{1}{s^3} \quad \text{and} \quad \mathbf{M}_{\text{ind}} \propto \frac{1}{s^3}. \tag{2.23}$$

A few important general observations can be made on the basis of this if we expand the force in powers of the inter-particle separation. First, the leading contribution to the force would be that between $\mathbf{M}_{\text{ext}}$ and $\mathbf{H}_{\text{ext}}$ — both independent of s. This is the force that any such magnetic particle would feel were it alone. The first correction to the interparticle force is the interaction between $\mathbf{M}_{\text{ind}}$ and $\mathbf{H}_{\text{ext}}$. This is inversely proportional to the separation cubed. The next correction, due to $\mathbf{H}_{\text{ind}}$ acting on $\mathbf{M}_{\text{ext}}$, is proportional to the fourth power. Lastly, there is a *van der Waals*-like, i.e. induced dipole-induced dipole, interaction of seventh order.

Here we restrict ourselves to the correction of leading order, the one due to the neighbouring particle changing $\mathbf{M}$. The two particles are both in a magnetic field which we take to be fairly homogeneous; sufficient to approximate the resulting field from either of the particles, here no. 1, as that of a dipole [15, 24],

$$\mathbf{H}_{\text{ind},1} = \frac{\chi}{\chi + 3} a^3 \left(\frac{3\big(\mathbf{H}(\mathbf{r_1}) \cdot \mathbf{s}\big)\mathbf{s}}{s^5} - \frac{\mathbf{H}(\mathbf{r_1})}{s^3} \right). \tag{2.24}$$

The field from particle 1 gives rise to a magnetization of particle 2 and by Eq. (2.19) a force

$$\mathbf{F}_{2\leftarrow 1} = 4\pi\mu_{\text{o}} \frac{\chi^2}{(\chi+3)^2} \frac{a^6}{s^3} \left(\frac{3}{s^2} \big(\mathbf{H}(\mathbf{r_1}) \cdot \mathbf{s}\big) \big(\mathbf{s} \cdot \boldsymbol{\nabla}\big) \mathbf{H}(\mathbf{r}_2) - \big(\mathbf{H}(\mathbf{r}_1) \cdot \boldsymbol{\nabla}\big) \mathbf{H}(\mathbf{r}_2) \right) \tag{2.25}$$

As anticipated, this is a force term that depends inversely on the distance cubed.

2.3 Magnetic particle in pure dipole field

The problem of two magnetizable spherical particles in an external field is a difficult one. It can be solved in the form of a triple recursion formula but this solution is very hard to

extract usable results from, [50, 51]. Here we will look at a simpler problem that admits a solution as a series expansion, specifically a multipole expansion: that of a sphere in a pure dipole field.

The idea is that we are going to immerse the particles in an external field which is mostly homogeneous and that the particles are separated somewhat. The dipole terms will then dominate. However, the dipole field from the other particle will induce higher order terms that we can take into account. This approximation falls in between ignoring the magnetic interaction, only retaining the terms due to the applied (external) field, and then solving the complete problem exactly, for example, expanding the fields of both to all orders.

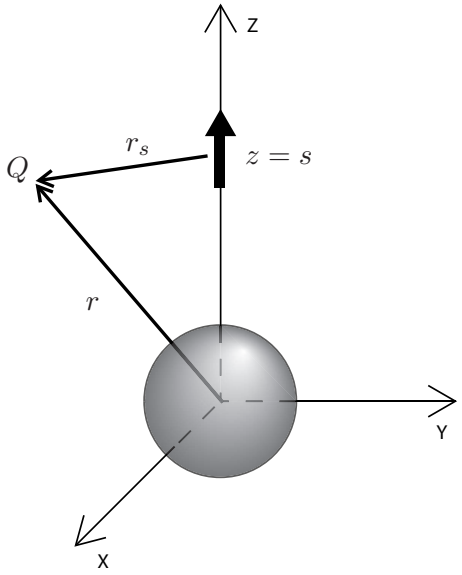

Figure 2.1: A magnetizable sphere centered at the origin and a point dipole directed in the z-direction indicated by the bold short arrow. For an arbitrary point Q, the distance r is calculated from the origin and the distance r_s is measured from the dipole at $z = s$.

We picture a sphere of radius a centered at the origin and a dipole at the point $z = s$ on the z-axis. We assume that everything is static and non-conducting so that $\mathbf{J} + \frac{\partial \mathbf{D}}{\partial t} = 0$ and thus $\boldsymbol{\nabla} \times \mathbf{H} = 0$. This means we can define the magnetic scalar potential, ψ, akin to the potential known from electrostatics. We take the dipole to be arranged in the direction of the z-axis, i.e. the scalar potential is [24, 25, 52]

$$\psi = \frac{m_z}{4\pi} \frac{\partial}{\partial z} \frac{1}{r_s}, \tag{2.26}$$

for some moment m_z and where r_s is the distance from the dipole. (The two other cases are found in an appendix.) This we expand as seen from the origin, i.e. the centre of the

sphere, in a multipole expansion

$$\frac{\partial}{\partial z}\frac{1}{r_s} = \frac{\partial}{\partial z}\frac{1}{s}\sum_n P_n(\cos\theta)\left(\frac{r}{s}\right)^n \tag{2.27}$$

i.e. an expansion in powers of distance r and with the (polar) angular dependence encapsulated in Legendre polynomials, P_n.

The differentiation can be carried out

$$\frac{\partial}{\partial z}\frac{1}{r_s} = \frac{1}{s}\sum_n \left(P_n(\cos\theta)\frac{n}{s}\left(\frac{r}{s}\right)^{n-1}\frac{\partial r}{\partial z} + P_n'(\cos\theta)(-\sin\theta)\left(\frac{r}{s}\right)^n\frac{\partial\theta}{\partial z}\right). \tag{2.28}$$

and we can then apply an identity for Legendre polynomials and the derivatives of polar coordinate functions in terms of Cartesian coordinates,

$$\frac{\partial r}{\partial x} = \sin\theta\,\cos\phi, \qquad \frac{\partial\theta}{\partial x} = \frac{1}{r}\cos\theta\,\cos\phi, \tag{2.29a}$$

$$\frac{\partial r}{\partial y} = \sin\theta\,\sin\phi, \qquad \frac{\partial\theta}{\partial y} = \frac{1}{r}\cos\theta\,\sin\phi, \tag{2.29b}$$

$$\frac{\partial r}{\partial z} = \cos\theta, \qquad \frac{\partial\theta}{\partial z} = -\frac{1}{r}\sin\theta. \tag{2.29c}$$

We do it one term at a time. First, we write out the derivative in the first term of Eq. (2.28)

$$P_n(\cos\theta)\frac{n}{s}\left(\frac{r}{s}\right)^{n-1}\frac{\partial r}{\partial z} = P_n(\cos\theta)\frac{n}{r}\left(\frac{r}{s}\right)^n\cos\theta \tag{2.30}$$

In the second term, we use the identity

$$-P_n'(x) = \frac{nx}{1-x^2}P_n(x) - \frac{n}{1-x^2}P_{n-1}(x) \tag{2.31}$$

to obtain

$$-P_n(\cos\theta)\left(\frac{r}{s}\right)^n\frac{n}{r}\cos\theta + P_{n-1}(\cos\theta)\left(\frac{r}{s}\right)^n\frac{n}{r}. \tag{2.32}$$

The terms can then be collected

$$\frac{\partial}{\partial z}\frac{1}{r_s} = \frac{1}{s^2}\sum_n (n+1)P_n(\cos\theta)\left(\frac{r}{s}\right)^n. \tag{2.33}$$

By sorting by order of Legendre polynomials, we get the multipole expansion.

This is the general expansion of the dipole potential. Now we write up the most general multipole expansion of the potential in ψ_{in} and around the sphere ψ_{ex}. First we observe that outside the sphere, the expansion of the potential cannot be in positive powers r^n as the potential must tend to a finite value, e.g. zero, at infinity. Conversely, in order to stay finite at the origin the potential cannot have terms with negative powers $1/r^n$. In short,

$$\psi_{\text{in}} = \sum_n A_n r^n\, P_n(\cos\theta) \tag{2.34}$$

$$\psi_{\text{ex}} = \sum_n B_n\frac{P_n(\cos\theta)}{r^{n+1}} + \frac{m_z}{4\pi}\frac{\partial}{\partial z}\frac{1}{r_s} \tag{2.35}$$

$$= \sum_n \left(B_n\frac{1}{r^{n+1}} + \frac{m_z}{4\pi s^2}(n+1)\left(\frac{r}{s}\right)^n\right) P_n(\cos\theta). \tag{2.36}$$

Now it remains to match $\psi_{\rm in}$ and $\psi_{\rm ex}$ at the boundary of the sphere, at $r = a$. We have two boundary conditions to help us. Firstly, that the H-field is finite across the boundary and as $\mathbf{H} = -\boldsymbol{\nabla}\psi$, so the potential must be continuous

$$\psi_{\rm in}|_{r=a} = \psi_{\rm ex}|_{r=a} \tag{2.37}$$

Secondly, that the normal component of **B**-field must be continuous, i.e.

$$-\mu_{\rm o}\frac{\partial\psi_{\rm ex}}{\partial r}\bigg|_{r=a} = -\mu\frac{\partial\psi_{\rm in}}{\partial r}\bigg|_{r=a}. \tag{2.38}$$

We employ these conditions in turn and use the fact that Legendre polynomials, $P_n(x)$, are orthogonal. First, equality of potentials at $r = a$, Eq. (2.37) gives

$$A_n = \frac{B_n}{a^{2n+1}} + \frac{m_z}{4\pi s^2}\frac{n+1}{s^n}. \tag{2.39}$$

Secondly, we require Eq. (2.38) so we need the derivatives

$$\frac{\partial\psi_{\rm in}}{\partial r} = \sum_n A_n n r^{n-1} P_n(\cos\theta) \tag{2.40}$$

and

$$\frac{\partial\psi_{\rm ex}}{\partial r} = \sum_n \left(-(n+1)\frac{B_n}{r^{n+2}} + \frac{m_z}{4\pi s^3} n(n+1)\Big(\frac{r}{s}\Big)^{n-1}\right) P_n(\cos\theta). \tag{2.41}$$

Applying the condition on the derivatives Eq. (2.38) gives

$$A_n = \frac{\mu_{\rm o}}{\mu}(n+1)\left\{-\frac{1}{n}\frac{B_n}{a^{2n+1}} + \frac{m_z}{4\pi s^2}\frac{1}{s^n}\right\}. \tag{2.42}$$

Subtracting Eqs. (2.39) and (2.42) enables us to find B_n which determines the expansion of the field external to the sphere as

$$B_n = -a^{2n+1} n(n+1)\frac{m_z}{4\pi s^{n+2}}\frac{\mu-\mu_{\rm o}}{n\mu + (n+1)\mu_{\rm o}}. \tag{2.43}$$

The induced nth-multipole moment of the sphere, $m^{(n)}$, is $4\pi B_n$. The dipole field creates multipole moments of all orders but the leading one is the dipole moment

$$m^{(1)} = -2m_z\frac{a^3}{s^3}\frac{\mu-\mu_{\rm o}}{\mu+2\mu_{\rm o}}. \tag{2.44}$$

This means the following: A dipole oriented in the z-direction of moment m_z induces a dipole moment $m^{(1)}$ in the sphere of permeability μ when they are separated by s in the z-direction.

2.4 Two magnetic spheres in an external magnetic field

Under the assumption that the materials are linearly paramagnetic the following argument applies if we think of two identical magnetic beads A and B of radii a separated by s with the line connecting the centres being the z-axis in an external magnetic field. The external field which we take to be homogeneous over the volume of either the two spheres and in the z-direction induces magnetic dipole moments m_z^A and m_z^B also in the z-direction in the magnetic spheres. These give rise to a field that adds to the external magnetic field and, in particular, modifies the field around the neighbouring sphere. The presence of two spheres changes the induced dipole moment from m_z^A and m_z^B due to external field to new values m_{tot}^A and m_{tot}^B. These values incorporate induced dipole moments $m_A^{(1)}$ and $m_B^{(1)}$ into

$$m_{\text{tot}}^A = m_z^A + m_A^{(1)} \qquad\qquad m_{\text{tot}}^B = m_z^B + m_B^{(1)} \tag{2.45}$$

where the $m_A^{(1)}$ and $m_B^{(1)}$ can be calculated from Eq. (2.44) and m_{tot}^B and m_{tot}^A. We thus have a set of simultaneous equations for m_{tot}^A and m_{tot}^A which can be solved to give us

$$m_{\text{tot}}^A = \frac{m_{\text{ext}}^A - 2m_{\text{ext}}^B \frac{a^3}{s^3}\frac{\mu-\mu_{\text{o}}}{\mu+2\mu_{\text{o}}}}{1 - 4\big(\frac{\mu-\mu_{\text{o}}}{\mu+2\mu_{\text{o}}}\big)^2 \frac{a^6}{s^6}} \tag{2.46}$$

$$m_{\text{tot}}^B = \frac{m_{\text{ext}}^B - 2m_{\text{ext}}^A \frac{a^3}{s^3}\frac{\mu-\mu_{\text{o}}}{\mu+2\mu_{\text{o}}}}{1 - 4\big(\frac{\mu-\mu_{\text{o}}}{\mu+2\mu_{\text{o}}}\big)^2 \frac{a^6}{s^6}}. \tag{2.47}$$

This can be compared with the magnetic dipole moment calculated from just having the sphere in the homogeneous external field and the pure dipole field from the neighbouring sphere assumed alone Eq. (2.44),

$$m_{\text{ext}}^B - 2m_{\text{ext}}^A \frac{a^3}{s^3}\frac{\mu-\mu_{\text{o}}}{\mu+2\mu_{\text{o}}} \qquad \text{and} \qquad m_{\text{ext}}^A - 2m_{\text{ext}}^B \frac{a^3}{s^3}\frac{\mu-\mu_{\text{o}}}{\mu+2\mu_{\text{o}}}. \tag{2.48}$$

The denominators in Eqs. (2.46) and (2.47) give the influence on a magnetizable sphere back on itself via coupling from the neighbouring one akin to summing contributions in a geometric series. We see that the denominator is positive as the two spheres do not overlap so $s > 2a$. This means that the effect of including contributions due to the proximity of two spheres is an increase in the magnetic dipole moments.

An analogous line of reasoning can be made if the field induces magnetic dipole moments in the x or y-directions and it can be extended to include higher multipole moments taking into account the couplings between them. This can be done by calculating the couplings from magnetic multipoles higher than the dipole obtaining analogues to Eq. (2.43) that gives the coupling from a dipole to arbitrary multipoles in a sphere. This can then be used to define a set of equations for the magnetic multipole moments of two spheres that can be solved to find the analogues of Eqs. (2.46) and (2.47) from which higher approximations to the magnetization and field inside of either spheres can be found. In turn, this can be used to find better approximations to the force between two spherical

particles than Eq. (2.25). We will not pursue this path as the corrections to the interaction force are presumably rather small. We will see in the next chapter that influence of magnetic interactions is dwarfed by effects of fluid flow in actual magnetic bead capturing geometries.

2.5 Discussion

We have carefully derived the expression for the force on a magnetic body in a general magnetic field from principles of thermodynamics and thus resolved a dispute arisen in the literature. This is a firm basis upon which one can build approximations in various actual situations of interest.

Then we found the interaction force between two spherical particles under the assumption that magnetic field was sufficiently homogeneous over the volume of the particles so one could calculate the magnetizations from the values of the magnetic field at the particle centres. This approximation is somewhat paradoxical in that the force stems from field inhomogeneities but just amounts to an assumption that the particles are small compared to the length scale over which the magnetic field varies.

A step was then taken beyond the assumption that the field is homogeneous over the volume of the particle and specifically we calculated the magnetic scalar potential in and around a spherical magnetizable particle in the case of the magnetic field from a magnetic dipole. Assuming that the most important magnetic multipole moment for a spherical particle is the dipole moment, we found the dipole moments for particles magnetized by a homogeneous magnetic field but close together. This outlines an approach for a detailed calculation of the magnetizations and magnetic fields in and around a pair of particles building on the couplings between multipole moments.

Chapter 3

Motion of few beads

Having duly considered magnetism and the forces on magnetic beads of magnetic origin, we, in the following, investigate the effect of the beads being immersed in a viscous, fluid medium. We find that fluid motion due to the beads moving sets up a long-range hydrodynamic interaction which affects bead motion. This interaction is then incorporated into a simulation of capturing of magnetic beads where we see that it has an effect on the ability to catch the beads.

3.1 Hydrodynamic interactions between beads

In actual magnetophoresis and magnetic bead capturing experiments in microfluidic channels there are other phenomena than magnetism contributing to the motion of the beads, notably what we term hydrodynamic interactions, i.e. the phenomenon that the beads are moving in as well as being moved by the surrounding fluid. However, in the literature on magnetic beads the motion of beads is treated as if they are moving individually, in isolation, cf. [55, 44, 8, 21]. If interactions between beads play a rôle, this approach is suspect and might even be incorrect. It is therefore interesting to establish the nature of hydrodynamic interactions, even if only in the context of bead capturing. It is not a purpose of the present to judge the validity of the approaches taken elsewhere; rather it is to bring hydrodynamic interactions to attention and to establish a framework from their study.

First, let us try to clarify what we mean by hydrodynamic interaction. The beads are subject to a magnetic force that moves them relative to the unperturbed fluid flow and this relative motion sets up a viscous drag from the fluid and thus a momentum transfer. This transfer of momentum gives rise to an additional flow, a change in fluid velocity, that affects, in principle, the global fluid flow pattern. In particular, the values of the fluid velocity around other beads are changed and the viscous drags on them are thus also changed. This means that the motion of these other beads is also changed as they accelerate to establish a new force balance between drag and the external magnetic force. We will later show that this force balance is established very quickly.

If we choose to ignore the specifics of the fluid flow, it appears that there is a fluid

mediated interaction between the beads that changes their motion relative to what one would expect if one applies Newton's laws to the magnetic forces calculated from the formulas of Chapter 2 and from the drag due to the unperturbed flow. There are thus two possible equivalent views: Either we calculate the full fluid flow taking into account the effect of beads and the external force on them, or we take the point of departure in the unperturbed fluid flow and then find a way to account for hydrodynamic interactions.

One possible, simple model is considering the effect of the beads on the unperturbed fluid flow as that of a point force. This can be described by a kind of hydrodynamic Green's function called the *stokeslet* (or Oseen tensor) similar to, for example, the Green's functions known from electrostatics that describe the electric field from a point charge [42, 49].

Furthermore, phenomena in a microfluidic channel occur in the vicinity of walls. This gives rise to effective interactions with the walls since the no-slip boundary condition must be fulfilled there. This can also be described by Green's function techniques [42].

3.1.1 Motion in a viscous fluid

Viscous action is a mechanism of dissipation of kinetic energy; it dampens velocity differences and gives rise to drags on bodies which move relative to the surrounding fluid. The drag force on a spherical bead of radius a in an unbounded fluid at rest of viscosity η is given by Stokes' law [27]

$$\mathbf{F}_\eta = -6\pi\eta a\mathbf{v} \tag{3.1}$$

as the sphere moves with velocity $\mathbf{v}$ relative to the fluid provided that this motion is laminar and slow in the sense that the Reynolds number Re is smaller than unity; the Reynolds number being defined by

$$\mathrm{Re} = \frac{\varrho u l}{\eta} \tag{3.2}$$

for some smallest length scale l entering the problem. A natural length scale in this case is the bead radius a. It should be noted that the validity of Stokes' law is not straightforward as pointed out by Oseen, cf. [26, 27].

An object, in our case, a spherical bead suddenly being subject to a changed external force, $\mathbf{F}_{\mathrm{ext}}$, will accelerate until the viscous force balances the external force on the object. By Newton's second law and Stokes' law for the viscous drag, we find

$$m\frac{\partial \mathbf{v}}{\partial t} = \mathbf{F}_{\mathrm{ext}} + \mathbf{F}_\eta = \mathbf{F}_{\mathrm{ext}} - 6\pi\eta a\mathbf{v}. \tag{3.3}$$

It is readily seen that the terminal velocity is $\mathbf{F}_{\mathrm{ext}}/6\pi\eta a$ and it is attained exponentially with a time constant of

$$\tau = \frac{m}{6\pi\eta a} = \frac{2\varrho a^2}{9\eta}. \tag{3.4}$$

assuming a neutrally bouyant spherical bead. This happens very fast: Assuming a viscosity of 10^{-3} kg/m s, that of water at room temperature, and a bead of radius 10^{-6} m, the time constant is less than 0.25 μs. During that time the bead will move less than a full diameter

even for a flow as fast as 1 m/s so we can safely ignore the acceleration phase. For a bead with a radius of 5 μm the time constant is 5.6 μs. This constitutes one of the most important approximations which we will use in the following.

The factor $(6\pi\eta a)^{-1}$ is called the mobility b and is interpreted as the speed a spherical bead attains when it is subject to a unit force.

3.1.2 Motion in fluid flow and external magnetic field

Let us now suppose that we have both a fluid flow and an external magnetic field acting on a magnetic bead. We assume, as suggested above, that viscous drag balances the external force at all times as acceleration relative to the surrounding fluid, This is possible because changes in the external force happens on a much shorter timescale than that of changes in the force experienced by the bead.

Stokes' law is only derived for unbounded fluid at rest, but often it is taken to hold for fluid flows in general. This is not strictly correct. If the fluid is translating with some fixed velocity we see by means of a Galilean transformation that we recover Stokes' law but for more complicated flows an additional term is needed to make up for non-uniform fluid velocity over the surface of the spherical particle or bead. This was first pointed out by Faxén [19]. The correct form of the drag is

$$\mathbf{F}_\eta = -6\pi\eta a(1 + \tfrac{1}{6}a^2\nabla^2)(\mathbf{v} - \mathbf{u}(\mathbf{r})) \tag{3.5}$$

with the Laplacian acting on the fluid flow $\mathbf{u}$ only [19, 20, 42]. We follow tradition and neglect this additional term though it could be included.

The balance of forces is then,

$$0 = \mathbf{F}_{\text{mag}} + \mathbf{F}_{\text{V}} = 2\pi\mu_{\text{o}}\, a^3 \frac{\chi}{\chi + 3}\, \boldsymbol{\nabla} H_{\text{ext}}^2 - 6\pi\eta a\, (\mathbf{v} - \mathbf{u}) \tag{3.6}$$

where $\mathbf{v}$ is the velocity of the bead and $\mathbf{u}$ is the fluid velocity — both taken in the lab frame. This equation, in effect, specifies the velocity of the bead

$$\mathbf{v} = \frac{\mu_{\text{o}} a^2}{3\eta} \frac{\chi}{\chi + 3}\, \boldsymbol{\nabla} H_{\text{ext}}^2 + \mathbf{u}. \tag{3.7}$$

The velocity of the fluid is not constant over the cross section of a channel, rather it assumes something like a parabolic profile with the maximum velocity in the centre and vanishing velocity at the walls. In the case of a circular channel — a pipe — the profile is known exactly and is parabolic as is the case for the flow parallel to two parallel planes of infinite extent. The case of a channel with rectangular cross section is also solvable analytically, not in closed form but rather in the form of a series expansion [27, 6]. For a parabolic fluid flow velocity profile, the Faxén term contributes only a constant.

As mentioned earlier, motion of beads in the fluid due to external forces acting on them perturbs the normal *Poiseuille* flow, parabolic or otherwise. In the following section we shall model the perturbation using Green's functions.

3.1.3 Hydrodynamic Green's functions

The flow of a viscous fluid like water in a microchannel only a fraction of a millimetre wide and at a speed in the range of millimetres per second is invariably laminar. If the microchannel is 1 mm wide and the fluid is water which flows with a maximum speed in the channel of 1 mm/s then we ascribe it a Reynolds number of 1. The small Reynolds number means that the mentioned laminar Poiseuille flow is a good description of the actual flow but also that it is permissible to simplify to the Navier-Stokes equation for incompressible flows

$$\varrho\frac{\partial \mathbf{u}}{\partial t} + \varrho(\mathbf{u}\cdot\boldsymbol{\nabla})\mathbf{u} = -\boldsymbol{\nabla}p + \eta\nabla^2\mathbf{u} + \mathbf{F}_{\text{vol}}, \tag{3.8}$$

for a velocity field $\mathbf{u}(\mathbf{r})$ and pressure field $p(\mathbf{r})$ in a fluid of density ϱ, viscosity η, subject to a force density acting on the fluid $\mathbf{F}_{\text{vol}}$. Instead of the non-linear Navier-Stokes equation we can neglect the left hand side for slow, steady-state flow and obtain the linear Stokes equation

$$0 = -\boldsymbol{\nabla}p + \eta\nabla^2\mathbf{u} + \mathbf{F}_{\text{vol}}. \tag{3.9}$$

Being linear, we stand a much better chance of solving it; even finding analytical solutions. The tool we are after is a Green's function that describes the flow due to a unit point force acting in the fluid at some point $\mathbf{r}_{\text{o}}$. This is reminiscent of our physical situation — a microscopic bead acting under the influence of a magnetic field causing a disturbance to the flow.

The Green's function, $G_{ij}(\mathbf{r},\mathbf{r}_{\text{o}})$, will then be a solution to Eq. (3.9) for the fluid velocity in the i-direction with the force term $\delta(\mathbf{r}-\mathbf{r}_{\text{o}})\,f_j$ acting in the j-direction corresponding to a point force $\mathbf{f}$ acting in the point $\mathbf{r}_{\text{o}}$. Conventionally, the solution to the Stokes equation is taken to be

$$u_i(\mathbf{r}) = \frac{1}{8\pi\eta}G_{ij}(\mathbf{r},\mathbf{r}_{\text{o}})\,f_j \tag{3.10}$$

and not directly the Green's function, G. Here and in the following we employ the convention of summing over repeated indices.

It is straightforward to solve the Stokes equation, Eq. (3.9) by Fourier transformation: One has to express the velocity $\mathbf{u}$ and the pressure p through their Fourier transforms in the Stokes equation and the incompressibility condition, carry out the differentiations, and thus obtain algebraic equations. The algebraic equations can then be solved for the transformed pressures and velocities and then transformed back to real space. We pause to show the method which is also used in Chapter 6.

First, write up the Fourier transform of the incompressibility condition

$$\boldsymbol{\nabla}\cdot\mathbf{u}(\mathbf{r}) = 0 \tag{3.11}$$

into

$$\boldsymbol{\nabla}\cdot\int\mathbf{u}(\mathbf{k})e^{i\mathbf{k}\cdot\mathbf{r}}\frac{d\mathbf{k}}{(2\pi)^3} = \int(i\mathbf{k})\cdot\mathbf{u}(\mathbf{k})e^{i\mathbf{k}\cdot\mathbf{r}}\frac{d\mathbf{k}}{(2\pi)^3} = 0 \tag{3.12}$$

then we multiply by $e^{-i\mathbf{k}_o\cdot\mathbf{r}}$ and integrate over all space to retrieve an algebraic equation equivalent to the incompressibility condition

$$\int d\mathbf{r}\int (i\mathbf{k})\cdot\mathbf{v}(\mathbf{k})e^{i(\mathbf{k}-\mathbf{k}_o)\cdot\mathbf{r}}\frac{d\mathbf{k}}{(2\pi)^3} = \int (i\mathbf{k})\cdot\mathbf{u}(\mathbf{k})\,\delta(\mathbf{k}-\mathbf{k}_o)\frac{d\mathbf{k}}{(2\pi)^3} = 0$$

yielding

$$i\mathbf{k}_o\cdot\mathbf{u}(\mathbf{k}_o) = 0. \tag{3.13}$$

The same procedure for the Stokes equation gives

$$\begin{aligned}&\boldsymbol{\nabla}\int p(\mathbf{k})\,e^{i\mathbf{k}\cdot\mathbf{r}}\frac{d\mathbf{k}}{(2\pi)^3} + \eta\nabla^2\int \mathbf{u}(\mathbf{k})\,e^{i\mathbf{k}\cdot\mathbf{r}}\frac{d\mathbf{k}}{(2\pi)^3} + \int \mathbf{f}\,e^{i\mathbf{k}\cdot\mathbf{r}}\frac{d\mathbf{k}}{(2\pi)^3}\\ &= \int \left((i\mathbf{k})\,p(\mathbf{k}) + \eta\,(-k^2)\,\mathbf{u}(\mathbf{k}) + \mathbf{f}\right)\,e^{i\mathbf{k}\cdot\mathbf{r}}\,\frac{d\mathbf{k}}{(2\pi)^3} = 0\end{aligned} \tag{3.14}$$

and upon multiplying by $e^{-i\mathbf{k}_o\cdot\mathbf{r}}$ and integrating, we retrieve the algebraic equation

$$i\mathbf{k}_o p(\mathbf{k}_o) - \eta k_o^2\,\mathbf{u}(\mathbf{k}_o) + \mathbf{f} = 0. \tag{3.15}$$

In this Fourier transformed version of the Stokes equation, we can eliminate the velocity by forming the scalar product with the vector $\mathbf{k}_o$ and using the incompressibility condition,

$$ik_o^2 p(\mathbf{k}_o) + \mathbf{k}_o\cdot\mathbf{f} = 0, \tag{3.16}$$

which lets us find the Fourier transform of the pressure

$$p(\mathbf{k}) = \frac{i(\mathbf{k}\cdot\mathbf{f})}{k^2} \tag{3.17}$$

where we from hereon drop the subscripts.

Returning to the Fourier transformed Stokes equation we can find the velocity

$$-\frac{\mathbf{k}(\mathbf{k}\cdot\mathbf{f})}{k^2} - \eta k^2\mathbf{u}(\mathbf{k}) + \mathbf{f} = 0 \tag{3.18}$$

or

$$\mathbf{u}(\mathbf{k}) = \frac{k^2\mathbf{f} - \mathbf{k}(\mathbf{k}\cdot\mathbf{f})}{\eta k^4} \tag{3.19}$$

Alternatively, we can apply the operator $\mathbf{1} - \mathbf{kk}/k^2$ to eliminate the pressure from the transformed Stokes equation. Regardless, we are only interested in the velocity field in real space so we Fourier transform back,

$$\mathbf{u}(\mathbf{r}) = \int \mathbf{u}(\mathbf{k})\,e^{i\mathbf{k}\cdot\mathbf{r}}\frac{d\mathbf{k}}{(2\pi)^3} = \int \frac{k^2\mathbf{f} - \mathbf{k}(\mathbf{k}\cdot\mathbf{f})}{\eta k^4}\,e^{i\mathbf{k}\cdot\mathbf{r}}\frac{d\mathbf{k}}{(2\pi)^3}. \tag{3.20}$$

Splitting up the integral in two $\mathbf{u} = \mathbf{u}_1 - \mathbf{u}_2$ and dealing with them one at the time, we take the easy one first

$$\mathbf{u}_1 = \int \frac{\mathbf{f}}{k^2}\, e^{i\mathbf{k}\cdot\mathbf{r}} \frac{d\mathbf{k}}{(2\pi)^3} = \int \frac{\mathbf{f}}{k^2}\, e^{ikr\cos\theta}\, 2\pi k^2 \frac{dk}{(2\pi)^3}\, d(\cos\theta)$$
$$= 2\pi\mathbf{f} \int_0^\infty \frac{e^{ikr} - e^{-ikr}}{ikr} \frac{dk}{(2\pi)^3} = \frac{\mathbf{f}}{4\pi r} \tag{3.21}$$

The second integral,

$$\mathbf{u}_2 = \int \frac{\mathbf{k}(\mathbf{k}\cdot\mathbf{f})}{\eta k^4}\, e^{i\mathbf{k}\cdot\mathbf{r}} \frac{d\mathbf{k}}{(2\pi)^3} \tag{3.22}$$

is evaluated by writing out the components in spherical coordinates with $\mathbf{r}$ pointing in the polar axis direction (z), dropping terms that vanish under azimuthal integration and performing the remaining integrals:

$$u_{2x} = \int_0^\infty \frac{dk}{(2\pi)^3} \int_{-1}^1 d(\cos\theta) \int_0^{2\pi} d\phi f_x \sin^2\theta\, \cos^2\phi\, e^{ikr\cos\theta} \tag{3.23a}$$

$$u_{2y} = \int_0^\infty \frac{dk}{(2\pi)^3} \int_{-1}^1 d(\cos\theta) \int_0^{2\pi} d\phi f_y \sin^2\theta\, \sin^2\phi\, e^{ikr\cos\theta} \tag{3.23b}$$

$$u_{2z} = \int_0^\infty \frac{dk}{(2\pi)^3} \int_{-1}^1 d(\cos\theta) \int_0^{2\pi} d\phi f_z \cos^2\theta \qquad e^{ikr\cos\theta}. \tag{3.23c}$$

The terms that vanish under azimuthal integration are of the forms $\sin\phi$, $\cos\phi$ and $\sin\phi\cos\phi$. The remaining three integrals are one for each of the three (Cartesian) vector components.

The ϕ and θ integrations are trivial whereas the k integral is more involved. The x and the y-components of the velocity are $f_x/8\pi\eta r$ and $f_y/8\pi\eta r$, respectively. The z-component vanishes identically. As we for the integrations chose the z-direction to coincide with the $\mathbf{r}$-vector, we can write this out as

$$\mathbf{u}_2 = \frac{1}{8\pi\eta}\left(\frac{\mathbf{f}}{r} - \frac{(\mathbf{f}\cdot\mathbf{r})\mathbf{r}}{r^3}\right). \tag{3.24}$$

Combining the results of the first integral Eq. (3.21) and the second Eq. (3.24) gives

$$\mathbf{u} = \mathbf{u}_1 - \mathbf{u}_2 = \frac{1}{8\pi\eta}\left(\frac{\mathbf{f}}{r} + \frac{(\mathbf{f}\cdot\mathbf{r})\mathbf{r}}{r^3}\right), \tag{3.25}$$

so that the velocity field due to a point force $\mathbf{f}$ (acting at the origin), in component notation, is

$$u_i(\mathbf{r}) = \frac{f_j}{8\pi\eta}\left(\frac{\delta_{ij}}{r} + \frac{r_i r_j}{r^3}\right). \tag{3.26}$$

The function in the brackets is called the stokeslet and is the Green's function for the flow due to a unit point force at the origin in an extended fluid [42]. The stokeslet is a tensor $\mathcal{S}$ where the (i,j)-component, $\mathcal{S}_{ij}$, is the flow in the direction i due to a unit force in the direction j.

It is remarkable that this kind of interaction falls off only as the inverse bead separation whereas the purely magnetic ones we considered in Sec. 2.2 falls off at least as separation to the power -3. For a given geometry, the two forces cannot be varied independently and, in some sense, they have the same origin both being proportional to the magnetic field squared and depending on the gradient of the magnetic field. The hydrodynamic and the magnetic interactions can thus be meaningfully compared and the longer range hydrodynamic interaction will dominate.

In restricted geometries, in the presence of walls, the Green's function needs to be modified [42]. It is only known explicitly in some particular, simple geometries like near an infinite plane wall. Having a wall means that a boundary condition has to be fulfilled; the no-slip condition. The correct Green's function in this situation must thus vanish by the wall. This is achieved by adding an image force and image flow singularities behind the wall in forming the Green's function.

Pozrikidis [42] gives the expression for the Green's function assuming the presence of a wall at the plane $x = w$,

$$\mathbf{G}^W(\mathbf{r}, \mathbf{r}_\mathrm{o}) = \mathcal{S}(\mathbf{r} - \mathbf{r}_\mathrm{o}) - \mathcal{S}(\mathbf{r} - \mathbf{r}_\mathrm{o}^\mathrm{im}) + 2h^2\mathbf{G}^D(\mathbf{r} - \mathbf{r}_\mathrm{o}^\mathrm{im}) - 2h\mathbf{G}^{SD}(\mathbf{r} - \mathbf{r}_\mathrm{o}^\mathrm{im}). \tag{3.27}$$

The terms require some explanation: We recognize the stokeslet $\mathcal{S}(\mathbf{r} - \mathbf{r}_\mathrm{o})$ at the position of the real point force but now there is also one at the mirror or image position $\mathbf{r}_\mathrm{o}^\mathrm{im} = (2w - x_\mathrm{o}, y_\mathrm{o}, z_\mathrm{o})$. Furthermore, there are two new kinds of sources, $\mathbf{G}^D$ and $\mathbf{G}^{SD}$. They are, respectively, the Green's functions for a source dipole and for a force dipole. Conventionally, the Green's functions are known as the *source doublet* and the *stokeslet doublet* and are given by

$$\mathbf{G}_{ij}^D(\mathbf{r}) = \pm\frac{\partial}{\partial r_j}\left(\frac{r_i}{r^3}\right) = \pm\left(\frac{\delta_{ij}}{r^3} - 3\frac{r_i r_j}{r^5}\right) \tag{3.28}$$

$$\mathbf{G}_{ij}^{SD}(\mathbf{r}) = \pm\frac{\partial \mathcal{S}_{i1}}{\partial r_j} = r_1\mathbf{G}_{ij}^D(\mathbf{r}) \pm \frac{\delta_{j1}r_i - \delta_{i1}r_j}{r^3} \tag{3.29}$$

where the minus signs occur when force is in the 1 or x-direction, i.e. towards the wall; plus sign otherwise. The distance from the point source to the wall is $h = x_\mathrm{o} - w$.

3.2 Simulations

To illustrate the effect of beads moving in the fluid as they are being caught, we turn to computer simulations. In this way, we can bring together the solution of the magnetic problem describing a magnetic bead separator with the fluid flow and hydrodynamic interaction due to bead motion. The flow and magnetostatic problems can be solved by the finite element method and we do this with aid of the Femlab software package [1] that is conveniently integrated with MATLAB computer programming environment [2]. The magnetostatic problem is solved by formulating the problem in terms of the magnetic vector potential with the magnetostatics application mode build into Femlab and the fluid flow problem is solved built-in Navier-Stokes solver application mode.

This will be the approach: First we solve the magnetostatic problem assuming that the influence of the magnetic beads on the total field is negligible. From the solution to the magnetostatic problem forces on beads can be worked out with the expressions found in Chapter 2. Then we solve the Poiseuille problem for the fluid flow. The equations of motion for beads moving under the influence of both the magnetic field and the fluid motion can then be solved. We can then add the influence of the motion of beads on each other, the hydrodynamic interaction, and influence of magnetic interactions.

The viscosity of the fluid is $\eta = 10^{-3}$ kg/m s in the simulations and the bead radius is 5 μm and the bead permeability is $\chi = 1$. The external homogeneous magnetic field that is applied to magnetize the strips of magnetic material has a field strength $\mathbf{H}_{\text{ext}} =$ 40000 A/m.

The concrete geometry we consider, inspired by experiments by Torsten Lund-Olesen (see Ref. [29]), is a two-dimensional slice of a fluid channel in the vicinity of the strips of magnetic material with a permeability of $1000\mu_{\text{o}}$. The channel is 100 μm wide and on either sides are 10 μm wide magnetic strips which are repeated periodically with a distance of 40 μm. The strips are 300 μm long and serve to create a magnetic field gradient in the channel that can catch the beads by focusing an applied magnetic field. Everything else is assumed to have the permeability of vacuum for the purposes of calculating the magnetic field.

The structure is assumed to be tall (perpendicular to the slice) so that the effects of the top and bottom walls can be assumed absent, if it helps picturing one can take the height to be infinite. However, the particles are assumed to be moving in three dimensions and they are taken to be three-dimensional themselves. The fall-off of the forces are different in two and three dimensions as are the Green's functions.

Trajectories for are then calculated for a bead i by solving the ordinary differential equation taking the bead velocity to be

$$\mathbf{v}_i = \mathbf{u}(\mathbf{r}_i) + (6\pi\eta a)^{-1}\mathbf{F}_i^{\text{mag}} \tag{3.30}$$

with $\mathbf{u}(\mathbf{r})$ being the fluid flow velocity at the point $\mathbf{r}$ and $\mathbf{F}_i^{\text{mag}}$ being the total magnetic force there. The fluid flow velocity is found by solving the Stokes equation in the absence of beads and then optionally adding the contributions to the flow from the Green's function for point forces at the positions of each of the other beads and the corresponding bead forces. At all times, the Green's function is chosen so that it takes into account the wall closest to the source bead and the total magnetic force on it is calculated from the external magnetic field with the aid of Eq. (2.21). Magnetic interaction can then be included or left out to study its influence by optionally adding a contribution from Eq. (2.25) to the total magnetic force $\mathbf{F}_{\text{mag}}$.

The simulation of the motion of up to 30 beads is done in a Matlab script that calls a Runge-Kutta-type routine for integrating the ordinary differential equations. The ability to turn on and off the magnetic and hydrodynamic interactions at will allows us to illustrate the relative influence of the two types of interactions.

3.2.1 Two-bead simulations

The effects of hydrodynamic interactions on bead trajectories are easy to illustrate whereas the magnetic ones are so small that they are only apparent when the case of including magnetic interactions are shown together with leaving them out in the same trajectory plot. Therefore we produce two figures; one including hydrodynamic interactions and one excluding them. In either of these two figures, we show the trajectories resulting from both including magnetic interactions and excluding them. This means that we have the results from four simulation runs compared in two figures, Figs. 3.1 and 3.2.

Fig. 3.1 illustrates the influence of hydrodynamic interactions. The figure shows the trajectories of two beads that move up against a fluid flow of 1 mm/s with and without magnetic interaction and under the mutual influence mediated by the fluid. Compare this with Fig. 3.2 where the only difference is that there is no hydrodynamic interaction. In the absence of interaction, the one bead is not caught and is flushed along with the fluid. This is because the hydrodynamic interaction is strong and long-range.

Looking closely at Fig. 3.1, we see that the beads are not caught at the same time but that the bead closer to the magnetic strip A is caught first and that trajectory of the other bead B has a cusp (indicated by a vertical black arrow) once the influence of the other, fast moving bead ceases as it has been caught. After the cusp, bead B moves much more slowly until getting close to the magnetic strip and being caught.

In contrast, the magnetic interaction gives almost indistinguishable pairs of trajectories as seen from both Fig. 3.1 and from Fig. 3.2. This supports our earlier observation based on the power to which the bead separation is raised in the expressions for the interactions: hydrodynamic interactions dominate the magnetic ones.

3.2.2 Few-bead simulations

What Figs. 3.1 and 3.2 tell us is that it can make a qualitative difference whether hydrodynamic interactions are included or not, however, this was on the basis of one illustrative but particular set of initial conditions for just two magnetic beads. In order to make a more persuasive argument, we will instead look at a number of randomly chosen initial positions of an increasing number of beads. If hydrodynamic interactions help bead capturing, then we will expect this effect to become more pronounced the more beads there are. We can quantify the influence of interactions by looking at the time it takes for all the beads to get caught in the presence of hydrodynamic interactions τ_{incl} and comparing it to the time it takes when we leave out the hydrodynamic interactions from the simulations τ_{excl}. The ratio of these $\tau_{\text{incl}}/\tau_{\text{excl}}$ is then taken as a measure of the importance of interactions in capturing. The simulations are performed with from one to thirty beads at a time and repeated for each number of beads twelve times with different initial positions. The results are shown in Fig. 3.3.

The results in Fig. 3.3 make a good case for the importance of hydrodynamic interactions. The relative speed-up increases with the number of beads as expected though no clear relation between bead number and speed-up can be readily identified. In the figure, a best fit linear relation has been added to help guide the eye. In a few of the non-interacting

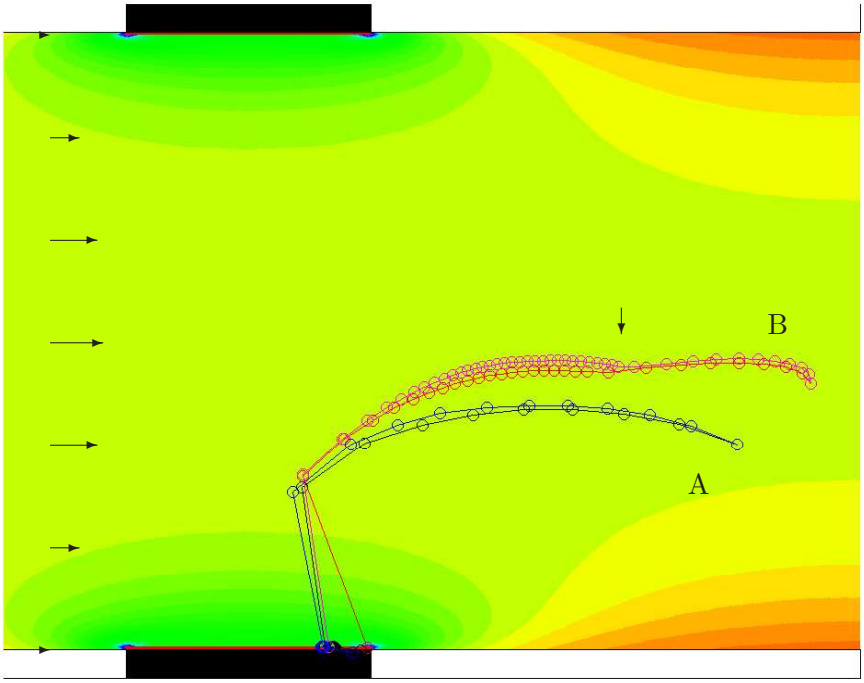

Figure 3.1: Motion of two beads, A and B (lines with open circles), under the influence of a magnetic field gradient (colour scale) and against a rightward-moving fluid flow (black horizontal arrows) in the presence of hydrodynamic interactions. The trajectories of the two beads are shown both in the cases of including and excluding magnetic interactions between the beads: the red and black tracks include magnetic interactions; the magenta and blue tracks exclude magnetic interactions. The parts of the strips of magnetic material nearest to the channel are indicated by black rectangles and the channel walls and non-magnetic surroundings by white. The beads are both caught as they drag fluid along, in turn dragging each other, so both beads are caught. The influence of magnetic interactions is so small that the trajectories are almost indistinguishable in the two cases. The figure covers an area 35 μm wide and 110 μm high. The maximum flow velocity is 1 mm/s.

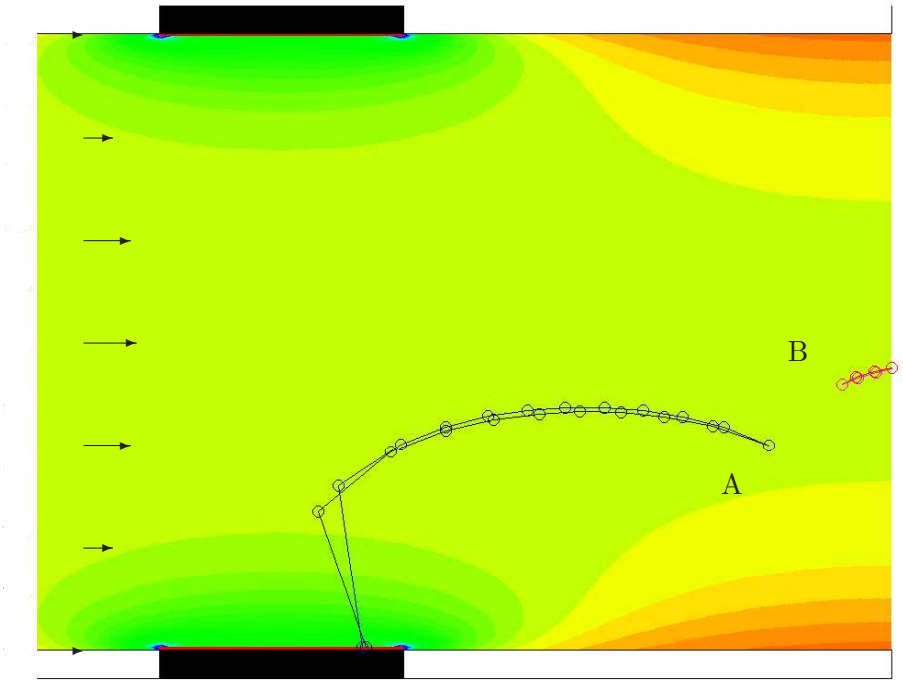

Figure 3.2: Same simulation as Fig. 3.1 but *without* including hydrodynamic interactions. Bead B is not caught as the local magnetic field gradient is small near the centre and because the fluid counter flow is too strong. In Fig. 3.1, the beads were caught because of the hydrodynamic interactions so when the interactions are turned off they do not help each other moving collectively and this leads to the qualitatively different result that Bead B escapes. There is little difference whether magnetic interactions are included (red and black tracks) or excluded (magenta and blue tracks).

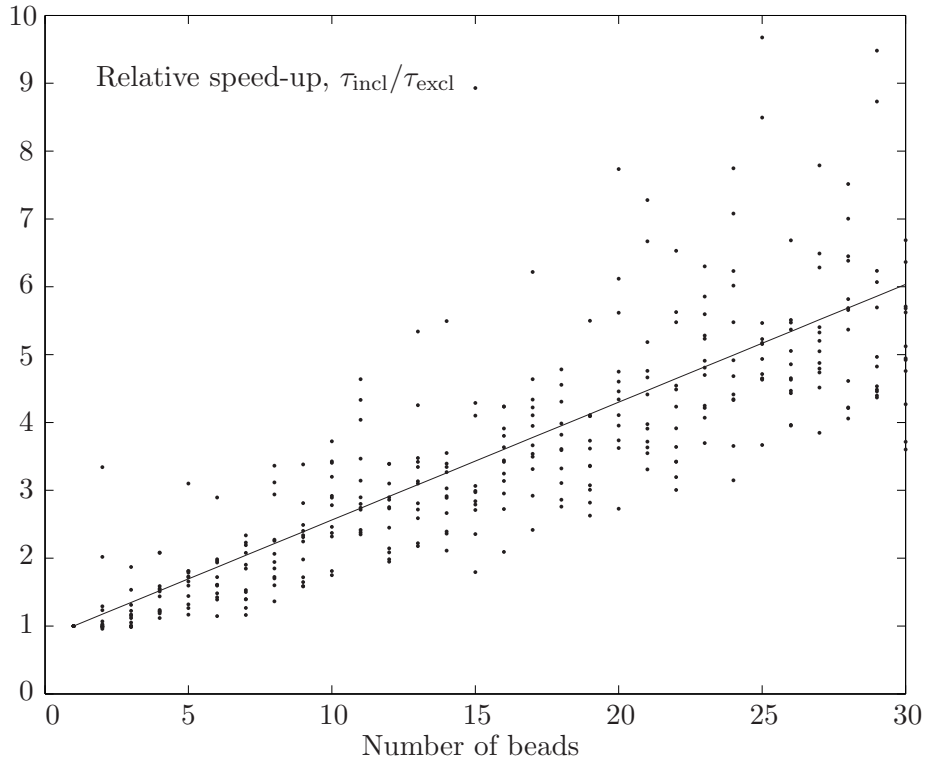

Figure 3.3: The speed-up $\tau_{\rm incl}/\tau_{\rm excl}$ resulting from including hydrodynamic interactions relative to leaving them out as function of the number of beads present in the simulation. For each number of beads, twelve simulations with randomly chosen initial bead positions are shown. The more beads present the larger speed-up. The line shown is a linear fit to guide the eye.

cases, not all of the beads were caught effectively making the relative speed-up infinite. These have been left out.

3.3 Discussion

We have found that beads moving in viscous fluid under an external force, such as one from an external magnetic field, transfer momentum to the fluid making them move differently. This can be interpreted as a hydrodynamic interaction between the beads.

Hydrodynamic interactions can be modeled simply by means of Green's functions for the Stokes' equations. The form of the stokeslet and the dependence on separation shows that it dominates over the magnetic interaction at large bead separations.

This is a long range interaction falling off as separation to the power -1 and can significantly affect the capturing of beads and in some cases even lead to qualitatively different results. The influence increases with larger numbers of beads simultaneously present leading to an effective speed-up that grows with bead number.

This means that taking into account hydrodynamic interactions is essential if we are to understand quantitatively the behaviour of devices relying on manipulation and in particular capturing of magnetic beads. Influence of hydrodynamic interactions also casts some doubt on quantitative measurements of the magnetic susceptibility of, for example, cells that rely on capturing or trajectories of moving cells unless the experiments are controlled for the concentration.

The approach taken above relies on the description of the fluid perturbation by means of Green's functions, however, this can be problematic as the beads can move quite rapidly during their capture. This means that the Stokesian approximation of vanishing Reynolds numbers might fail. The walls are also only approximately taken into account so it could be enlightening to have a complementary way to account for hydrodynamic interactions.

Chapter 4

Motion of many beads

In the preceeding chapter we found that the presence of more than one magnetic bead moving under forces due to an external field qualitatively changes bead capturing behaviour in certain situations. The interactions were taken into account on an almost bead-by-bead basis and so was the presence of walls. We found that magnetic interactions will generally be negligible so they will not be included. In this chapter, we try to take a step closer to the conditions in actual experiment with an approach complementary to the few bead view. We describe the beads not individually but on a larger scale where they appear as a continuum and can be described by a distribution. The aim is to investigate whether hydrodynamic interactions influence capturing by studying concentration dependency and artificially disregarding interactions.

4.1 Introduction

In the few bead approach we take into account the effect of the motion of the beads on the surrounding fluid by means of Green's functions that modify the flow. In the present continuum approach, we will incorporate the effect with a separate term in the Navier-Stokes equation and add a separate bead distribution or concentration field. In this way, we can make sure that the boundary conditions are properly fulfilled at all times and that we can, in principle, account for a non-zero Reynolds number but this happens at the expense of leaving the full solution of a coupled flow and advection problem to the finite element method solver.

Using the continuum model, we can study aspects of the capturing process for a variety of flow conditions and magnetic field strengths. Both the time evolution of capturing and the resulting stationary states can be studied though in the following we will look exclusively at the latter.

4.2 The physical problem

The separation of magnetic beads from the dispersion involves an interplay between forces of several kinds deciding the dynamics of the process: (a) Magnetic forces stemming from

the application of a strong magnetic field and strong magnetic field gradients. (b) Drag forces due to the motion of the beads with respect to the immediately surrounding fluid. (c) Gravity, as typically the beads are denser than the fluid so they settle under the action of gravity by themselves; a point we will ignore in the following.

Of particular interest is the effect of drag forces as these do two things. First, they transfer momentum from beads moving under the influence of external forces to the fluid. Second, they create an effective interaction between the beads. The external forces on a bead make it move relative to the surrounding fluid. This gives rise to a drag and a transfer of momentum to the fluid as mentioned and thus fluid motion. The extra fluid motion will change the fluid velocity around other beads and thus the drag on them. This gives rise to an effective interaction.

A significant simplification is afforded by the fact that for the magnetic beads typically employed inertial effects are completely unimportant: Except for acceleration phases much shorter than microseconds the external forces are exactly balanced by drag forces and the beads move with constant velocity, cf. Eq. (3.4).

We consider a flat microchannel as a full three-dimensional model is computationally expensive. This two-dimensional model we imagine as a slice of a channel that is translationally invariant in the one direction with a source of a magnetic field that serves to capture magnetic beads that are being carried past by a fluid flow.

4.3 Continuum model

We consider the distribution of a large number of identical spherical beads of radius a taken to be 1μm dispersed in a fluid of viscosity η equal to that of water $\eta = 10^{-3}$ kg m^{-1}s^{-1}. The concentration we denote by c and define as the number of beads per unit volume. The model consists of three parts coupled together: a flow problem, a bead advection problem and a magnetic force problem.

The geometry we consider, sketched in Fig. 4.1, consists of two plane, parallel, infinite walls at $z = 0$ and $z = h$ between which the fluid flows from left to right, i.e. in the positive x-direction. In the simulations, we set the height $h = 50$ μm and simulate a section 350 μm long. The system is assumed translationally invariant in the y-direction, effectively reducing the problem to a two-dimensional one. Perpendicularly to the xz-plane, in the y-direction, near $(x, z) = (250\ \mu\text{m}, 55\ \mu\text{m})$ is a pair of straight parallel wires with equal and oppositely directed currents which generate the magnetic field that attracts and collects some fraction of the beads advected with the fluid.

4.3.1 Fluid flow

The beads are dispersed in the fluid which is launched with a parabolic velocity profile past a magnetic field gradient that serves to retain them. The magnetic field acts with a force on the magnetic beads and this transfers momentum to the fluid, hence changes the flow. As we are going to use numerical methods anyway we can describe fluid flow

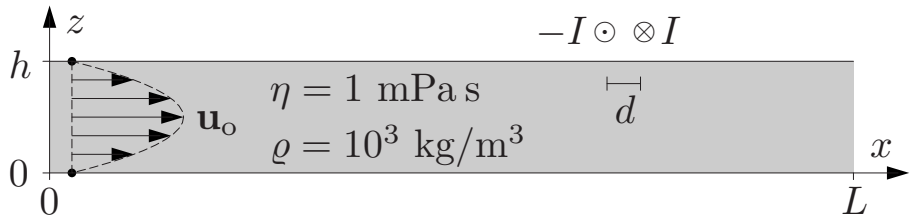

Figure 4.1: Sketch of the microfluidic system with $L = 350$ μm and $h = 50$ μm. A dispersion of paramagnetic beads enters at $x = 0$ with a parabolic Poiseuille flow profile, $\mathbf{u}_o$, and leaves at $x = L$. Beads are caught by the pair of wires placed 100 μm from the outlet at the top and carrying currents $\pm I$.

velocity $\mathbf{u}$ by the full Navier-Stokes equation,

$$\varrho \frac{\partial \mathbf{u}}{\partial t} + \varrho(\mathbf{u} \cdot \boldsymbol{\nabla})\mathbf{u} = -\boldsymbol{\nabla} p + \eta \nabla^2 \mathbf{u} + c\mathbf{F}_{\text{ext}}(\mathbf{r}) \tag{4.1}$$

where the momentum transfer from beads to fluid is included by setting the bulk force term $\mathbf{F}_{\text{Vol}} = c\mathbf{F}_{\text{ext}}(\mathbf{r})$ in Eq. (3.8). This bulk force term is proportional to the number density of beads and the magnetic (external) force on an individual bead at position $\mathbf{r}$. This term is crucial in the model in that it connects flow with bead distribution and magnetic field.

The flow is at all times assumed incompressible as we have done elsewhere so $\boldsymbol{\nabla} \cdot \mathbf{u} = 0$ as well. These equations are implemented in an application mode in Femlab which.

4.3.2 Bead motion

Beads move both due to advection and due to the applied magnetic field so it is necessary to describe the motion of beads as well, that is, an equation of motion for the bead number density. As the beads neither appear, nor disappear in the bulk the density must obey a continuity equation

$$\frac{\partial c}{\partial t} + \boldsymbol{\nabla} \cdot \mathbf{j} = 0. \tag{4.2}$$

for some bead current $\mathbf{j}$ to be defined.

As model for the bead current we have used the Nernst-Planck-type expression [43]

$$\mathbf{j} = -D\boldsymbol{\nabla} c + c\mathbf{u} + cb\mathbf{F}_{\text{ext}}, \tag{4.3}$$

which contains contributions from diffusion, advection and magnetic attraction of beads. The contribution from diffusion is proportionl to the diffusion constant D and the bead migration due to the external magnetic force is proportional to the bead Stokes' law mobility $b = (6\pi\eta a)^{-1}$.

For a spherical particle of radius a the diffusion constant is given by the Einstein expression

$$D = \frac{k_B T}{6\pi\eta a} \tag{4.4}$$

which equals 2.2×10^{-13} m^2/s for a bead of radius 1 μm at room temperature. This is small compared to other dimension entering the problem in the following sense. The time-scale for a bead to diffuse across the height h of the channel is $\tau_{\text{diff}} \sim h^2/D$ which we can compare with the timescale for advection over a similar distance $\tau_{\text{adv}} \sim h/u_{\text{o}}$. From these time-scales we form a dimensionless quantity, the Péclet number, hu/D as the ratio $\tau_{\text{diff}}/\tau_{\text{adv}}$. A Péclet number larger than unity indicates that advection dominates over diffusion. Alternatively, we could form a similar number from the bead mobility and the external force. In the simulations below we, however, artifically increase the magnitude of the diffusion constant in order to stabilize the computations so that we can use a coarser mesh and thus save computation time. Later, we will investigate this assumption and find that it is permissible.

4.3.3 Magnetic force

The magnetic beads are taken to be superparamagnetic with constant magnetic susceptibility χ of unity. In an external field $\mathbf{H}_{\text{ext}}(\mathbf{r})$ the force on such a bead is given by Eq. (2.21) assuming that the bead is sufficiently small so that we can take the external field $\mathbf{H}_{\text{ext}}$ to be approximately constant over a bead radius, i.e. $a|\boldsymbol{\nabla}\mathbf{H}_{\text{ext}}| \ll |\mathbf{H}_{\text{ext}}|$ when determining the magnetization $\mathbf{M}$.

As source for the magnetic field we imagine a pair of long thin wires held together closely with equal and opposite currents. The wires, and thus currents, go perpendicularly through the plane of the simulation domain creating a magnetic field that is translationally invariant. This field was chosen in order to have a definite model in mind that respects the translational symmetry of the problem at the same time as having a not-too-slow decay of the magnetic field. If we were to perform a full three-dimensional calculation we could choose a compact current distribution, a flat circular current loop, that would yield a dipole field at large distances r, i.e. an $1/r^3$-dependence and a $1/r^7$-force law but at close range a linear force law. The field resulting from the configuration of two parallel wires can be found in the following manner:

From Ampère's law, we readily find the magnetic field, $\mathbf{H}$, around a straight circular wire by integration along a circular path. In this way we find,

$$\mathbf{H}(\mathbf{r}) = \frac{\mathbf{J} \times \mathbf{r}}{2\pi r^2} \tag{4.5}$$

where the electrical current vector, $\mathbf{J}$, is along the wire, orthogonal to the position vector $\mathbf{r}$ which we can take to be in the plane of the simulation domain.

The magnetic field $\mathbf{H}_{\uparrow\downarrow}$ resulting from two anti-parallel wires close together is found by imagining them separated by $\mathbf{d}$ in the xz-plane, and then decreasing the separation, d, as the total current, $I = |\mathbf{J}|$ is increased keeping the product of separation distance and current constant. Formally, this is the same as performing a differentiation along the $\mathbf{d}$-direction leaving

$$\mathbf{H}_{\uparrow\downarrow} = \frac{1}{2\pi r^2}\left(\mathbf{J} \times \mathbf{d} - \frac{2(\mathbf{J} \times \mathbf{r})(\mathbf{d} \cdot \mathbf{r})}{r^2}\right). \tag{4.6}$$

From this, we find with Eq. (2.19), the total magnetic force on a spherical bead in the vicinity of the wire pair

$$\mathbf{F}_{\text{ext}} = -\frac{2}{\pi}\frac{\chi}{\chi+3}\mu_{\text{o}}a^3(I\,d)^2\,\frac{\mathbf{r}}{r^6}; \tag{4.7}$$

a manifestly attractive central force, independent of the direction of $\mathbf{d}$. The fact that the angular dependence drops out is in some sense fortuitous and restricted to the $1/r^2$ field dependence.

4.3.4 Boundary conditions

Finally, boundary conditions for the flow and bead motion need to be specified. For the flow this is simple as we take the velocity at the inlet, $x = 0$ to be a parabola across the inlet with a maximum flow speed of $4u_{\text{o}}$ and an average flow speed of u_{o}

$$\mathbf{u}(0, y, z) = 4u_{\text{o}}\,\hat{\mathbf{x}}\,z(h - z) \quad \text{for} \quad 0 \leq z \leq h \tag{4.8}$$

directed into the channel in the x-direction, i.e. in the direction of the unit vector $\hat{\mathbf{x}}$. At the outlet, we demand that the fluid velocity in directed straight out, parallel to $\hat{\mathbf{x}}$, but is otherwise free to take on any value. At the walls, we assume no-slip.

The evolution of the bead concentration is governed by Eq. (4.2). In addition to the bulk equations, we need appropriate boundary conditions but these are somewhat involved. First, we consider the situation at the walls. We are interested in allowing the beads to move out to the walls and settle there so merely demanding that the normal components of the bead current vector $\mathbf{j}$ vanishes is not correct, rather, we need to let the bead current be free to take on any value as long as the current component normal to the channel wall is directed into the wall. However, as we do not wish beads to enter the bulk from a wall, they stick in a sense, we demand that the normal current projection vanishes if the force projection is directed out of a wall. Symbolically, the boundary condition at a wall with $\mathbf{n}$ as the outward normal seen from the channel can be written

$$\mathbf{c}\cdot\mathbf{j} = \mathbf{n}\cdot(-D\boldsymbol{\nabla}c + c\mathbf{u} + cb\mathbf{F}_{\text{ext}}) \tag{4.9}$$

$$= bc\,(\mathbf{n}\cdot\mathbf{F}_{\text{ext}})\,\Theta(\mathbf{n}\cdot\mathbf{F}_{\text{ext}}) \tag{4.10}$$

with the function $\Theta(x)$ being the Heaviside function that is 0 for $x < 0$ and 1 for $x > 0$. The second equality holds because the fluid velocity vanishes at the wall and that we do not permit beads to diffuse in and out of the walls.

The two openings of the channel section, the inlet and the outlet, need special consideration when it comes to the boundary conditions. The boundary conditions specifying normal bead currents are Neumann ones but at the inlet we instead only assume that the fluid comes in with the constant initial number density c_0. At the outlet, we let the bead current take on any value, however, the situation is slightly different from that at the walls. There we assume that there is no fluid flowing into the wall (essentially the meaning of having a wall, regardless of assumptions of no-slip or not) whereas the outlet manifestly permits outflow. We can formulate the boundary conditions to be the same but the meaning is slightly different as the current has a contribution from advection at the outlet but not at the walls.

4.3.5 Simulations

The model is implemented as a Matlab script using Femlab as finite element solver. The fluid flow and the Navier-Stokes equation are implemented through a Femlab application mode as is the bead motion. Matlab code implements the magnetic problem and joins together the individual parts of the model.

The primary control parameters are the current through the pair of wires times the wire separation $I\,d$, the fluid in-flow velocity $\mathbf{u}_\mathrm{o}$, and the initial bead number density c_o. The wire current-distance product ultimately decides the magnetic force on the beads which is needed to balance the fluid flow that carries the beads past the capturing area. As we are investigating the effects from hydrodynamically mediated bead interaction, what we are really after are properties that depend on the bead number density, in particular those that do so nonlinearly.

The simulation domain is meshed into approximately 3500 triangles with extra refinement in the vicinity of the wires. The size of the mesh is a trade-off between computational time and, resolution and stability. When diffusion dominates over advection on the scale of a mesh element then simulations are stable. This means that a finer mesh leads to stability. In the region near the wires the force on beads becomes large which can lead to numerical instabilities which we partly alleviate by refining locally. At the highest initial concentrations and largest values of $I\,d$, it can be difficult to get the simulations to work at all. This can be seen in some of the results shown in the following where numerical artefacts appear.

We choose initial concentrations c_o in the range 10^{13} m^{-3} to 10^{16} m^{-3} which are comparable to those of commercially available concentrated magnetic bead dispersions and the diluted samples used in experiments [46]. This corresponds to concentrations of $10^7 - 10^{10}$ beads per millilitre. We can take $c_\mathrm{o}^{-1/3}$ as a characteristic interbead distance which corresponds to approximately 4.6 μm for the highest concentrations which is comparable to the 1 μm radius. At the lowest concentrations, we can estimate the number of particles in a volume of the typical length scale entering into the problem h to be $c_\mathrm{o}h^3 = 1.25$. The range of concentrations should thus cover a reasonable range of values from the beads being quite close together to only a few beads in the channel at a time. The average speed at the inlet u_o we take to be in the range of a few hundred μm/s, typically 300 μm/s, which is realistic albeit somewhat slow but the small value promotes numerical stability in the simulations.

4.4 Results

4.4.1 Qualitative picture

The simplest results we obtain are the steady state distributions of beads in the microchannel. The currents in the wires create the magnetic field that scoops out beads as illustrated for three values of wire current distance product $I\,d$ and a comparatively low concentration in Fig. 4.2(b)–(d). A sketch of the geometry, Fig. 4.2(a), has been duplicated in the figure for reference. For small currents only a thin region is emptied but increasing the current

makes the region expand until it covers the whole width of the channel. The force on the beads makes them migrate away from the opposing wall, creating an empty region there as well.

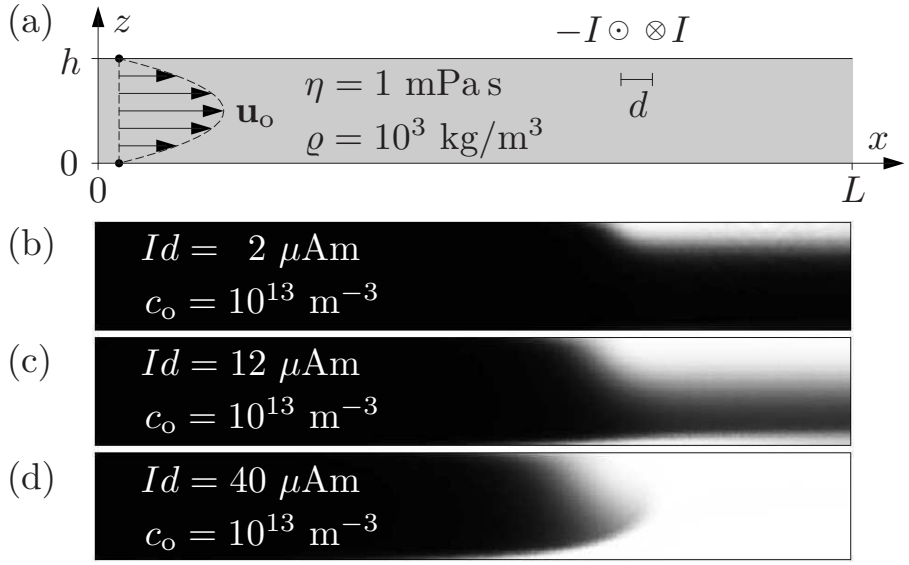

Figure 4.2: (a) Sketch of the microfluidic system with $L = 350$ μm and $h = 50$ μm. A dispersion of paramagnetic beads enters at $x = 0$ with a parabolic Poiseuille flow profile, $\mathbf{u}_o$, and leaves at $x = L$. Beads are caught by the pair of wires placed 100 μm from the outlet at the top and carrying currents $\pm I$. (b)–(d) Simulated stationary density of the beads ranging from zero (white) to c_o (black) for increasing values of the current-distance product Id as indicated. At $x = 0$ the concentration is $c_o = 10^{13}$ m^{-3} and the maximum flow speed is 300 μm/s.

The magnetic field dragging magnetic beads affects the flow of fluid and sets up a small vortex superimposed on the parabolic velocity profile where the fluid moves upstream (to the left) by the wall opposite the wires and faster downstream (to the right) by the wall close to the wires. If we subtract the parabolic flow from the velocity pattern calculated in simulation we can see how this vortex works. The vortex flushes beads close past the wires thus helping the capture. We interpret this as a consequence of hydrodynamic interactions where the motion of the beads influences fluid flow and in turn bead motion.

At the upper wall, we find that the beads settle right by the wires near $x = 250$ μm. This can be seen in Fig. 4.4 where the normal projection of the bead current vector has been plotted as function of position along the upper wall, by the wires.

Another sign of influence of hydrodynamic interactions is dependence on initial concentration. If there are many beads, i.e. a high concentrations, they will move collectively and the results from simulations will be different from the case of few beads and low concentrations. In Fig. 4.5 we duplicate the conditions from Fig. 4.2 but at a high initial concentration c_o. Qualitatively, the picture looks the same; concentrated fluid enters from the left and some of the beads have been caught leaving diluted fluid to exit at the

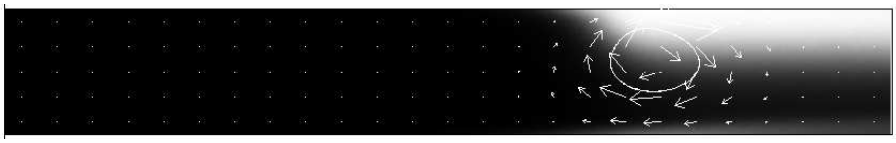

Figure 4.3: The flow roll set up in capturing of magnetic beads. The arrows show the difference between the fluid velocity and unperturbed Poiseuille flow setting up the indicated vortex. The grey scale indicates the concentration of beads. The initial concentration is 10^{13} m^{-3} and the maximum flow speed is 100 μm/s.

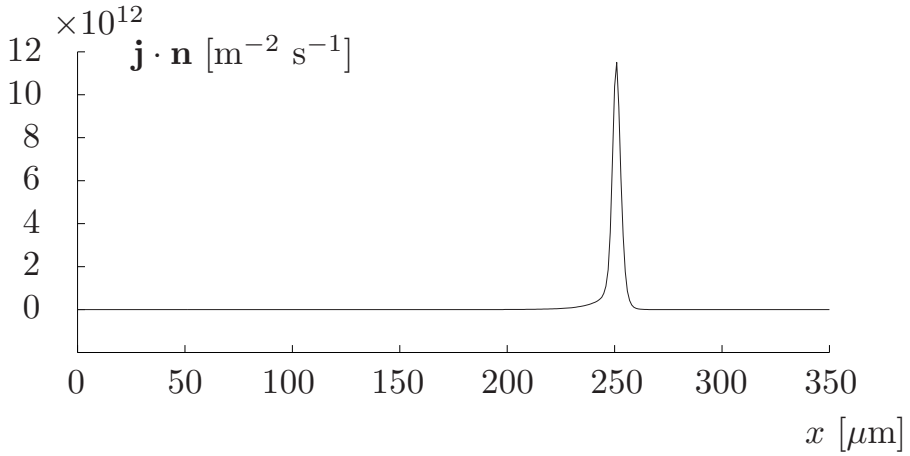

Figure 4.4: The normal projection of the bead current $\mathbf{j} \cdot \mathbf{n}$ along the wall close to the wires. This shows the settling rate per unit area as function of position. The beads settle at the edge with a rate that is strongly peaked about the position of the wires $x = 250$ μm.

right. However, the details of the pictures are different. The emptied regions are slightly larger and the bead concentration patterns are slightly different with a tendency of the bead stream to wiggle at intermediate currents and a different bead concentration profile due to a strong vortex at high currents. Seemingly, hydrodynamic interactions have some influence that should be quantified.

4.4.2 Quantitative measures

To quantify the effectiveness of capturing, we need to keep track of which beads are captured and of which are flushed through the channel. We keep tally by integrating the outward normal component of the bead currents along each segment i of the domain boundary,

$$\gamma_i = \int_i \mathbf{j} \cdot \mathbf{n} \, d\ell. \tag{4.11}$$

The rate of beads being captured is defined as the sum of the rates for each of the walls, $\gamma_{\text{cap}} = \gamma_{\text{lower}} + \gamma_{\text{upper}}$. In any stationary state the bead flux in and out of the domain

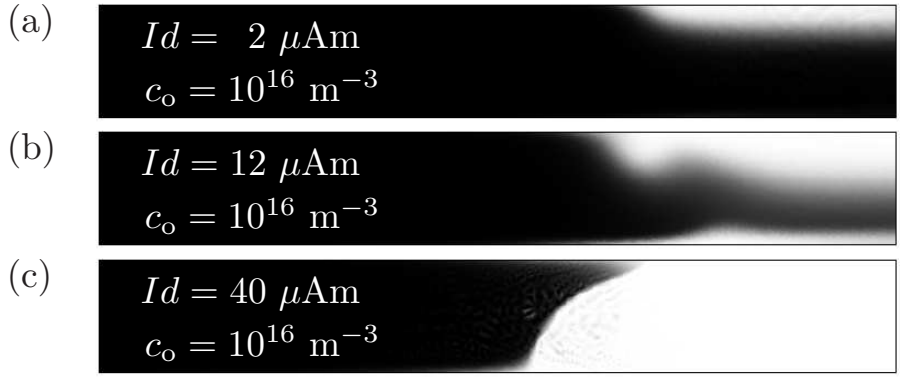

Figure 4.5: (a)–(c) Simulated stationary density of the beads ranging from zero (white) to c_o (black) for increasing values of the current-distance product Id as indicated. The inlet concentration is $c_o = 10^{16}$ m^{-3} and the maximum flow speed is 300 μm/s. Notice that though qualitatively similar to Fig. 4.2 the distribution patterns are different and somewhat more complicated; notice the wiggling in (b). This is attributed to the interactions present at higher concentrations.

counted with sign must equal zero,

$$\gamma_{\text{cap}} + \gamma_{\text{inlet}} + \gamma_{\text{outlet}} = 0, \tag{4.12}$$

as there cannot be any accumulation of beads. This provides a useful check.

There is a competition between beads being carried along by the flow and being caught by the magnetic field. A simple measure of the capturing is the ratio of bead capture rate to bead in-flow rate,

$$\beta = \frac{\text{“capture rate”}}{\text{“in-flow rate”}} = \frac{\gamma_{\text{cap}}}{\gamma_{\text{inlet}}} \tag{4.13}$$

If capturing dominates then this fraction tends to 1, if flushing dominates it tends to 0. Fig. 4.6 shows this in that slow flow and strong current leads to a high capturing fraction whereas fast flow and weak current leads to a small fraction of beads caught. The actual rate of beads caught as function of wire current and flow velocity is shown in the inset in Fig. 4.6. Clearly, in the limit of strong current and high magnetic field almost all beads are caught so that the rate of beads caught tends to the rate of beads carried in.

If there is a competition between magnetic capturing and flushing, then we would expect that the data could be described essentially by the ratio of the magnetic forces to the fluid flow speed which is proportional to the square of the current-distance product divided by the fluid flow speed. In Fig. 4.7, we plot the data from Fig. 4.6 as function of this combined parameter and we see that the data mostly collapse to one curve. This collapse is not perfect and is not expected to be as the underlying flow and bead distribution patterns are different for the various flow and magnetic field configurations as we saw from Figures 4.2 and 4.5. The pattern is repeated at the higher initial concentration in Fig. 4.8, however, the results are marred by numerical artefacts that makes them much less convincing.

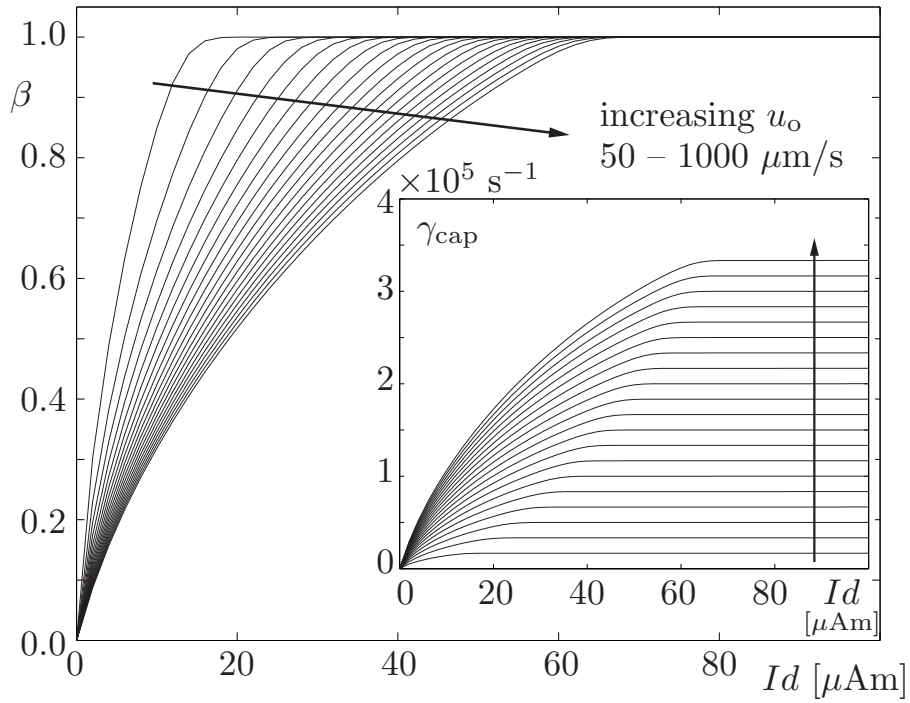

Figure 4.6: The fraction β of beads caught as function of the current-distance product Id for twenty different flow speeds (50 – 1000 μm/s; indicated by the arrows). Larger current leads to higher β; faster flow to smaller β. In this simulation the initial concentration is low, $c_o = 10^{13}$ m^{-3}. *Inset:* Rate γ_{cap} of bead capture as function of Id, for the flows above. The faster flow or the larger current, the higher γ_{cap}.

4.4.3 Concentration dependence

Simulation permits the separation of otherwise intertwined effects. Here we can study the effect of the external force on the beads acting back on the fluid flow. This is an effective interaction between beads as described in section 4.2. At low bead densities and in the absence of the bulk force term in the Navier-Stokes equation we expect that the beads move as if they were alone. At higher bead number densities the force acting on the beads contributes a significant force on the fluid affecting fluid flow and giving rise to the mentioned effective hydrodynamic interaction. The strength of this interaction must thus depend on the density of particles. In Fig. 4.9 this is illustrated; capturing was simulated at fixed in-flow speed $u_o = 300$ μm/s and a fixed value of the current-wire distance product $I\,d = 8$ μAm but for a range of bead number densities. At low densities we find that capturing is roughly independent of density and the fraction of beads captured, β, has some intermediate value whereas for high densities all beads are caught. This we interpret as evidence of hydrodynamic interactions that assist in capturing. In comparison, leaving out the bulk force term $c\mathbf{F}_{ext}$ in the Navier-Stokes equation, i.e. the force acting on the fluid, gives concentration *in*dependence as illustrated. We clearly see that the coupling

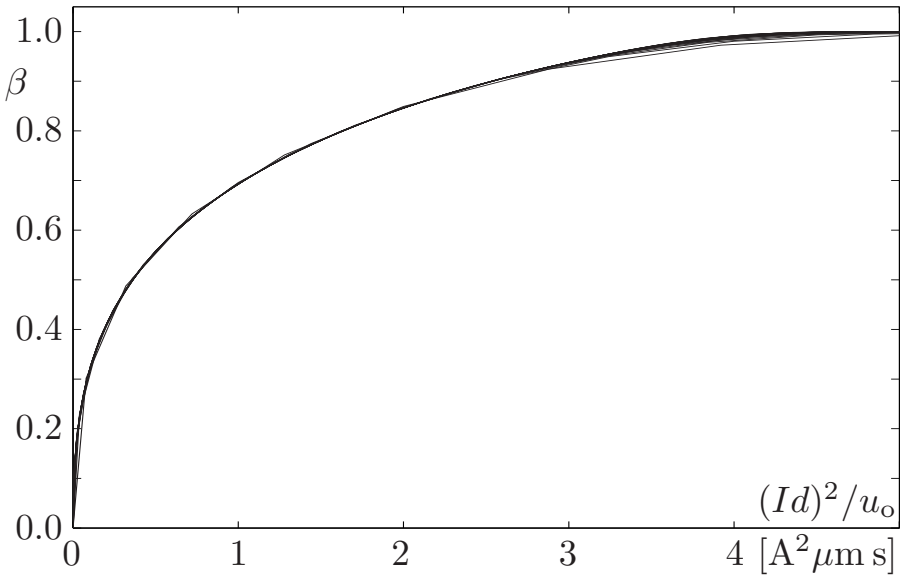

Figure 4.7: The fraction β of beads caught versus $(Id)^2/u_\mathrm{o}$, the ratio of the current-distance product squared and the fluid flow velocity. This demonstrates scaling in the competition between capturing and flushing: the twenty curves from Fig. 4.6 approximately collapse to one single.

from the external force acting on the beads to the fluid changes the behaviour and helps capturing.

At very strong applied fields, corresponding to large values of $I\,d$, we expect all beads to be captured regardless of interactions and independently of concentration. Similarly, for weak fields and small values of the current-distance product $I\,d$ almost no beads will be caught regardless of the presence or absence of beads. However, at intermediate currents and fields we expect a significant effect and benefit from hydrodynamic interactions.

Defining β_incl as the fraction of beads caught when the force term $c\mathbf{F}_\mathrm{ext}$ is included in the Navier-Stokes equation, Eq. (4.1), and β_excl when this term is left out, we calculate the difference in the two fractions,

$$\Delta\beta = \beta_\mathrm{incl} - \beta_\mathrm{excl}. \tag{4.14}$$

If our prediction is correct, we expect $\Delta\beta$ to be independent of current for small concentrations but to peak at some positive value for intermediate currents at high concentrations. Fig. 4.10 shows that this is also the case. At high concentrations, interactions mean an increase in the fraction of beads captured of more than fifty per cent of the beads *flowing into the channel*. This is important as one can ease requirements on magnetic fields in devices by going to higher concentrations of beads where interactions matter more.

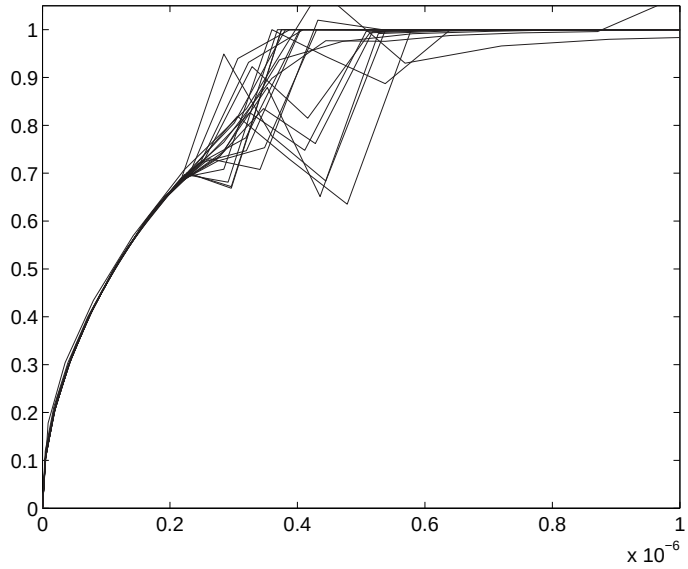

Figure 4.8: The fraction β of beads caught versus $(Id)^2/u_o$, the ratio of the current-distance product squared and the fluid flow velocity as in Fig. 4.7 but for an initial concentration of $c_o = 10^{16}$ m^{-3} instead of $c_o = 10^{13}$ m^{-3}. This indicates the competition between capturing and flushing where twenty curves of β as function of $I\,d$ approximately collapse to one, however, problems of numerical instability related to a too coarse mesh and large mesh Péclet numbers partially precludes confirmation of the collapse. Notice that the common curve appears shifted to the left by a factor of five compared to Fig. 4.7.

4.4.4 Influence of diffusion constant

As mentioned above, it has been necessary to increase the diffusion constant to stabilize simulations and aid convergence. It has been done on a simulation by simulation basis in order to keep it as close to the correct value given by Eq. (4.4) as possible. Mostly, the value has been kept at $D = 2 \times 10^{-12}$ m^2/s but occasionally for high initial concentrations and high $I\,d$ it has been as high as $D = 5 \times 10^{-11}$ m^2/s.

This artificial use of the diffusion constant makes it necessary to investigate more closely the influence of the magnitude of the diffusion constant on the results obtained. This is illustrated in Fig. 4.11 where our main variable of interest, the fraction of beads caught β, is shown as function of the diffusion constant D for four values of the initial number density (10^{13} m^{-3}, 10^{14} m^{-3}, 10^{15} m^{-3}, and 10^{16} m^{-3}). We see that β is relatively independent of the diffusion constant for values up to about 10^{-10} m^2/s where diffusion starts to influence results significantly. Inspecting bead distribution similar to Fig. 4.2 and Fig. 4.5 for different values of the diffusion constant also shows a transition to diffusion dominated behaviour at values around 10^{-10} m^2/s.

Alternatively, we can compare with the Péclet number that reaches unity at a diffusion constant of 1.5×10^{-8} m^2/s which roughly corresponds to the point in Fig. 4.11 where the curves for the four different concentrations coalesce. The maximum value of the diffusion

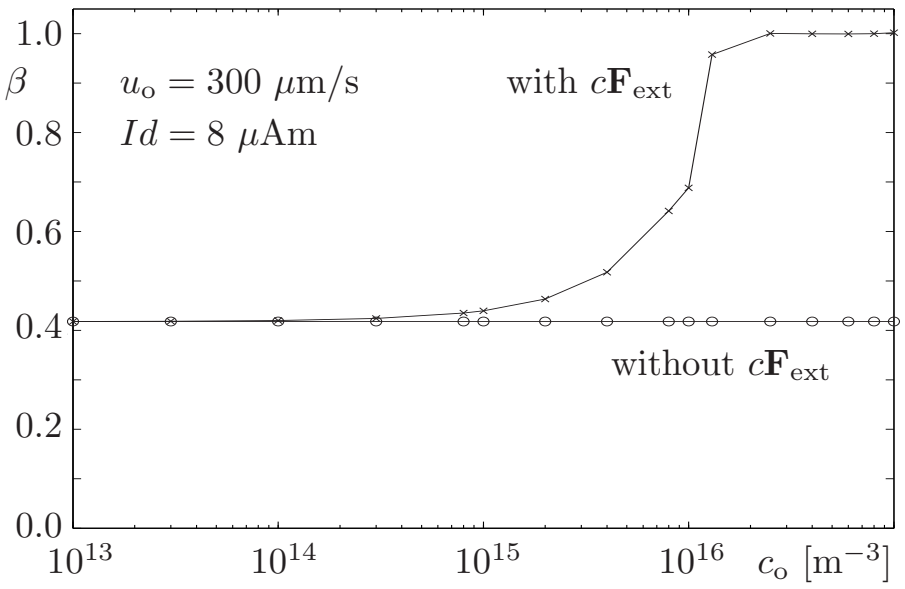

Figure 4.9: Fraction β of beads caught as function of initial bead number density with and without the bulk force term $c\mathbf{F}_{\text{ext}}$ in Eq. (3.8). The fixed values for the current-distance product Id and the maximum in-flow speed u_o are shown. At low densities less than 50% are caught; at high densities the collective motion of the beads leads to 100% capture.

constant $D = 10^{-10}$ m^2/s corresponds to a Péclet number of $hu_o/D = 150$ which is in the advection dominated regime.

4.4.5 Other force laws

The model of the force law that we have employed so far is special in that it is very short range and one might imagine that this helps in setting up the vortex that flushes beads into the attracting region because the force predominantly acts in the one side leaving the necessary counterflow at the other side of the channel undisturbed. If we then imagine a force law that depends on distance to the power -3 instead of -5,

$$\mathbf{F}_{\text{ext}} = -K\frac{\mathbf{r}}{r^4}, \tag{4.15}$$

the counterflow will be affected somewhat more. At the same time, capturing of beads would become somewhat more effective overall as a larger part of the channel and thus more of the beads will be affected by the attractive force. The expected net result is a reduced influence of hydrodynamic interactions on capturing and a smaller concentration dependence on the presence or absence of the bulk force term.

This effect is illustrated on Fig. 4.12 which duplicates Fig. 4.10 but with this changed force law. The vertical axis is comparable between the two figures and we see that the effect of interactions is less dramatic but still visible. Note, however, that the first axes are not comparable.

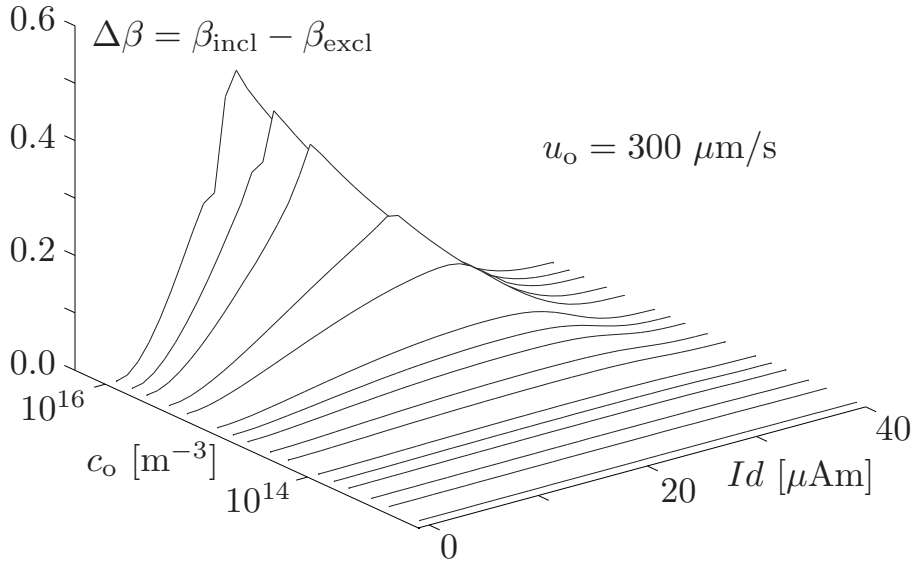

Figure 4.10: The difference $\Delta\beta = \beta_{\text{incl}} - \beta_{\text{excl}}$ in captured bead fractions between two situations: including and excluding the bulk force term $c\mathbf{F}_{\text{ext}}$ in the Navier–Stokes equation (4.1). At high concentrations ($c_{\text{o}} > 10^{15}$ m^{-3}) there is an appreciable difference between including and excluding the bulk force term, corresponding to hydrodynamic bead-bead interactions.

4.5 Bead current for finite size beads

The Nernst-Planck expression for the bead current Eq. (4.3) is linear in concentration, however, one might expect proximity of beads, and thus concentration, to influence the bead current. The beads are of finite size and this leads to a correction we derive below.

A bead subject to an external force such as the magnetic force, $\mathbf{F}_{\text{ext}}$, will move relative to the surrounding fluid until an equal and opposite drag force has been set up as described above. This drag force on a spherical bead of radius a alone in unbounded fluid in the Stokes limit was found by Faxén [19, 42] and equals

$$\mathbf{F}_{\text{drag}} = 6\pi\eta a(1 + \tfrac{1}{6}a^2\nabla^2)(\mathbf{u} - \mathbf{v}), \tag{4.16}$$

where $\mathbf{v}$ is the translational velocity of the bead. We take this as the starting point for the derivation of an alternative expression for the bead current that takes into account the size of the beads. Under the action of the external force, the translational velocity will be set up such that

$$\mathbf{v} = (1 + \tfrac{1}{6}a^2\nabla^2)\mathbf{u} + \frac{1}{6\pi\eta a}\mathbf{F}_{\text{ext}}. \tag{4.17}$$

The translational velocity of a single bead gives a bead current upon multiplication with the number concentration giving $c(1 + \frac{1}{6}a^2\nabla^2)\mathbf{u} + cb\mathbf{F}_{\text{ext}}$ where b is the (Stokes' law) bead mobility $(6\pi\eta a)^{-1}$. We include diffusion which needs to be taken into account for

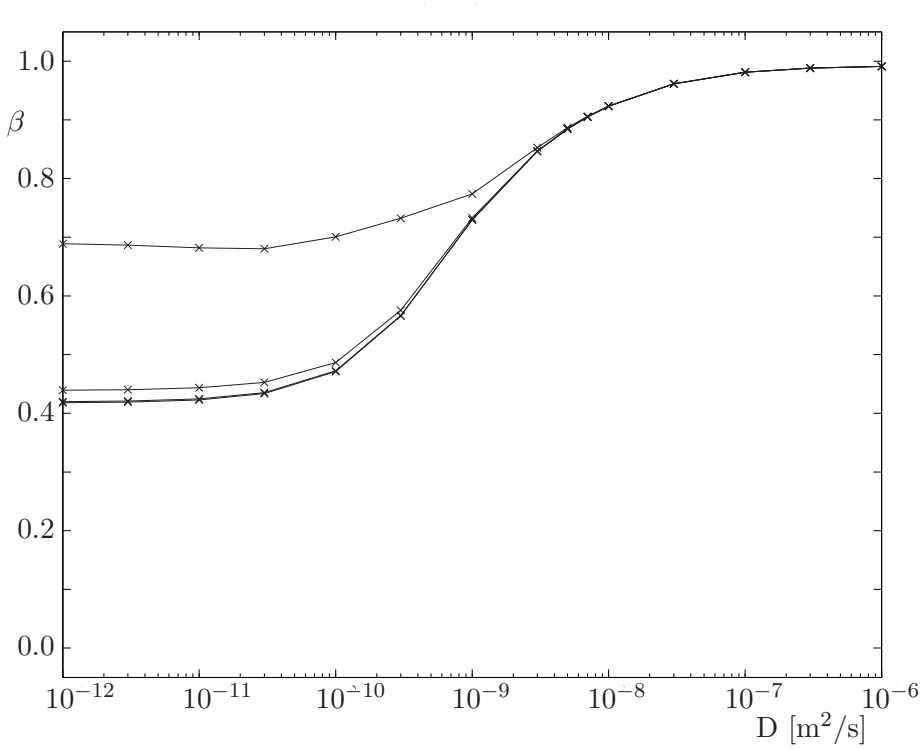

Figure 4.11: Fraction of particles caught as function of diffusion constant. At low values of the diffusion constant, D, the results are essentially independent of it. If we keep increasing it we get to a regime where the beads diffuse so readily that they are caught as they invariably diffuse into area where the magnetic field is strong enough to catch them. The four curves represent the initial concentrations $c_\mathrm{o} = 10^{13}$ m^{-3}, 10^{14} m^{-3}, 10^{15} m^{-3} and 10^{16} m^{-3}. The two curves corresponding to the lowest initial concentrations are indistinguishable then β increases with higher concentrations. The current distance product is $I\,d = 8$ μAm and the in-flow speed is 300 μm/s.

the smallest beads and as mentioned above helps stabilize simulations. This gives the alternative bead current, $\mathbf{j}_F$ we required above,

$$\mathbf{j}_F = -D\boldsymbol{\nabla} c + c(1 + \tfrac{1}{6}a^2\nabla^2)\mathbf{u} + cb\mathbf{F}_\mathrm{ext} \tag{4.18}$$

with the diffusion current $-D\boldsymbol{\nabla} c$ and subscript F for Faxén.

If the flow velocity profile is purely parabolic across the channel and constant along it then the Faxén term contributes a constant, trivial amount. The Faxén term $a^2\nabla^2\mathbf{u}$ is effectively an interaction term that makes a coupling between beads through the perturbations made by the moving beads to the quiescent flow that exists in their absence. The wake from a bead changes the flow pattern globally as there is a momentum transfer as discussed above but also very locally on the scale of a bead radius where the bead drags along fluid and creates a fluid velocity gradient. We can distinguish two situations in which the Faxén term can be estimated.

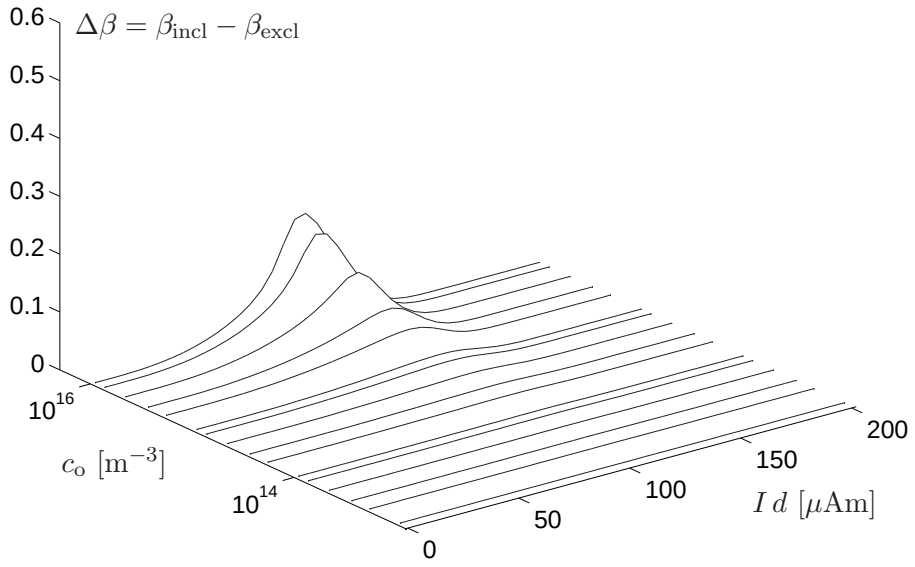

Figure 4.12: A distance to the power -3 force law. The difference $\Delta\beta = \beta_{\text{incl}} - \beta_{\text{excl}}$ in captured bead fractions between two situations: including and excluding the bulk force term $c\mathbf{F}_{\text{ext}}$ in the Navier–Stokes equation (3.8). At high concentrations ($c_{\text{o}} > 10^{15}$ m^{-3}) there is a smaller difference between including and excluding the bulk force term, corresponding to lessened importance of hydrodynamic bead-bead interactions relative to the directed influence of the magnetic force on individual beads.

When the neighbour distance is comparable to the bead radius then the Faxén term will be important due to the perturbations of the flow on small scales. This happens when $a^2c^{2/3}$ is comparable to unity which corresponds to number densities at or in excess of 10^{17} m^{-3} which is about the highest in the present study. At lower densities, say 10^{13} m^{-3}, this effect is negligible.

Our continuum model effectively coarse-grains and averages out the small scales comparable to individual beads so the Faxén term only takes into account large scale velocity variations like the one related to the superimposed vortex. In this view, the velocity variations are on the scale of the microchannel height h and should be compared with the bead radius a so the relevant 'small parameter' would be $(a/h)^2$ which is 1/2500 in our geometry. For beads small in comparison with the channel height, this will also be negligible.

It has proven difficult to incorporate this into the simulations, possibly as we need to solve a third order partial differential equation numerically. This is because we need the divergence of the bead current term which now involves a laplacian. Instead we choose to neglect the Faxén term all together, however, noting that this might not be permissible at the very highest concentrations and for large beads.

4.6 Simplified view

We can understand the capturing in the two-dimensional channel in the limit of low concentrations and in the absence of interactions in a rather simpler manner by considering the motion of a single bead on its own. We assume again that the motion is completely dominated by friction such that we have a set of equations for the velocity rather than the acceleration. In the absence of external forces, the bead follows a flow which is undisturbed because we only consider a single bead.

For reasons of convenience, we choose a slightly different set of coordinates than earlier with x and y as coordinates in the plane of the channel and a slightly different placement of the channel. For a channel of width w delimited above and below by $y = 0$ and $y = -w$ with a central attractive force directed towards $(0, 0)$ falling off as distance to the power five, the velocity of a bead will be

$$x' = v_x = -\frac{Kx}{(x^2+y^2)^3} - 4u_o y(1+\frac{y}{w}) \qquad \text{for} \quad x \in \,]-\infty, \infty[\tag{4.19}$$

$$y' = v_y = -\frac{Ky}{(x^2+y^2)^3} \qquad \text{for} \quad y \in \,[-w, 0]. \tag{4.20}$$

The equation system defines an abstract two-dimensional flow that can be analysed [53]. The constants K and u_o give the strength of the attractive force and the maximum flow speed, respectively, K is related to Eq. (4.7) through the mobility b

$$K = b\frac{2}{\pi}\frac{\chi}{\chi+3}\mu_o a^3 (Id)^2 = \frac{a^2}{3\pi^2}\frac{(Id)^2}{\eta}\frac{\mu_o \chi}{\chi+3} \tag{4.21}$$

such that the attractive r^{-5}-law in Eqs. (4.19) and (4.20) is a law for velocity rather than force.

We proceed by finding fix-points for Eqs. (4.19) and (4.20) and finding the separatrices origining at those points. There are two interesting fixed points, i.e. points with vanishing derivatives that define non-trivial separatrices, $(-\infty, -w)$ and $(\infty, 0)$. Finding trajectories by solving the differential equations numerically defines the separatrix that separates those points that are caught and those that escape to infinity and the separatrix that separates those that cannot be reached from the inlet on the left.

This is illustrated in Fig. 4.13 where separatrices are shown for a range of strengths of the attractive force increasing from Fig. 4.13(a) to Fig. 4.13(e). As the force is increased, a larger fraction of the beads entering by the inlet are caught as seen by the shifting the one separatrix (marked by dashes) towards the lower wall, expanding the region I. At a certain point, the separatrix reaches the lower wall so that all beads entering by the inlet are caught, Fig. 4.13(e).

We can compare this to Fig. 4.2. For weak fields as in Fig. 4.2(b), a thin region near and to the right of the attractive wires is partly emptied for beads. Comparing this with Fig. 4.13, we see that it is not because the partly emptied region cannot be reached by beads entering from the left. The region appears empty because beads entering near the separatrix are spread out to make up for those caught making the region appear empty.

At slightly stronger fields as in Fig. 4.2(c), a region opposite the wires appears that is not reached by beads entering at the inlet corresponding to region III in Fig. 4.13(c). At the highest field strengths, Fig. 4.13, region I covers the entire width of the channel the separatrix curving backwards right by the attracting wires accounting for the convex bulge shape of the dark area seen in Fig. 4.2(d).

Do we instead compare with the simulations for high initial concentrations, Fig. 4.5, we see that this cannot be explained as well as in the low concentration limit by our simple single bead model. This is best seen for strong attraction as the bulge is replaced by a concave taper shape of the dark area which is not accounted for by the simplified model. This is another indication that hydrodynamic interactions at high concentrations influences the details of capturing.

4.7 Discussion

We have implemented a model that treats the beads as a continuum and which takes into account the effect of the transfer of momentum from the external magnetic field through the beads to the fluid. Since the fluid advects the beads as seen by the $c\mathbf{u}$ contribution to the bead current, Eq. (4.3), the effect of the momentum transfer set up by nearby beads is an effective hydrodynamic interaction.

It is very important to include the action from the beads on the fluid medium when studying capturing. Simply leaving it out will give qualitatively incorrect results for high concentrations of beads as the effective interaction significantly helps capturing. It should make detectable differences depending on whether there are a few or some hundreds of particles in actual experiments. This should be considered when choosing operating conditions for microfluid devices based on capturing of beads as higher bead number densities potentially ease requirements for external magnets and allow faster flushing.

The effectiveness of capturing is well-described as a trade-off between flushing and attraction. The simulation data essentially collapse onto a single curve when they are plotted as function of the square of the current divided by the average flow speed for all the other parameters kept fixed.

We point out that there are other ways in which particles may interact such as via a *Faxén* term which we have derived. The influence of this term has not been included here but it might play a role at the highest bead number densities.

A simple model of beads as single particles can describe some features of capturing at low concentrations but fails to explain similar features at the high concentrations where we see interactions play a rôle. The simple model can thus not be used to treat the realm of hydrodynamic interactions as it is explicitly based on beads moving in isolation.

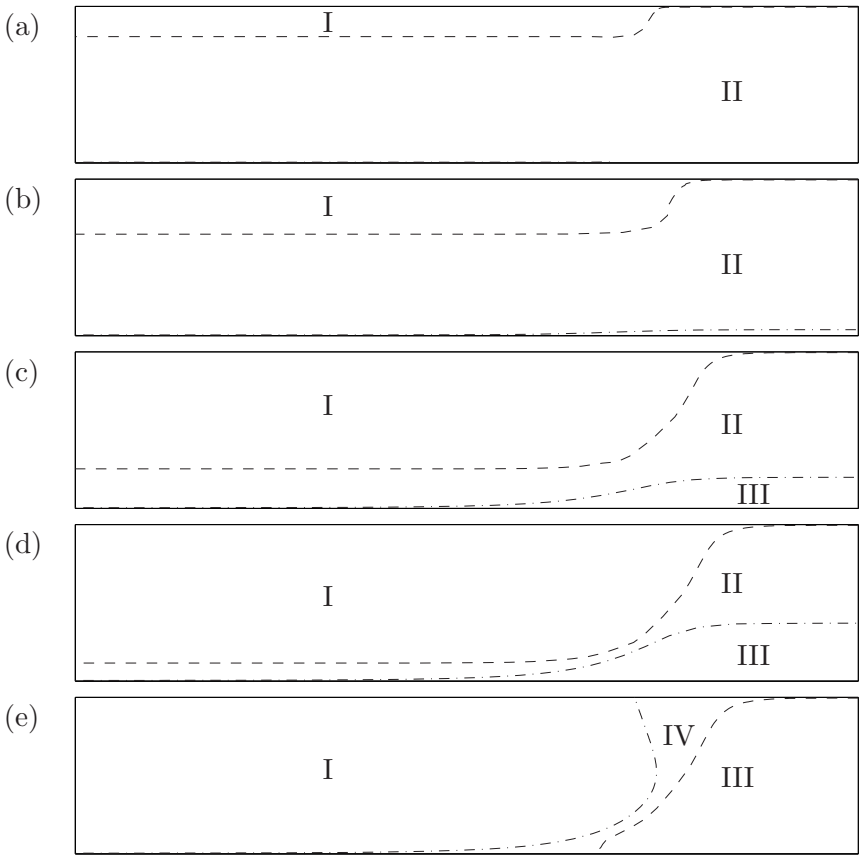

Figure 4.13: (a)–(e) Separatrices separating regions of beads that are captured at the wires and regions that cannot be reached from the inlet to the left for increasing strengths of the attractive force. Region I: Beads entering from the inlet (left) are caught by the attractive force. Region II: Beads entering from the inlet escape to the right. Region III: Cannot be reached by beads from the inlet but would escape to the right. Region IV: Cannot be reached from the inlet but beads would be caught. With increasing field strength (a)–(e), region I expands until it covers the whole inlet width in (e).

Chapter 5

Experimental test

In order to establish experimentally the influence of hydrodynamic interactions on bead capturing, an experiment has been devised in collaboration with Kristian Smistrup, Anders Brask and my supervisors and is currently being pursued. The idea is to carry out experiments at a range of concentrations in a localized magnetic field which is too weak to capture individual beads but strong enough to make them move somewhat. This corresponds to the range of intermediate strength magnetic fields in Fig. 4.10 where concentration has the largest influence on capturing.

5.1 Principle

The experimental setup is somewhat different from the one described theoretically in Chapter 4 in that it is not a bead capturing setup where the beads are retained because it is difficult to quantify the number of beads caught once they have settled. Rather, the idea is to create a weak magnetic force by a field and field gradient which are just sufficient to move single beads on their own. We have chosen three parallel laminar flows of fluid instead of walls in a flat geometry. On their own, the beads are not able to move from one flow to another but collectively they migrate to one of the buffer flows and can be counted. The flat geometry is chosen to resemble the two-dimensional flow studied in Chapter 4.

The three flows consists of a dispersion of beads of known uniform initial concentration at the centre and two buffer flows, one on either side, to catch migrating beads. The flows are kept laminar at as low Reynolds numbers as practical so that mixing of the three flows is kept negligible. This has been tested with a dyed solution instead of beads and some transfer of dye from the central from to the buffer flows is found. However, the diffusivity of a dye molecule is much higher than that of a one-micrometre diameter bead so this is not expected to be a problem. If need be, one might consider adjusting the viscosities of the fluids slightly with additives such as glycerol or trace amounts of guar or xanthan gum.

The magnetic force is then adjusted so that single beads do not move appreciably from the central fluid flow into the buffer flow close to the magnetic field when the bead concentration is low. The other buffer flow acts as a negative control that indicates

influence of mixing, diffusion and motion of beads for other reasons than the magnetic field.

When the bead concentration of the in-flowing bead dispersion is increased, we will expect beads to move collectively due to forces mediated by hydrodynamic interactions and that this leads to beads migrating from the central flow to the one buffer flow.

The three flows passing through the device are collected during the experiment so that the magnetic moment can be measured by means of a vibrating sample magnetometer (VSM) to give a measure of the number of beads in either of the two buffer flows and in the dispersion. An excess of beads in the buffer flow closer to the magnetic field is then attributed to bead migration due to the magnetic field.

The magnetic polystyrene beads employed are so dense (specific density 1800 $\mathrm{kg\,m^{-3}}$) that they sediment appreciably from the aqueous dispersion so that it is necessary to incorporate this effect into the design of the experiment. By orienting the flow device vertically so that the flows are vertical as well, we avoid migration of beads from the dispersion to either of the buffer flows on account of gravity alone.

5.2 Implementation and design

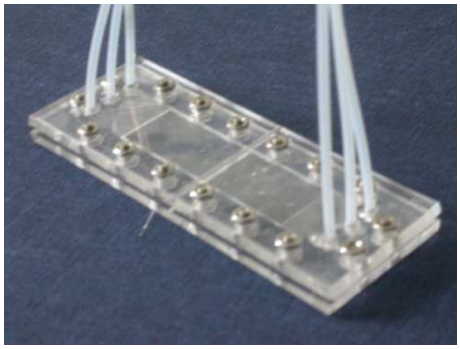

Figure 5.1: Picture of the laminated flow device to be used in the experiment. The six tubes leading the flows into the device are visible as are the screws that are used to keep the layers together.

The flow device itself is made from seven sheets of acrylic plastic (poly(methyl methacrylate) often referred to as PMMA) cut out by means of a CO_2-laser and laminated together. The sheets are cut to define the top and bottom lids, spacers for flow channels and separator layers between the in- and outflow channels. Referring to Fig. 5.2, the layers are as follows: The top lid, not shown in Fig. 5.2, is a 250 μm thick sheet only with holes cut out to feed-through the two buffer flows and the bead dispersion. The next layer is a spacer layer 90 μm thick defining the flow of the first buffer flow leaving a 40 mm long and 12.5 mm wide rectangular channel as well as tapering sections at either end in order to spread out the flow over the whole channel width, Fig. 5.2α. The next layer is a separator layer 250 μm thick that keeps the buffer and dispersion flows separate except

for the 40 mm by 12.5 mm rectangular flow channel Fig. 5.2β. The bead dispersion is launched and collected in two tapered sections at either end of the rectangular channel Fig. 5.2γ. The sequence is then repeated in reverse with a thick separator layer, Fig. 5.2β', and a thinner buffer flow layer Fig. 5.2α' and a thick bottom lid which is not shown.

The model of the magnetic field used in the simulations of Chapter 4, a pair of wires with opposite currents, is inappropriate for experiment. The magnetic field decays very rapidly, distance to the power -5, so that very strong wire currents would be necessary as the wires cannot be right next to the bead flow in the three flow configuration. In Chapter 4, the wires were 5 μm from the bead flow whereas in the experiment, it will have to be at least 500 μm away. This means a tightening of requirements for the current wire distance product $I\,d$ by a factor 10^{10} which is prohibitive. Instead, we can generate a more or less homogeneous magnetic field externally and then induce a field gradient by placing a magnetizable object close by the channel thus eliminating problems of high currents and heat dissipation in the device.

As source of the magnetic field and field gradient we choose a set of electromagnets that magnetize a piece of magnetizable, special stainless steel wire with radius $r_c = 50$ μm through a polepiece. As model of this magnetic field, we use the field around a right-circular cylinder, $\mathbf{H}_{\rm cyl}$, homogeneously magnetized perpendicularly to the cylinder axis by an external magnetic field, $\mathbf{H}_{\rm o}$, which can be found in a similar manner to the homogeneously magnetized sphere from the magnetic scalar potential. From measurements, it is known that the magnetization is linear in the applied field such that we assume a constant permeability of the wire $\mu_{\rm wire}$. In this manner, we find that the field external to the wire is

$$\mathbf{H}_{\rm cyl}(\mathbf{r}) = \mathbf{H}_{\rm o} + \frac{r_c^2}{r^2}\frac{\chi}{\chi+2}\left(-\mathbf{H}_{\rm o} + \frac{(\mathbf{H}_{\rm o}\cdot\mathbf{r})\mathbf{r}}{r^2}\right). \tag{5.1}$$

with $\mathbf{r}$ being the position vector from the center of the cylindrical wire. We already know that the magnetization of a spherical bead in a field that is approximately constant over the bead is

$$\mathbf{M} = \frac{3\chi}{\chi+3}\mathbf{H}_{\rm ext}. \tag{5.2}$$

The susceptibility of the bead material is denoted χ and the permeability $\mu_{\rm bead} = (1+\chi)\mu_{\rm o}$. The force on a bead of radius a is then given by Eq. (2.21)

$$\begin{aligned}\mathbf{F}_{\rm bead} =& 2\pi\mu_{\rm o}a^3\frac{\mu_{\rm bead}-\mu_{\rm o}}{\mu_{\rm bead}+2\mu_{\rm o}}\frac{\mu_{\rm wire}-\mu_{\rm o}}{\mu_{\rm wire}+\mu_{\rm o}}\\ &\left[\mathbf{r}\left(H_{\rm o}^2\frac{4r_c^2}{r^4} - H_{\rm o}^2\frac{4r_c^4}{r^6}\frac{\mu_{\rm wire}-\mu_{\rm o}}{\mu_{\rm wire}+\mu_{\rm o}} - \frac{6r_c^4}{r^8}\frac{\mu_{\rm wire}-\mu_{\rm o}}{\mu_{\rm wire}+\mu_{\rm o}}(\mathbf{H}_{\rm o}\cdot\mathbf{r})^2 - \frac{8r_c^2}{r^6}(\mathbf{H}_{\rm o}\cdot\mathbf{r})^2\right)\right.\\ &\left. + 2\mathbf{H}_{\rm o}(\mathbf{H}_{\rm o}\cdot\mathbf{r})\left(-\frac{r_c^4}{r^6}\frac{\mu_{\rm wire}-\mu_{\rm o}}{\mu_{\rm wire}+\mu_{\rm o}} + 2\frac{r_c^2}{r^4}\right)\right]\end{aligned} \tag{5.3}$$

which consists of a term directed along the applied external field, $\mathbf{H}_{\rm o}$, and a radial term along the direction to the centre of the cylindrical wire. We see that the leading order force terms are of order -3 in the distance from the wire r. We know from the simulations

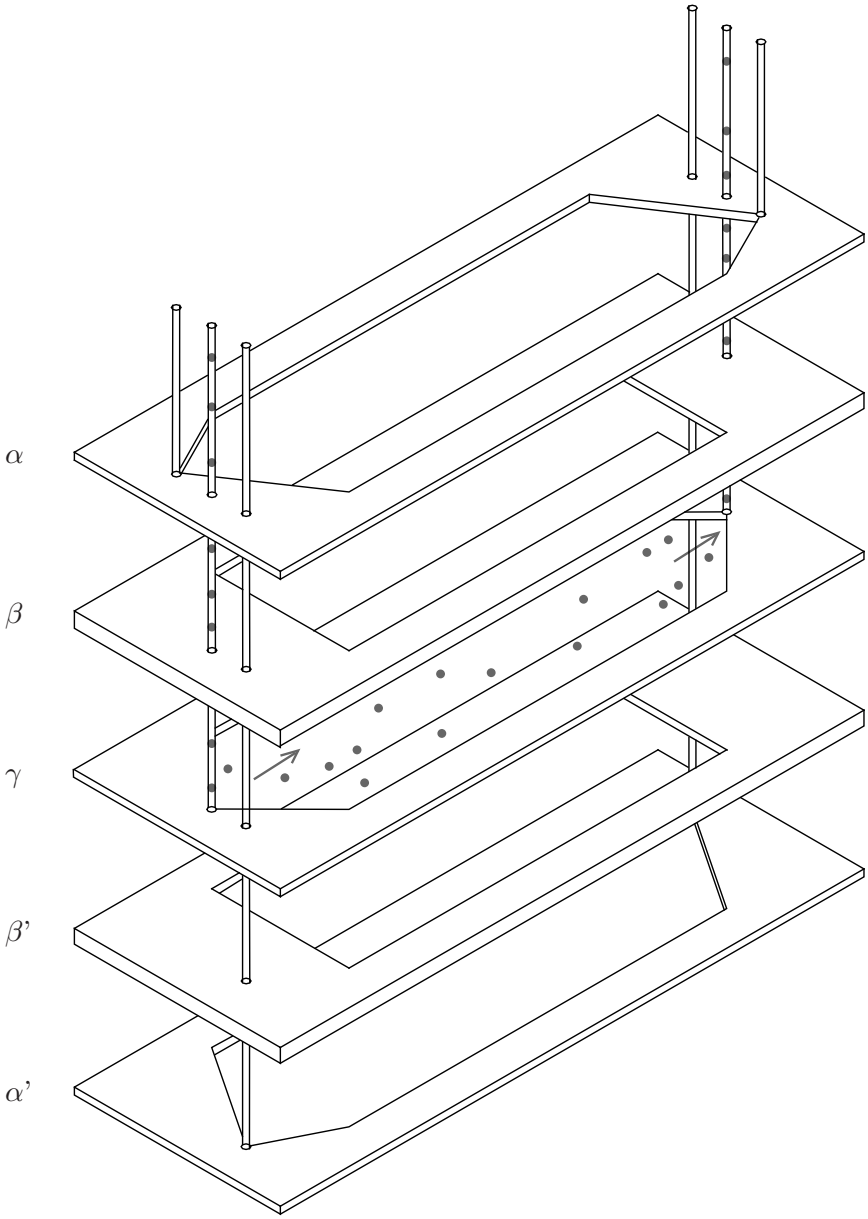

Figure 5.2: Sketch of the laminated flow device without top and bottom lids before assembly. The remaining five layers are the two buffer flow spacer layers α and α', the flow separator layers β and β', and the layer in which the bead dispersion flows γ. The three flows enter through three tubes that are lead through to the respective layers. The beads are indicated in the central layer γ. The magnetizable steel wires are not shown.

that a short range force only effectively pulls beads at the one side of the flow sets up a vortex superposed on the flow pattern and sweeps beads towards the wall. However, it seems impossible to make a force law of order -5 as in the simulations that would at the same time provide a sufficient force to attract the beads from the dispersion into the buffer flow. By placing another similar wire asymmetrically at the other side of the channel but at a greater distance it is possible to get a somewhat steeper force law than the order -3 [46].

5.3 Simulations

In order to have theoretical predictions of the behaviour of the configuration chosen for the flow device and in order to verify that the principle of the device can work, attempts were made to simulate it with the actual dimensions and parameters for the device. It proved impossible.

The dimensions of the necessary simulation domain become so large that it is impossible to handle it on a normal desktop computer. The mesh that is used by the finite element algorithm becomes prohibitively large. The problem is that the stability of the algorithm for this problem is related to the balance between advection and diffusion on the scale of a mesh element similar to the Péclet number described in Sec. 4.3.2. This effectively sets a maximum size for a mesh element if the simulations are to be stable, however, a large number of elements take more computer memory. The simulations were then moved to the DTU High Performance Computing centre under a grant from Danish Center for Scientific Computing. Unfortunately, the combination Matlab and Femlab is only able to address about 4 GB of memory which is not sufficient.

Reducing the simulation domain has not worked for a variety of reasons. The first approach was attempting to refine selectively the mesh in regions where the mesh element Péclet number, i.e. the ratio lu/D for some mesh element characteristic length l, was too large. Secondly, it was attempted to simulate a smaller section of the device, however, this is problematic when the force acting on the beads is too large by the domain inlet. In an experiment, the flow pattern will have changed appreciably from Poiseuille flow and the concentration of beads will have changed from the initial value but this is precisely what we want to simulate. This means that there is an effective lower limit on the domain size which along with the effective upper limit on the mesh element size gives a minimum requirement on memory that far exceeds what is available to Femlab and Matlab.

5.4 Discussion

Experiments are under way and the essential parts have been manufactured. The idea is to test the influence of hydrodynamic interactions between beads that move due to an external field in an as clean and simple system as possible. The principle of having laminar flows and using buffer flows as controls means that the experiment can be run for long periods of time to accumulate data without having a build-up of beads in the channel.

It has not been possible to make concrete predictions for the experiment to which results can be compared save for the qualitative prediction of Chapter 4 that in some range of intermediate magnetic field strengths there will be an increase with bead concentration in the number of beads that migrate from the central flow to the buffer flow nearer the source of magnetic field inhomogeneity, the magnetic wire.

Chapter 6

The induced force method

Until now we have seen that a fluid medium effectively mediates forces between particles and the surrounding microchannel or container walls. We have attempted to take this into account in various *ad hoc* ways, however, this is inherently unsatisfactory and there seems to be a place for a systematic approach that treats not just single particles treated a points but encompasses the rigid body motion of extended particles in confined geometries as found in a microfluidic system.

Below we develop and extend a method that has been used for studying the sedimenting or settling particles as well as diffusion into a systematic approach that can be used to model particle motion in a wide variety of geometries. We set up the basic machinery and illustrate the workings by calculating the mobility of a single sphere placed inside a cubic microchannel or box.

6.1 Principle

A different approach from the ones employed above is to focus exclusively on the particle motion and develop a formalism in the Stokes limit in terms of forces on particles and the interactions between the particles mediated by the fluid. In such an approach, the fluid steps into the background and only show up as a field. Here we will follow the theory due to Mazur, Beenakker and Saarloos [5, 31, 34] where the problem of interacting particles in a flow is formulated in terms of the forces on the surfaces of the particles and connections between them. Their approach was only developed for spherical particles and a single plane wall but they were able to extend it to the case of particles in a spherical container by making one particle enclose the others [4]. In the following, we extend and develop further their "induced force method" to include rectangular finite walls so that a we can take into account the effects of a rectangular microchannel, for example.

First, we consider N spherical particles. The lth particle has radius a_l, linear velocity $\mathbf{v}_l$ and angular velocity $\boldsymbol{\omega}_l$ moving in a fluid with viscosity η. The particles are moving under the influence of external forces $\mathbf{F}_l^{\text{ext}}$ and torques $\mathbf{T}_l^{\text{ext}}$ that cause them to move in the fluid. The fluid is otherwise at rest but flows with velocity $\mathbf{u}(\mathbf{r}, t)$ due to the motion of the particles. The starting point for the description is again the stationary Stokes equation

for the fluid

$$-\boldsymbol{\nabla} p + \eta \nabla^2 \mathbf{u} = -\boldsymbol{\nabla} \cdot \boldsymbol{\sigma} = 0 \tag{6.1}$$

and the condition of incompressibility

$$\boldsymbol{\nabla} \cdot \mathbf{u} = 0. \tag{6.2}$$

We have here constructed the stress tensor $\boldsymbol{\sigma}$ from pressure p and the viscous stress

$$\sigma_{\alpha\beta} = p\delta_{\alpha\beta} - \eta \left(\frac{\partial u_\alpha}{\partial r_\beta} + \frac{\partial u_\beta}{\partial r_\alpha} \right) \tag{6.3}$$

where we employed component notation.

The idea is to extend these equations to all of space including the volumes of the particles and in the process formulate the no-slip boundary conditions on the particles in terms of the force distributions necessary to maintain no-slip.

The spherical particles move according to the equations of motion; the lth particle under the influence of the forces $\boldsymbol{\sigma} \cdot \hat{\mathbf{n}}$ due to the fluid and the external force $\mathbf{F}_l^{\text{ext}}$ and torque $\mathbf{T}_l^{\text{ext}}$

$$m_l \frac{d\mathbf{u}_l}{dt} = -\int_{S_l(t)} \boldsymbol{\sigma} \cdot \hat{\mathbf{n}}_l \, dS + \mathbf{F}_l^{\text{ext}}, \tag{6.4}$$

$$I_l \frac{d\boldsymbol{\omega}_l}{dt} = -\int_{S_l(t)} (\mathbf{r} - \mathbf{R}_l) \times (\boldsymbol{\sigma} \cdot \hat{\mathbf{n}}_l) \, dS + \mathbf{T}_l^{\text{ext}}. \tag{6.5}$$

Since $\hat{\mathbf{n}}_l$ above is the local *outward* normal unit vector on the lth particle together with the definition of the stress tensor we have the negatives of the surface integrals. The particle masses, m_l, and moments of inertia, I_l, appear above along with the position vectors $\mathbf{R}_l(t)$ for the centers and the surfaces $S_l(t)$ for each particle l at time t.

As the particles are assumed to be rigid spherical particles the velocity of the particle surface must be a combination of translation and rotation and since we assume no-slip this holds true for the fluid velocity $\mathbf{u}$ at the surface as well

$$\mathbf{u}(\mathbf{r}, t) = \mathbf{v}_l + \boldsymbol{\omega} \times (\mathbf{r} - \mathbf{R}_l(t)), \qquad \text{for} \quad |\mathbf{r} - \mathbf{R}_l(t)| = a_l. \tag{6.6}$$

In order to fulfil this condition, the rigid particles excert forces at the surface on the fluid and we extend Eq. (6.1) all over space by introducing these [33, 30]

$$\boldsymbol{\nabla} \cdot \boldsymbol{\sigma} = \sum_j \mathbf{F}_j(\mathbf{r}, t), \tag{6.7}$$

where the force $\mathbf{F}_j(\mathbf{r}, t)$ due to the jth particle vanishes except where $|\mathbf{r} - \mathbf{R}_j| = a_j$ as there are no induced forces in the inside of the particles either. In their interior we let $p = 0$.

The idea is to consider not just N spherical particles but a rectangular box as well. The box encloses all the particles and has walls at the six planes $x = -L_x$, $x = L_x$,

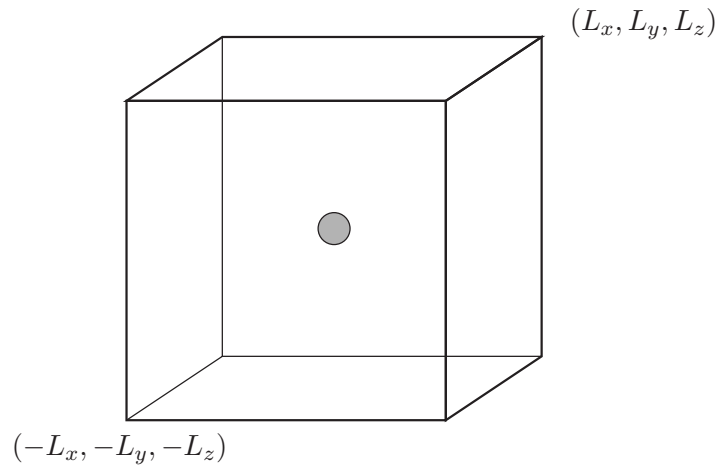

Figure 6.1: A single spherical particle at the centre of a cubic box. The box is centered around the origin and has sidelengths $2L_x$, $2L_y$ and $2L_z$.

$y = -L_y$, $y = L_y$, $z = -L_z$, and $z = L_z$. Although the walls are assumed immobile, we can take a similar approach exchanging no-slip boundary conditions in terms of velocity into boundary conditions in terms of the forces necessary to keep the fluid at the walls at rest. This means that we have an additional sum of force densities over the walls

$$\boldsymbol{\nabla} \cdot \boldsymbol{\sigma} = \sum_{j \in \text{beads}} \mathbf{F}_j(\mathbf{r}, t) + \sum_{w \in \text{walls}} \mathbf{F}_w(\mathbf{r}, t). \tag{6.8}$$

A formal solution to the Stokes equation can be formulated in reciprocal space, **k**-space, in terms of the induced forces which we expand in a multipole expansion for the spherical particles and Legendre polynomials for the walls. Together with the equations of motion for the particles and the boundary conditions we derive the equations that link the motion of particles with induced forces. In steady state, the zeroth and first multipoles of the forces on the spherical particles must correspond to the applied forces and torques so it is possible to develop equations linking applied forces to induced forces to particle motion.

With force terms for walls and particles, the Stokes equation becomes

$$-\boldsymbol{\nabla} p + \eta \nabla^2 \mathbf{u} = -\sum_{i \in \text{beads}} \mathbf{F}_l(\mathbf{r}) - \sum_{w \in \text{walls}} \mathbf{F}_w(\mathbf{r}) \tag{6.9}$$

where we have added the forces from beads and walls alike.

Along with the condition of incompressibility $\boldsymbol{\nabla} \cdot \mathbf{u} = 0$, this can be Fourier transformed into an algebraic equation just as we did for the Green's functions in Chapter 3. Below, we employ the following conventions for the Fourier transform

$$\mathbf{u}(\mathbf{r}) = \int \frac{d\mathbf{k}}{(2\pi)^3} \, e^{i\mathbf{k}\cdot\mathbf{r}} \mathbf{u}(\mathbf{k}), \tag{6.10}$$

$$\mathbf{u}(\mathbf{k}) = \int d\mathbf{r} \, e^{-i\mathbf{k}\cdot\mathbf{r}} \mathbf{u}(\mathbf{r}). \tag{6.11}$$

and similarly for the forces and pressure. Proceeding this way, we arrive at the following transformed equations in $\mathbf{k}$-space

$$\eta k^2 \mathbf{u}(\mathbf{k}) + i\mathbf{k}p(\mathbf{k}) = \sum_{j\in\text{beads}} e^{-i\mathbf{k}\cdot\mathbf{R}_j}\mathbf{F}_j(\mathbf{k}) + \sum_{w\in\text{walls}} \mathbf{F}_w(\mathbf{k}) \tag{6.12}$$

and

$$\mathbf{k}\cdot\mathbf{u}(\mathbf{k}) = 0, \tag{6.13}$$

from which we can eliminate p and the need for the second equation by applying the operator $(\mathbf{1}-\hat{\mathbf{k}}\hat{\mathbf{k}})$ to both equations. Here and in the following we will use dyadic notation and let a 'hat' denote a unit vector so that $\hat{\mathbf{k}}$ means $\mathbf{k}/k$. This leaves the formal solution for $\mathbf{u}(\mathbf{k})$ which we will use repeatedly

$$\mathbf{u}(\mathbf{k}) = \sum_{j\in\text{beads}} \frac{1}{\eta k^2}\, e^{-i\mathbf{k}\cdot\mathbf{R}_j}(\mathbf{1}-\hat{\mathbf{k}}\hat{\mathbf{k}})\cdot\mathbf{F}_j(\mathbf{k}) + \sum_{w\in\text{walls}} \frac{1}{\eta k^2}\,(\mathbf{1}-\hat{\mathbf{k}}\hat{\mathbf{k}})\cdot\mathbf{F}_w(\mathbf{k}). \tag{6.14}$$

Here we have used that the fluid would be at rest in the absense of external forces on the particles. This is not an essential restriction as one could include an unperturbed flow, see for example the remarks in Ref. [34].

6.2 Expansions of forces and velocities

On the basis of the formal solution we will be working towards a hierarchy of linear equations that couple expansions of forces on particles and walls with expansions of their velocities. The coefficients in these equations are termed "connectors" following Mazur [34].

6.2.1 At the spherical particles

The next step is to expand the unknown induced forces on each of the spherical particles in a series with tensorial force multipole expansion coefficients $\mathsf{F}_l^{(p+1)}$,

$$\mathbf{F}_l(\mathbf{k}) = \sum_{p=0}^{\infty}(a_l k/i)^p\,\overline{\hat{\mathbf{k}}^p}\odot\overline{\frac{\partial^p}{\partial\mathbf{k}^p}}\,\mathbf{F}_l(\mathbf{k})\frac{(i/a_l)^p}{p!}\bigg|_{\mathbf{k}=0} = \sum_{p=0}^{\infty}(a_l k/i)^p\,\overline{\hat{\mathbf{k}}^p}\odot\mathsf{F}_l^{(p+1)}. \tag{6.15}$$

The notation here warrants some explanation. The symbol $\hat{\mathbf{k}}^p$ is the p-dimensional (polyadic) tensor formed as an ordered product of the vector $\hat{\mathbf{k}}$ p times. The circled dot, $\odot$, denotes full tensor contraction so that

$$\mathsf{A}\odot\mathsf{B} = \sum_{j,k,l,\ldots} A_{\ldots,l,k,j}B_{j,k,l,\ldots}, \tag{6.16}$$

i.e., we contract with aa many indices as available starting with the innermost. We use this and the polyadic notation to reduce the amount of dummy indices needed. The

overbracket $\overline{\mathsf{A}}$ indicates that the tensor A has been made irreducible in the sense that it has been symmetrized in any pair of indices and that it has been made to vanish under contraction in any pair of indices [23]. Below we only encounter the explicit forms of the irreducible tensors in the two simplest cases

$$\overline{a_\alpha} = a_\alpha \qquad \text{and} \qquad \overline{a_\alpha a_\beta} = a_\alpha a_\beta - \tfrac{1}{3}\delta_{\alpha\beta}\, a^2 \tag{6.17}$$

in component notation.

Mazur and Saarloos [34, 35] goes on to show that this expansion can be expressed in terms of spherical Bessel functions j_p [24] as

$$\mathbf{F}_l(\mathbf{k}) = \sum_{p=0}^{\infty} (2p+1)!!(-i)^p j_p(ka_l)\, \overline{\hat{\mathbf{k}}^p} \odot \mathsf{F}_l^{(p+1)}. \tag{6.18}$$

The double factorial $n!!$ is defined as the product $n(n-2)(n-4)\cdots$ down to either 1 or 2 depending on whether n is odd or even.

6.2.2 At the walls

Similarly, we expand the induced forces at the walls. In the following w, $\underline{w}$ and $\overline{w}$ will be used to denote x, y and z such that the triplet $w\underline{w}\overline{w}$ makes up a cyclic permutation of xyz. This is just to keep track of walls and directions. We look at the wall at $w = -L_w$ as example but it carries through for all six walls w from $x = -L_x$ to $z = L_z$. The force density is confined to the wall so that

$$\mathbf{F}_{+L_w}(\mathbf{r}) = \mathbf{F}_{+L_w}(\underline{w}, \overline{w})\, \Omega(\underline{w}/L_{\underline{w}}, \overline{w}/L_{\overline{w}})\, \delta(w - L_w) \tag{6.19}$$

where

$$\Omega(\underline{w}/L_{\underline{w}}, \overline{w}/L_{\overline{w}}) = \begin{cases} 1 & \text{for} \quad (\underline{w}, \overline{w}) \in [-L_{\underline{w}}, L_{\underline{w}}] \times [-L_{\overline{w}}, L_{\overline{w}}] \\ 0 & \text{elsewhere.} \end{cases} \tag{6.20}$$

The force density on the finite-sized wall can be expanded in a terms of Legendre polynomials, P_n, because of the finite extent

$$\mathbf{F}_{+L_w}(\underline{w}, \overline{w}) = \frac{1}{4L_{\underline{w}}L_{\overline{w}}} \sum_{n,m} P_n(\underline{w}/L_{\underline{w}})\, P_m(\overline{w}/L_{\overline{w}})\, \mathbb{F}_{+L_w}(n,m), \tag{6.21}$$

so that in $\mathbf{k}$-space we have

$$\mathbf{F}_{+L_w}(\mathbf{k}) = \int d\mathbf{r} e^{-i\mathbf{k}\cdot\mathbf{r}}\, \mathbf{F}(\mathbf{r}) = \int d\mathbf{r} e^{-i\mathbf{k}\cdot\mathbf{r}} \mathbf{F}(\underline{w}, \overline{w}) \Omega(\underline{w}/L_{\underline{w}}, \overline{w}/L_{\overline{w}}) \delta(w - L_w) \tag{6.22}$$

$$= e^{-ik_w L_w} \frac{1}{4L_{\underline{w}}L_{\overline{w}}} \sum_{n,m} \int_{-L_{\underline{w}}}^{L_{\underline{w}}} d\underline{w} \int_{-L_{\overline{w}}}^{L_{\overline{w}}} d\overline{w}\, e^{-i(k_{\underline{w}}\underline{w} + k_{\overline{w}}\overline{w})} P_n(\underline{w}/L_{\underline{w}}) P_m(\overline{w}/L_{\overline{w}}) \mathbb{F}_{+L_w}(n,m) \tag{6.23}$$

$$= e^{-ik_w L_w} \sum_{n,m} (-i)^{n+m} j_n(k_{\underline{w}} L_{\underline{w}}) j_m(k_{\overline{w}} L_{\overline{w}}) \mathbb{F}_{+L_w}(n,m). \tag{6.24}$$

In the last line we used Rodrigues' formula and introduced the spherical Bessel functions $j_n(x)$ [48].

6.3 Equation hierarchy

We now need to make the connection to fluid velocity. We do this by evaluating surface averages $\overline{x}^{S_l}$ of the multipole moments $\overline{\hat{\mathbf{n}}^p}\,\mathbf{u}(\mathbf{r})$ of the fluid velocity,

$$\begin{aligned}\overline{\overline{\hat{\mathbf{n}}^p}\,\mathbf{u}(\mathbf{r})}^{S_l} &= \frac{1}{4\pi a_l^2} a_l^{-p} \int d\mathbf{r}\, \overline{(\mathbf{r}-\mathbf{r}_l)^p}\,\mathbf{u}(\mathbf{r})\,\delta(|\mathbf{r}-\mathbf{R}|-a_l) \\ &= (-i/a_l)^p \int \frac{d\mathbf{k}}{(2\pi)^3} \Big(\overline{\frac{\partial^p}{\partial \mathbf{k}^p}\frac{\sin ka_l}{ka_l}}\Big)\, e^{i\mathbf{k}\cdot\mathbf{R}_l}\mathbf{u}(\mathbf{k}) \\ &= i^p \int \frac{d\mathbf{k}}{(2\pi)^3}\,\overline{\hat{\mathbf{k}}^p}\, j_p(ka_l)\, e^{i\mathbf{k}\cdot\mathbf{R}_l}\mathbf{u}(\mathbf{k}). \end{aligned} \tag{6.25}$$

The Dirac delta-function ensures that the first integral can be extended all over real space and the second equality stems from the identity

$$\overline{\frac{\partial^p}{\partial \mathbf{k}^p}\frac{\sin k}{k}} = (-1)^p\,\overline{\hat{\mathbf{k}}^p}\, j_p(k) \tag{6.26}$$

see Ref. [31].

These averages can then be handled in turn starting with the zeroth moment corresponding to translation for the particles and similarly for the walls.

6.3.1 Translational velocity

As the spherical particles are rigid bodies only two of these moments are non-vanishing and they correspond to the translation and rotation velocities respectively. The surface average, i.e., the moment with $p = 0$ gives

$$\overline{\mathbf{u}(\mathbf{r})}^{S_l} = \int \frac{d\mathbf{k}}{(2\pi)^3}\,\mathbf{u}(\mathbf{k}) e^{i\mathbf{k}\cdot\mathbf{R}_l} j_0(ka_l). \tag{6.27}$$

Together with the trivial average of the boundary condition for a single particle we can insert the formal solution of the equations of motion Eq. (6.14) and obtain an equation for the translational velocity $\mathbf{v}_l$ of the lth particle,

$$\begin{aligned}\mathbf{v}_l = \overline{\mathbf{u}(\mathbf{r})}^{S_l} &= \sum_{j\in\text{beads}} \int \frac{d\mathbf{k}}{(2\pi)^3}\,(\eta k^2)^{-1}\,(\mathbf{1}-\hat{\mathbf{k}}\hat{\mathbf{k}})\cdot\mathbf{F}_j(\mathbf{k})\, e^{i\mathbf{k}\cdot(\mathbf{R}_l-\mathbf{R}_j)} j_0(ka_l) \\ &+ \sum_{w\in\text{walls}} \int \frac{d\mathbf{k}}{(2\pi)^3}\,(\eta k^2)^{-1}\,(\mathbf{1}-\hat{\mathbf{k}}\hat{\mathbf{k}})\cdot\mathbf{F}_w(\mathbf{k})\, e^{i\mathbf{k}\cdot\mathbf{R}_l} j_0(ka_l). \end{aligned} \tag{6.28}$$

We can now use the expansion of the force on the jth spherical particle into multipole moments Eq. (6.18) and the expansion of forces at the walls Eq. (6.21)

$$\begin{aligned}\mathbf{v}_l = (6\pi\eta a_l)^{-1} \sum_{j\in\text{beads}} \sum_{p=0}^{\infty} \int d\hat{\mathbf{k}} \int_{-\infty}^{\infty} dk\, \frac{3a_l}{8\pi^2}(2p+1)!!(-i)^p\, (\mathbf{1}-\hat{\mathbf{k}}\hat{\mathbf{k}})\cdot\overline{\hat{\mathbf{k}}^p}\odot\mathsf{F}_j^{(p+1)} \\ \times j_p(ka_l)e^{i\mathbf{k}\cdot(\mathbf{R}_l-\mathbf{R}_j)}\, j_0(ka_l) \\ +(6\pi\eta a_l)^{-1} \sum_{w\in\text{walls}} \sum_{n,m} \int d\hat{\mathbf{k}} \int_0^{\infty} dk\, \frac{3a_l}{4\pi^2}\, (\mathbf{1}-\hat{\mathbf{k}}\hat{\mathbf{k}})\cdot\mathbb{F}_w(n,m) \\ \times e^{i(\mathbf{k}\cdot\mathbf{R}-k_w L_w)}(-i)^{n+m} j_n(k_{\underline{w}}L_{\underline{w}})\, j_m(k_{\overline{w}}L_{\overline{w}})\, j_0(ka_l).\end{aligned} \tag{6.29}$$

Collecting terms allows us to write this in terms of so-called connectors,

$$\begin{aligned}\mathbf{v}_l = (6\pi\eta a_l)^{-1}\mathsf{F}_l^{(1)} + (6\pi\eta a_l)^{-1} \sum_{j\neq i} \sum_{p=0}^{\infty} \mathsf{A}_{lj}^{1\leftarrow p+1} \odot \mathsf{F}_j^{(p+1)} \\ + (6\pi\eta a_l)^{-1} \sum_{w\in\text{walls}} \sum_{n,m} \mathsf{U}_{lw}^{1\leftarrow(n,m)} \cdot \mathbb{F}_w(n,m),\end{aligned} \tag{6.30}$$

where the connectors, $\mathsf{A}_{lj}^{1\leftarrow p+1}$, are defined for all $j \neq l$ by

$$\mathsf{A}_{lj}^{1\leftarrow p+1} = \frac{3a_l}{8\pi^2}(2p+1)!!(-i)^p \int d\hat{\mathbf{k}} \int_{-\infty}^{\infty} dk\, (\mathbf{1}-\hat{\mathbf{k}}\hat{\mathbf{k}})\,\overline{\hat{\mathbf{k}}^p}\, j_p(ka_j)\, j_0(ka_l) e^{ik\hat{\mathbf{k}}\cdot(\mathbf{R}_l-\mathbf{R}_j)}. \tag{6.31}$$

and the connectors $\mathsf{U}_{lw}^{1\leftarrow(n,m)}$ by

$$\mathsf{U}_{lw}^{1\leftarrow(n,m)} = \frac{3a_l}{4\pi^2} \int d\hat{\mathbf{k}} \int_0^{\infty} dk\, (\mathbf{1}-\hat{\mathbf{k}}\hat{\mathbf{k}})(-i)^{n+m} e^{i(\mathbf{k}\cdot\mathbf{R}_l - k_w L_w)} j_n(k_{\underline{w}}L_{\underline{w}})\, j_m(k_{\overline{w}}L_{\overline{w}})\, j_0(ka_l). \tag{6.32}$$

Notice that there is no connector in front of the zeroth force multipole term in 6.30, only the factor $(6\pi\eta a_l)^{-1}$ known from Stokes' law. This can be shown from Eq. (6.15) by complex integration [34].

The connectors serve to 'connect' or couple terms in the expansions of the forces on particles and walls to the corresponding expansions of velocities on particles and walls. The connector $\mathsf{A}_{lj}^{1\leftarrow p+1}$ is thus the coupling of the pth force multipole moment from the jth particle to the translational velocity of the lth particle. Below we will introduce similar connectors for the rotational and higher order velocity moments $\mathsf{A}_{lj}^{n\leftarrow p+1}$. In an analogous manner, the connector $\mathsf{U}_{lw}^{1\leftarrow(n,m)}$ is the coupling of the (n,m)-term in the force expansion at the wall w to the translational velocity of the lth particle.

6.3.2 Rotational velocity

We can repeat the above considerations for the rotation of the particles. In this case we determine the surface average $\overline{\hat{\mathbf{n}}\,\mathbf{u}(\mathbf{r})}^{S_l}$ considering the boundary condition

$$\begin{aligned}\overline{\hat{\mathbf{n}}\,\mathbf{u}(\mathbf{r})}^{S_l} &= \overline{\hat{\mathbf{n}}\,\mathbf{v}_l(\mathbf{r})}^{S_l} + \overline{\hat{\mathbf{n}}\,(\boldsymbol{\omega}_l \times (\mathbf{r}-\mathbf{R}_l))}^{S_l} = \overline{\hat{\mathbf{n}}\,(\boldsymbol{\omega}_l \times (\mathbf{r}-\mathbf{R}_l))}^{S_l} \\ &= \frac{a_l}{4\pi}\int \hat{\mathbf{n}}\,(\boldsymbol{\omega}_l \times \hat{\mathbf{n}})\,dS = \frac{a_l\boldsymbol{\epsilon}\cdot\boldsymbol{\omega}_l}{4\pi}\int \hat{\mathbf{n}}\,\hat{\mathbf{n}}\,dS = \tfrac{1}{3}a_l\boldsymbol{\epsilon}\cdot\boldsymbol{\omega}_l \end{aligned} \tag{6.33}$$

where we used that the average containing the (constant) translational velocity vanishes. The fourth equality stems from writing out the cross product in terms of the rank three completely antisymmetric tensor $\boldsymbol{\epsilon}$ and pulling constant terms out in front of the integral. Again by virtue of the formal solution Eq. (6.14)

$$\begin{aligned} a_l\boldsymbol{\epsilon}\cdot\boldsymbol{\omega} = {}& \frac{3!!i}{(2\pi)^3}\sum_{j\in\text{beads}}\int d\mathbf{k}\,(\eta k^2)^{-1}\,\hat{\mathbf{k}}(\mathbf{1}-\hat{\mathbf{k}}\hat{\mathbf{k}})\cdot\mathbf{F}_j(\mathbf{k})\,e^{i\mathbf{k}\cdot(\mathbf{R}_l-\mathbf{R}_j)}\,j_1(ka_l) \\ &+ \frac{3!!i}{(2\pi)^3}\sum_{w\in\text{walls}}\int d\mathbf{k}\,(\eta k^2)^{-1}\,\hat{\mathbf{k}}\,(\mathbf{1}-\hat{\mathbf{k}}\hat{\mathbf{k}})\cdot\mathbf{F}_w(\mathbf{k})\,e^{i\mathbf{k}\cdot\mathbf{R}_l}\,j_1(ka_l) \end{aligned} \tag{6.34}$$

and expanding with Eqs. (6.18) and (6.21)

$$\begin{aligned} a_l\boldsymbol{\epsilon}\cdot\boldsymbol{\omega} = {}& (6\pi\eta a_l)^{-1}\mathsf{B}^{2\leftarrow 2}\odot\mathsf{F}_l^{(2)} + (6\pi\eta a_l)^{-1}\sum_{j\in\text{beads},j\neq l}\sum_{p=0}^{\infty}\mathsf{A}^{2\leftarrow p+1}\odot\mathsf{F}_j^{(p+1)} \\ &+ (6\pi\eta a_l)^{-1}\sum_{w\in\text{walls}}\sum_{n,m}\mathsf{U}_{lw}^{2\leftarrow(n,m)}\cdot\mathbb{F}_w(n,m) \end{aligned} \tag{6.35}$$

with

$$\mathsf{B}^{2\leftarrow 2} = \frac{3!!3}{8\pi^2}\int d\hat{\mathbf{k}}\,\hat{\mathbf{k}}(\mathbf{1}-\hat{\mathbf{k}}\hat{\mathbf{k}})\hat{\mathbf{k}}, \tag{6.36}$$

$$\mathsf{A}^{2\leftarrow p+1} = \frac{3ia_l 3!!(2p+1)!!}{8\pi^2}(-i)^p\int d\hat{\mathbf{k}}\int_{-\infty}^{\infty}dk\,\hat{\mathbf{k}}(\mathbf{1}-\hat{\mathbf{k}}\hat{\mathbf{k}})\,\overline{\hat{\mathbf{k}}^p}\,j_p(ka_j)j_1(ka_l), \tag{6.37}$$

$$\mathsf{U}_{iw}^{2\leftarrow(n,m)} = \frac{3ia_l 3!!}{4\pi^2}\int d\hat{\mathbf{k}}\int_0^{\infty}dk\,\hat{\mathbf{k}}\,(\mathbf{1}-\hat{\mathbf{k}}\hat{\mathbf{k}})\,(-i)^{n+m}e^{i(\mathbf{k}\cdot\mathbf{R}_l-k_wL_w)}\,j_n(k_{\underline{w}}L_{\underline{w}})\,j_m(k_{\overline{w}}L_{\overline{w}})\,j_1(ka_l). \tag{6.38}$$

6.3.3 Higher order velocity moments

As the particles are rigid, the higher velocity moments must vanish. For example,

$$\overline{\mathbf{u}(\mathbf{r})\,\overline{\hat{\mathbf{n}}\hat{\mathbf{n}}}}^{S_l} = 0, \tag{6.39}$$

which we express in terms of the surface multipole moments and the formal solution Eq. (6.14)

$$\begin{aligned}\overline{\overline{\overline{\overline{5!!\mathbf{u}(\mathbf{r})}^{S_l}\,\hat{\mathbf{n}}\hat{\mathbf{n}}}}} &= \frac{5!!i^2}{(2\pi)^3}\int d\mathbf{k}\,\overline{\hat{\mathbf{k}}\hat{\mathbf{k}}}\,\mathbf{u}(\mathbf{k})e^{i\mathbf{k}\cdot\mathbf{R}_l}\,j_2(ka_l)\\ &= (6\pi\eta a_l)^{-1}\frac{3i^2a_l\cdot 5!!}{8\pi^2}\Bigg[\int d\hat{\mathbf{k}}\int_{-\infty}^{\infty}dk\,\overline{\hat{\mathbf{k}}\hat{\mathbf{k}}}(\mathbf{1}-\hat{\mathbf{k}}\hat{\mathbf{k}})\cdot\mathbf{F}_l(\mathbf{k})\,j_2(ka_l)\\ &+\sum_{j\in\text{beads},j\neq i}\int d\hat{\mathbf{k}}\int_{-\infty}^{\infty}dk\,\overline{\hat{\mathbf{k}}\hat{\mathbf{k}}}(\mathbf{1}-\hat{\mathbf{k}}\hat{\mathbf{k}})\cdot\mathbf{F}_j(\mathbf{k})\,j_2(ka_l)e^{i\mathbf{k}\cdot(\mathbf{R}_l-\mathbf{R}_j)}\\ &+\sum_{w\in\text{walls}}2\int d\hat{\mathbf{k}}\int_0^{\infty}dk\,\overline{\hat{\mathbf{k}}\hat{\mathbf{k}}}\,(\mathbf{1}-\hat{\mathbf{k}}\hat{\mathbf{k}})\cdot\mathbf{F}_w(\mathbf{k})\,j_2(ka_l)e^{i\mathbf{k}\cdot\mathbf{R}_l}\Bigg]\end{aligned}\tag{6.40}$$

which with the aid of the expansion 6.18 becomes

$$0=-\mathsf{B}^{3\leftarrow 3}\odot\mathsf{F}_l^{(3)}+\sum_{j\in\text{beads},j\neq l}\sum_{p=0}^{\infty}\mathsf{A}^{3\leftarrow p+1}\odot\mathsf{F}_j^{(p+1)}+\sum_{w\in\text{walls}}\sum_{n,m}\mathsf{U}_{lw}^{3\leftarrow(m,n)}\cdot\mathbb{F}_w(n,m)\tag{6.41}$$

where

$$\mathsf{B}^{3\leftarrow 3}=-\frac{9\cdot 5!!}{8\pi}\int d\hat{\mathbf{k}}\,\overline{\hat{\mathbf{k}}\hat{\mathbf{k}}}(\mathbf{1}-\hat{\mathbf{k}}\hat{\mathbf{k}})\,\overline{\hat{\mathbf{k}}\hat{\mathbf{k}}}\tag{6.42}$$

$$\mathsf{A}_{lj}^{3\leftarrow p+1}=\frac{3i^2a_l5!!(2p+1)!!}{8\pi^2}i^p\int d\hat{\mathbf{k}}\int_{-\infty}^{\infty}dk\,\overline{\hat{\mathbf{k}}\hat{\mathbf{k}}}(\mathbf{1}-\hat{\mathbf{k}}\hat{\mathbf{k}})\,\overline{\hat{\mathbf{k}}^p}\,j_p(ka_l)j_2(ka_l)e^{i\mathbf{k}\cdot(\mathbf{R}_l-\mathbf{R}_j)}\tag{6.43}$$

$$\begin{aligned}\mathsf{U}_{lw}^{3\leftarrow(n,m)}=\frac{3i^2a_l\cdot 5!!}{4\pi^2}\int d\hat{\mathbf{k}}\int_0^{\infty}dk\,\overline{\hat{\mathbf{k}}\hat{\mathbf{k}}}\,(\mathbf{1}-\hat{\mathbf{k}}\hat{\mathbf{k}})\,(-i)^{n+m}e^{i(\mathbf{k}\cdot\mathbf{R}_l-k_wL_w)}\\ \times\; j_n(k_{\underline{w}}L_{\underline{w}})j_m(k_{\overline{w}}L_{\overline{w}})j_2(ka_l)\end{aligned}\tag{6.44}$$

These expressions can be generalized for higher order velocity moments, however, the structure of the expressions should be clear.

6.3.4 Walls

Finally, we need to take care of the boundary conditions at the walls. We have assumed that the walls are stationary such that no-slip implies that $\mathbf{u}(\mathbf{r})=0$ for all values of $\mathbf{r}$ lies on a wall. However, this needs to be translated into a condition on $\mathbf{u}(\mathbf{k})$. The condition that $\mathbf{u}(\mathbf{r})=0$ for all $\mathbf{r}$ on the wall corresponds to a uncountable number of conditions, one for each point on the wall. However, the wall is finite so we can write up a denumerable infinity of conditions by multiplying by a product Π of Legendre polynomials and the indicator function for the wall

$$\Pi=\frac{1}{4L_{\underline{v}}L_{\overline{v}}}P_N(\underline{v}/L_{\underline{v}})\,P_M(\overline{v}/L_{\overline{v}})\,\Omega(\underline{v}/L_{\underline{v}},\overline{v}/L_{\overline{v}})\,\delta(v-L_v)\tag{6.45}$$

for each pair of non-negative integers (N, M) and integrating

$$\begin{aligned} 0 &= \frac{1}{4L_{\underline{v}}L_{\overline{v}}} \int d\mathbf{r}\, P_N(\underline{v}/L_{\underline{v}})\, P_M(\overline{v}/L_{\overline{v}})\, \Omega(\underline{v}/L_{\underline{v}}, \overline{v}/L_{\overline{v}})\, \delta(v - L_v)\mathbf{u}(\mathbf{r}) \\ &= \frac{1}{4L_{\underline{v}}L_{\overline{v}}} \int d\mathbf{r} \int \frac{d\mathbf{k}}{(2\pi)^3}\, P_N(\underline{v}/L_{\underline{v}})\, P_M(\overline{v}/L_{\overline{v}})\, \Omega(\underline{v}/L_{\underline{v}}, \overline{v}/L_{\overline{v}})\, \delta(v - L_v)\, e^{i\mathbf{k}\cdot\mathbf{r}}\mathbf{u}(\mathbf{k}) \\ &= \int \frac{d\mathbf{k}}{(2\pi)^3}\, (-i)^{N+M} j_N(k_{\underline{v}}L_{\underline{v}})\, j_M(k_{\overline{v}}L_{\overline{v}})\, e^{ik_vL_v}\mathbf{u}(\mathbf{k}). \end{aligned} \tag{6.46}$$

We thus see that we need only specify N and M; as forseen the problem has been reduced to a denumerable number of conditions.

We now use the formal solution Eq. (6.14) to obtain

$$\begin{aligned} 0 = &\sum_{j\in\text{beads}} \int \frac{d\mathbf{k}}{(2\pi)^3}\, (-i)^{N+M}\, j_N(k_{\underline{v}}L_{\underline{v}}) j_M(k_{\overline{v}}L_{\overline{v}})(\eta k^2)^{-1}\, e^{i(k_vL_v - \mathbf{k}\cdot\mathbf{R}_j)}(\mathbf{1} - \hat{\mathbf{k}}\hat{\mathbf{k}})\cdot\mathbf{F}_j(\mathbf{k}) \\ + &\sum_{w\in\text{walls}} \int \frac{d\mathbf{k}}{(2\pi)^3}\, (-i)^{N+M}\, j_N(k_{\underline{v}}L_{\underline{v}}) j_M(k_{\overline{v}}L_{\overline{v}})(\eta k^2)^{-1}\, e^{ik_vL_v}(\mathbf{1} - \hat{\mathbf{k}}\hat{\mathbf{k}})\cdot\mathbf{F}_w(\mathbf{k}). \end{aligned} \tag{6.47}$$

Then we can use the previously derived expansions Eqs. (6.18) and (6.21) to arrive at

$$\begin{aligned} 0 = &\sum_{j\in\text{beads}} \sum_{p=0}^{\infty} \int \frac{d\mathbf{k}}{(2\pi)^3}\, \frac{(2p+1)!!(-i)^{p+N+M}}{\eta k^2}\, j_N(k_{\underline{v}}L_{\underline{v}})\, j_M(k_{\overline{v}}L_{\overline{v}})\, j_p(ka_l) \\ &\qquad \times e^{-i\mathbf{k}\cdot\mathbf{R}_j}(\mathbf{1} - \hat{\mathbf{k}}\hat{\mathbf{k}})\cdot\overline{\hat{\mathbf{k}}^p}\odot\mathsf{F}_j^{(p+1)} \\ + &\sum_{w\in\text{walls}} \int \frac{d\mathbf{k}}{(2\pi)^3}\, \frac{(-i)^{n+m+N+M}}{\eta k^2}\, j_N(k_{\underline{v}}L_{\underline{v}})\, j_M(k_{\overline{v}}L_{\overline{v}})\, j_n(k_{\underline{w}}L_{\underline{w}})\, j_m(k_{\overline{w}}L_{\overline{w}}) \\ &\qquad \times e^{i(k_vL_v - k_wL_w)}\, (\mathbf{1} - \hat{\mathbf{k}}\hat{\mathbf{k}})\cdot\mathbb{F}_w(n,m). \end{aligned} \tag{6.48}$$

This we also express in terms of connectors, this time $\tilde{\mathsf{U}}$ and V,

$$0 = \sum_{j\in\text{beads}} \sum_{p=0}^{\infty} \tilde{\mathsf{U}}_{vj}^{(N,M)\leftarrow p+1} \odot \mathsf{F}_j^{(p+1)} + \sum_{w\in\text{walls}} \sum_{n,m} \mathsf{V}_{vw}^{(N,M)\leftarrow(n,m)} \cdot \mathbb{F}_w(n,m). \tag{6.49}$$

These connectors take into account the influence of particles and other walls, respectively, on any wall v

$$\begin{aligned} \tilde{\mathsf{U}}_{vj}^{(N,M)\leftarrow p+1} = &\int \frac{d\mathbf{k}}{(2\pi)^3}\, \frac{(2p+1)!!(-i)^{N+M+p}}{\eta k^2}\, j_N(k_{\underline{v}}L_{\underline{v}})\, j_M(k_{\overline{v}}L_{\overline{v}})\, j_p(ka_l) \\ &\qquad \times e^{-i\mathbf{k}\cdot\mathbf{R}_j + ik_vL_v}(\mathbf{1} - \hat{\mathbf{k}}\hat{\mathbf{k}})\cdot\overline{\hat{\mathbf{k}}^p} \end{aligned} \tag{6.50}$$

$$\mathsf{V}_{vw}^{(N,M)\leftarrow(n,m)} = \int \frac{d\mathbf{k}}{(2\pi)^3} \frac{(-i)^{n+m+N+M}}{\eta k^2} j_N(k_{\underline{v}} L_{\underline{v}})\, j_M(k_{\overline{v}} L_{\overline{v}})\, j_n(k_{\underline{w}} L_{\underline{w}})\, j_m(k_{\overline{w}} L_{\overline{w}}) \times e^{i(k_v L_v - k_w L_w)} (\mathbf{1} - \hat{\mathbf{k}}\hat{\mathbf{k}}). \quad (6.51)$$

As the connectors A and U had simple interpretations so do the connectors $\tilde{\mathsf{U}}_{vj}^{(N,M)\leftarrow p+1}$ and $\mathsf{V}_{vw}^{(N,M)\leftarrow(n,m)}$. The former is the coupling of the pth force multipole on the jth particle to the (N,M)-term of the would-be velocity of the immobile wall v; the latter is the coupling from the (n,m)-term of the expansion of induced forces at the wall w.

6.4 Solution procedure

Before proceeding any further, it is beneficial to get an overview of the structure of the problem. We are setting up a system of linear equations, Eqs. (6.30), (6.35), (6.41) and (6.49), that couple the externally applied forces $\mathbf{F}_l^{\text{ext}}$ and torques $\mathbf{T}_l^{\text{ext}}$ on particles l enclosed in a rectangular box to the translational and rotational velocities of the particles. These equations involve expansions of the forces on the particles and the walls and the couplings between them. To proceed, we truncate the expansions at some order and calculate the couplings, the so-called connectors, between the terms in the expansions.

In the following, we restrict ourselves to the very simplest case of a single particle at the center of a cube with sides $2L_x = 2L_y = 2L_z = 2$ and only the lowest multipole moment of force for the spherical particle and the $(0,0)$-force term for each of the walls. Evaluation of the connectors is not easy but it turns out that the integrals can be found in closed form for the radial integration when they are written in polar coordinates as we have done above, leaving the angular integrations to numerical methods. We will not pause to write out the quite complicated intermediate results, however, for our particular instance the Us, $\tilde{\mathsf{U}}$s and Vs can be determined.

To lowest order and with one particle and six walls we have seven equations, seven unknowns and one free parameter, the external force on the particle. The unknowns are the forces on the walls and the translational velocity of the particle. These equations can be rewritten in the form

$$\begin{pmatrix} \mathbf{v} \\ 0 \\ 0 \\ 0 \\ 0 \\ 0 \\ 0 \end{pmatrix} = (6\pi\eta a)^{-1} \begin{pmatrix} \mathbf{1} & \mathsf{U}_{+x} & \mathsf{U}_{-x} & \mathsf{U}_{+y} & \mathsf{U}_{-y} & \mathsf{U}_{+z} & \mathsf{U}_{-z} \\ \tilde{\mathsf{U}}_{+x} & \mathsf{V}_{+x+x} & \mathsf{V}_{+x-x} & \mathsf{V}_{+x+y} & \mathsf{V}_{+x-y} & \mathsf{V}_{+x+z} & \mathsf{V}_{+x-z} \\ \tilde{\mathsf{U}}_{-x} & \mathsf{V}_{-x+x} & \mathsf{V}_{-x-x} & \mathsf{V}_{-x+y} & \mathsf{V}_{-x-y} & \mathsf{V}_{-x+z} & \mathsf{V}_{-x-z} \\ \tilde{\mathsf{U}}_{+y} & \mathsf{V}_{+y+x} & \mathsf{V}_{+y-x} & \mathsf{V}_{+y+y} & \mathsf{V}_{+y-y} & \mathsf{V}_{+y+z} & \mathsf{V}_{+y-z} \\ \tilde{\mathsf{U}}_{-y} & \mathsf{V}_{-y+x} & \mathsf{V}_{-y-x} & \mathsf{V}_{-y+y} & \mathsf{V}_{-y-y} & \mathsf{V}_{-y+z} & \mathsf{V}_{-y-z} \\ \tilde{\mathsf{U}}_{+z} & \mathsf{V}_{+z+x} & \mathsf{V}_{+z-x} & \mathsf{V}_{+z+y} & \mathsf{V}_{+z-y} & \mathsf{V}_{+z+z} & \mathsf{V}_{+z-z} \\ \tilde{\mathsf{U}}_{-z} & \mathsf{V}_{-z+x} & \mathsf{V}_{-z-x} & \mathsf{V}_{-z+y} & \mathsf{V}_{-z-y} & \mathsf{V}_{-z+z} & \mathsf{V}_{-z-z} \end{pmatrix} \begin{pmatrix} \mathbf{F}^{\text{ext}} \\ \mathbb{F}_{+x} \\ \mathbb{F}_{-x} \\ \mathbb{F}_{+y} \\ \mathbb{F}_{-y} \\ \mathbb{F}_{+z} \\ \mathbb{F}_{-z} \end{pmatrix} \quad (6.52)$$

where all the entries in the matrix are three-by-three tensors and the components of the column vectors are three-vectors. The indicies indicate walls whereas the superfluous index for the particle has been suppressed. The form of this system of equations is a little unusual in that there are unknowns on either side of the equality. In block form, Eq. (6.52)

looks like

$$\begin{pmatrix} \mathbf{v} \\ \underline{0} \end{pmatrix} = (6\pi\eta a)^{-1} \begin{pmatrix} \mathbf{1} & \underline{\mathsf{U}} \\ \underline{\tilde{\mathsf{U}}} & \underline{\underline{\mathsf{V}}} \end{pmatrix} \begin{pmatrix} \mathbf{F}^{\text{ext}} \\ \underline{\mathbb{F}} \end{pmatrix} \tag{6.53}$$

where we have grouped the various blocks in the matrix in Eq. (6.52) into the 1×6 matrix $\underline{\mathsf{U}}$, the 6×6 matrix $\underline{\underline{\mathsf{V}}}$ and the 6×1 matrix $\underline{\tilde{\mathsf{U}}}$. We solve for $\mathbf{v}$ as

$$\mathbf{v} = (6\pi\eta a)^{-1} \left[\mathbf{1} - (\underline{\mathsf{U}}\, \underline{\underline{\mathsf{V}}}^{-1}\, \underline{\tilde{\mathsf{U}}}) \right] \mathbf{F}^{\text{ext}}. \tag{6.54}$$

The linear relationship between the force applied to the particle and its velocity lets us interpret

$$\mathsf{b} = (6\pi\eta a)^{-1} \left(\mathbf{1} - \underline{\mathsf{U}}\, \underline{\underline{\mathsf{V}}}^{-1}\, \underline{\tilde{\mathsf{U}}} \right) \tag{6.55}$$

as the mobility tensor for a spherical particle alone in a box.

6.4.1 An application

Let us further specialize the above by calculating the Us and Vs in a concrete example. We are going to consider the mobility of a single spherical particle of dimensionless radius 0.1 at the center of the cube with sides of length 2 in dimensionless units. This must be the simplest practically relevant case as we truncate all expansions retaining only the lowest order terms.

Because of symmetries, we only need to calculate one form of the U and three types of Vs corresponding to the connector of a wall onto itself, from a wall to the wall opposite, and from a wall to either of its four adjacent walls. The connectors U and $\tilde{\mathsf{U}}$ differ only in numerical factors.

The $\mathsf{U}_{+z}^{1\leftarrow(0,0)}$-connector is found by a combination of symbolic radial integration and numerical integration of the angular part as in Eq. (6.32). However, writing the integral out in Cartesian coordinates in *lieu* of polar as we did, makes it apparent that $\mathsf{U}_{+z}^{1\leftarrow(0,0)}$ must be diagonal which is not so surprising as this means that a force on a wall in some direction along the box axes causes the particle to move in the same direction. This reduces the calculation task somewhat. We have

$$\mathsf{U}_{+z}^{1\leftarrow(0,0)} \approx \frac{3 \cdot 0.1}{4\pi^2} \begin{pmatrix} 73.4 & 0 & 0 \\ 0 & 73.4 & 0 \\ 0 & 0 & 103.2 \end{pmatrix}. \tag{6.56}$$

Notice that the two first are identical as expected from symmetry; the particle being at the center of the cube is also symmetrically placed with respect to either of the walls. Also note that the term corresponding to a force perpendicular to the wall is approximately $\sqrt{2}$-times bigger than the two other entries. The reason for this has not been found.

The expression for $\mathsf{U}_{-z}^{1\leftarrow(0,0)}$ is identical and the ones for $\mathsf{U}_{+x}^{1\leftarrow(0,0)}$, $\mathsf{U}_{-x}^{1\leftarrow(0,0)}$, $\mathsf{U}_{+y}^{1\leftarrow(0,0)}$ and $\mathsf{U}_{-y}^{1\leftarrow(0,0)}$ are found by suitable rotations.

The lowest order connector from a wall onto itself can be found in closed form

$$\mathsf{V}_{+z\,+z}^{(0,0)\leftarrow(0,0)} = \frac{16\pi^2}{3} \left[1 - \sqrt{2} + 3\ln(1+\sqrt{2}) \right] \begin{pmatrix} 1 & 0 & 0 \\ 0 & 1 & 0 \\ 0 & 0 & 2 \end{pmatrix} \approx \begin{pmatrix} 117.4 & 0 & 0 \\ 0 & 117.4 & 0 \\ 0 & 0 & 234.8 \end{pmatrix}, \tag{6.57}$$

and from this the five others are readily found through rotations as above.

The remaining two types of connectors were also found by means of a combination of symbolic and numeric integration. The opposing walls connector is

$$\mathsf{V}^{(0,0)\leftarrow(0,0)}_{-z\,+z} \approx \begin{pmatrix} 119.7 & 0 & 0 \\ 0 & 119.7 & 0 \\ 0 & 0 & 119.7 \end{pmatrix}, \tag{6.58}$$

and the connector between the adjacent walls at $+L_z$ and $+L_y$ is

$$\mathsf{V}^{(0,0)\leftarrow(0,0)}_{+y\,+z} \approx \begin{pmatrix} 131.6 & 0 & 0 \\ 0 & 147.2 & 0 \\ 0 & 0 & 147.2 \end{pmatrix} \tag{6.59}$$

where the remaining connectors can be found from suitable rotations.

With all the elements determined, the mobility tensor for a particle with radius 0.1 placed at the centre of a cubic microchannel is found from Eq. (6.55)

$$\mathsf{b} = 0.130\,(6\pi\eta a)^{-1}\mathbf{1} \tag{6.60}$$

where we note that it is about a factor of seven smaller than the value for a particle in unbounded fluid and that it is isotropic as we would expect from the symmetry of the problem. However, we should not over-emphasize the actual numerical value of the mobility as the work of Mazur [31, 32] shows dramatical "non-additivity" of hydrodynamic interactions and that in the case of no container and many particles it is essentially never permissible to neglect many-particle interactions at least as far as three-particle interactions and something similar might hold true for our truncation of the various force and velocity expansions. Furthermore, we lack in this problem a "small parameter" in which we can develop these expansions except, perhaps, for the particle radius. The arbitrary but convenient truncation of the expansions that we have employed does not afford any control over the error thus committed.

All this said, we can compare with known results for a *spherical* container with a particle at its centre [4]. The mobility of a spherical particle of radius a_i in a sphere of radius A is

$$b = \left(1 - \frac{9a_i}{4A} + \frac{5a_i^3}{2A^3}\right)(6\pi\eta a)^{-1}\,\mathbf{1}. \tag{6.61}$$

Inserting an outer sphere radius $A = 1$ and a particle radius of $a_i = 0.1$, we find the mobility

$$b = 0.7775\,(6\pi\eta a)^{-1}\,\mathbf{1} \tag{6.62}$$

which is quite different from the value calculated in the case of a cubic geometry. Naturally, we are comparing two different physical arrangements, however, it seems reasonable that the errors committed in truncating the expansions are the dominant ones.

One can imagine a number of tests of our approach. We could compare results from our method applied to the case of one single plane wall with exact results calculated from the Lorentz method of reflecting the solution to the flow problem in unbounded fluid in an infinite plane wall [42, 5, 22]. Also, one could compare with results for rotational mobility instead of translational in a spherical geometry for which exact results are known [26, 27]. Regardless, it seems valuable to include in the analysis contributions to higher orders.

6.5 Outlook

The promise of the method for plane walls developed herein is that it can be extended systematically and that its application is not limited to a regular shape such as a cube or a sphere. It would be straightforward to decompose a complicated microchannel geometry into rectangular, plane walls and then calculate the necessary connectors between any reasonable number of particles and the walls up to some order that is deemed sufficient from the nature of the problem considered. At the moment, the calculation of the connectors is quite tedious and it has not been possible to find explicit or closed form formulas for any but a few, however, it should not be ruled out that this is possible. The methods used for similar problems today, the motion of particles in a so-called bumper array, are based on the solution of differential equations by, for example, the finite element method, however, only in two-dimensions. The method of induced forces is not restricted to two-dimensions by constraints of computing power, especially if explicit expressions for the connectors can be found.

Another, more adventurous, path to tread is to try to extend the method to elliptical or even thin cylindrical particles. This might be significantly more challenging technically to carry out, however, not all interesting objects flowing in a microfluidic channel are round. There could easily be interesting phenomena to explore in the tumbling of an elliptical polymer bead or the motion of a rigid essentially one-dimensional molecule such as xanthane or guar gum or maybe a carbon nanotube.

In this chapter we have only outlined the method and there would be the need for further refinements as pointed out and especially the need for some striking predictions and experiments to test them. Let us speculate, that it could be possible by meaning of a non-invasive technique such as optical tweezers to actually measure the hydrodynamic interaction forces between glass or polymer beads and nearby walls. A study of this could be interesting and worthy of a PhD-project in itself. Maybe the induced force method could find a niche of its own as the “house” method of choice for particles in microfluidic systems.

Chapter 7

Summary and outlook

In the preceding five chapters, we have explored aspects of the physics of magnetic beads in microfluidic channels. Surprisingly, hydrodynamic interactions seem to have a more profound influence on the motion of microscopic beads than their mutual magnetic interaction. The influence of a bead moving relative to the surrounding fluid creates a disturbance to the flow that we have interpreted as a hydrodynamic interaction between the beads and this interaction is seen to decay as bead separation to the power -1. The leading magnetic interaction term decays much faster, as separation to the power -3, than the hydrodynamic one. This is the most important and simplest observation made above.

It means that except in the very simplest descriptions of magnetic bead capture or motion, hydrodynamic interactions should not be left out. We went on to illustrate this point through computer simulations where in certain situations the presence or absence of hydrodynamic interactions made all the difference to the workings of the model magnetic bead separator. Admittedly, while nicely illustrating a point, the circumstances were somewhat concocted so a fairer and random set of initial conditions was compared on the basis of the time taken for a varying number of magnetic beads to be captured in the presence and absence of hydrodynamic interactions. As expected from the notion of hydrodynamic interactions helping beads move collectively, an increasing speed-up in the interacting case is seen over the non-interacting case as bead number increases.

The methods employed have been rather *ad hoc* and the Green's function approach has left something to be desired in terms of handling more than a few beads and in handling more complicated channel geometries. It has provided us with the key insight of the slow decay of interactions with bead separation but does not go so well with numerical simulations. Two paths have then been laid out: One is treating the bead distribution as a field in its own right, coupling it with the fluid equations of motion, and solving the resulting equations numerically. The other is an analytical one in which a systematic machinery for treating bead motion in arbitrary geometries has been outlined. The latter hints at an approach that could be extended to a proper many-particle theory of spherical particles in a fluid confined in arbitrary geometries. This prospect seems the most exciting prospect to be hinted to from this work. The careful study of many-particle effects has been most rewarding in so many other branches of physics that this should be worthy of

consideration here as well.

Many-particle physics is a grand enterprise but a much more modest one could also be interesting. We pointed out that it is possible to manipulate microscopic beads with optical tweezers and the technique allows not just manipulation of many beads simultaneously (see for example Ref. [18]) but also the measurement of the forces involved. This could be used to measure forces on beads moving near walls or near one another and systematically compare this with predictions derived from the method of induced forces. This would not warrant bold extensions of the theory developed herein and the significant agility of modern optical tweezer methods would make this idea not just interesting and worthwhile but also realistic.

Appendix A

Field from sphere in pure dipole fields: x and y-dipoles

In section 2.3 we calculated the magnetization and in particular the potential of a magnetic sphere with permeability μ of radius a in the field from a point dipole at a distance s in the z-direction. However, we only considered the case of a dipole oriented along the z-direction as this case is a little less complicated.

In this appendix, we treat the more involved but analogous cases of dipoles oriented along the x and y-directions. The derivation is elaborated in a fair amount of detail to make checking easier.

A.1 Dipole along the x-direction

Here we jump in at Eq. (2.28) where we differentiate with respect to x instead of z as this is dipole we want now,

$$\frac{\partial}{\partial x}\frac{1}{r_s} = \frac{1}{s}\sum_n \left(P_n(\cos\theta)\,\frac{n}{s}\Big(\frac{r}{s}\Big)^{n-1}\frac{\partial r}{\partial x} + P_n'(\cos\theta)\,(-\sin\theta)\Big(\frac{r}{s}\Big)^n\frac{\partial\theta}{\partial x}\right) \tag{A.1}$$

Looking at the first term in the sum

$$P_n(\cos\theta)\frac{n}{r}\Big(\frac{r}{s}\Big)^n \sin\theta\cos\phi. \tag{A.2}$$

and the second term

$$\frac{n\cos\theta\cos\phi}{r\sin\theta}\Big(\cos\theta\,P_n(\cos\theta) - P_{n-1}(\cos\theta)\Big)\Big(\frac{r}{s}\Big)^n. \tag{A.3}$$

Combining the terms in the sum gives us

$$\frac{\partial}{\partial x}\frac{1}{r_s} = \frac{1}{s}\sum_n \frac{n}{r}\frac{\cos\phi}{\sin\theta}\Big(\frac{r}{s}\Big)^n\Big(P_n(\cos\theta) - \cos\theta\,P_{n-1}(\cos\theta)\Big). \tag{A.4}$$

or by order of multipoles

$$\frac{\partial}{\partial x}\frac{1}{r_s} = \frac{1}{s}\frac{\cos\phi}{r\sin\theta}\sum_n P_n(\cos\theta)\left(\frac{r}{s}\right)^n\Big(n-(n+1)\frac{r\cos\theta}{s}\Big). \tag{A.5}$$

We write up the general expression of the magnetic scalar potential like this

$$\psi_{\text{in}} = \sum_n A_n r^n\, P_n(\cos\theta) \tag{A.6}$$

$$\psi_{\text{ex}} = \sum_n B_n\frac{P_n(\cos\theta)}{r^{n+1}} + \frac{m_x}{4\pi}\,\frac{\partial}{\partial x}\frac{1}{r_s} \tag{A.7}$$

$$= \sum_n \left(B_n\frac{1}{r^{n+1}} + \frac{m_x}{4\pi s}\,\frac{\cos\phi}{r\sin\theta}\Big(\frac{r}{s}\Big)^n\Big(n-(n+1)\frac{r\cos\theta}{s}\Big)\right)P_n(\cos\theta). \tag{A.8}$$

First, we use the condition of continuity of potentials

$$A_n = \left(\frac{B_n}{a^{2n+1}} + \frac{m_x}{4\pi s}\,\frac{\cos\phi}{a\sin\theta}\frac{1}{s^n}\Big(n-(n+1)\frac{a\cos\theta}{s}\Big)\right). \tag{A.9}$$

The second condition depends on derivatives of the potentials, in particular that of ψ_{ex},

$$\frac{\partial\psi_{\text{ex}}}{\partial r} = \sum_n P_n(\cos\theta)\Bigg(-(n+1)\frac{B_n}{r^{n+2}} + \frac{m_x}{4\pi s^2}\,\frac{\cos\phi}{\sin\theta}\Big(\frac{r}{s}\Big)^{n-1} n\Big(\frac{n-1}{r}-(n+1)\frac{\cos\theta}{s}\Big)\Bigg). \tag{A.10}$$

Applying the condition yields

$$A_n = \frac{\mu_{\text{o}}}{\mu}\left\{-\frac{n+1}{n}\frac{B_n}{a^{2n+1}} + \frac{m_x}{4\pi s}\frac{\cos\phi}{\sin\theta}\frac{1}{s^n}\left(\frac{n-1}{a}-(n+1)\frac{\cos\theta}{s}\right)\right\} \tag{A.11}$$

We can now find B_n

$$B_n \;=\; -a^{2n+1}\frac{n\mu}{n\mu+\mu_{\text{o}}(n+1)}\frac{m_x}{4\pi s}\frac{\cos\phi}{\sin\theta}\frac{1}{s^n}\left(\Big(1-\frac{\mu_{\text{o}}}{\mu}\Big)\Big(\frac{n}{a}-\frac{\cos\theta}{s}(n+1)\Big)+\frac{1}{a}\frac{\mu_{\text{o}}}{\mu}\right) \tag{A.12}$$

A.2 Dipole along the y-direction

Carrying out the exact same programme for y,

$$\frac{\partial}{\partial y}\frac{1}{r_s} = \frac{1}{s}\sum_n\left(P_n(\cos\theta)\frac{n}{s}\Big(\frac{r}{s}\Big)^{n-1}\frac{\partial r}{\partial y} + P_n'(\cos\theta)(-\sin\theta)\Big(\frac{r}{s}\Big)^n\frac{\partial\theta}{\partial y}\right) \tag{A.13}$$

Looking at the first term in the sum

$$P_n(\cos\theta)\frac{n}{r}\Big(\frac{r}{s}\Big)^n\sin\theta\,\sin\phi \tag{A.14}$$

and the second term

$$P_n(\cos\theta)\Big(\frac{r}{s}\Big)^n \frac{n\cos^2\theta\,\sin\phi}{r\sin\theta} - P_{n-1}(\cos\theta)\Big(\frac{r}{s}\Big)^n \frac{n\cos\theta\,\sin\phi}{r\sin\theta}. \tag{A.15}$$

Combining the terms in the sum gives us

$$\frac{\partial}{\partial y}\frac{1}{r_s} = \frac{1}{s}\frac{\sin\phi}{r\sin\theta}\sum_n n\Big(\frac{r}{s}\Big)^n \big(P_n(\cos\theta) - \cos\theta\, P_{n-1}(\cos\theta)\big) \tag{A.16}$$

which can be sorted by the order of Legendre polynomials

$$\frac{\partial}{\partial y}\frac{1}{r_s} = \frac{1}{s}\frac{\sin\phi}{r\sin\theta}\sum_n \Big(\frac{r}{s}\Big)^n P_n(\cos\theta)\big(n-(n+1)\frac{r\cos\theta}{s}\big). \tag{A.17}$$

We write up the general expression of the magnetic scalar potential like this

$$\psi_{\text{in}} = \sum_n A_n r^n\, P_n(\cos\theta) \tag{A.18}$$

$$\psi_{\text{ex}} = \sum_n B_n \frac{P_n(\cos\theta)}{r^{n+1}} + \frac{m_y}{4\pi}\,\frac{\partial}{\partial y}\frac{1}{r_s} \tag{A.19}$$

$$= \sum_n \left(B_n \frac{1}{r^{n+1}} + \frac{m_y}{4\pi s}\,\frac{\sin\phi}{r\sin\theta}\Big(\frac{r}{s}\Big)^n \Big(n-(n+1)\frac{r\cos\theta}{s}\Big)\right) P_n(\cos\theta). \tag{A.20}$$

First, we use the condition of continuity of potentials

$$A_n = \frac{B_n}{a^{2n+1}} + \frac{m_y}{4\pi s}\frac{\sin\phi}{\sin\theta}\frac{1}{s^n}\Big(\frac{n}{a} - (n+1)\frac{\cos\theta}{s}\Big). \tag{A.21}$$

The second condition depends on derivatives of the potentials, in particular that of ψ_{ex},

$$\frac{\partial\psi_{\text{ex}}}{\partial r} = \sum_n \left(-(n+1)\frac{B_n}{r^{n+2}} + \frac{m_y}{4\pi s}\frac{\sin\phi}{\sin\theta}\frac{n}{r}\Big(\frac{r}{s}\Big)^n\Big(\frac{n-1}{r} - (n+1)\frac{\cos\theta}{s}\Big)\right) P_n(\cos\theta). \tag{A.22}$$

Applying the condition yields

$$A_n = \frac{\mu_{\text{o}}}{\mu}\left\{-\frac{n+1}{n}\frac{B_n}{a^{2n+1}} + \frac{m_y}{4\pi s}\frac{\sin\phi}{\sin\theta}\frac{1}{s^n}\Big(\frac{n-1}{a} - (n+1)\frac{\cos\theta}{s}\Big)\right\} \tag{A.23}$$

We can now find B_n

$$0 = \frac{B_n}{a^{2n+1}}\Big(1+\frac{\mu_{\text{o}}}{\mu}\frac{n+1}{n}\Big) + \frac{m_y}{4\pi s}\frac{\sin\phi}{\sin\theta}\frac{1}{s^n}\left(\Big(1-\frac{\mu_{\text{o}}}{\mu}\Big)\Big\{\frac{n}{a} - (n+1)\frac{\cos\theta}{s}\Big\} + \frac{1}{a}\frac{\mu_{\text{o}}}{\mu}\right) \tag{A.24}$$

Appendix B

Implementation in Matlab

In order to carry out the overall programme, we need a set of Matlab programmes. The magnetostatic and hydrodynamical problems can readily be solved by the finite element solver, FEMlab.

The contents of this section mostly serves to document central parts of the Matlab routines that calculates trajectories. The actual routines have some embellishments that makes them work faster. There is also a bit of housekeeping code.

We need to solve an ordinary differential equation and to that end we need to supply the time-derivative of position, the velocity. In the approximation, we made before we assume that there is no inertia. The velocity of a particle will become equal to that of the liquid immediately if the external force vanishes because we have from above

$$\mathbf{u}_a = \mathbf{v}(\mathbf{r}_a) + \frac{\mathbf{F}_a}{6\pi\eta a} \tag{B.1}$$

or as Matlab-code for two particles:

```
drdt(1) = v1x + F1x/(6*pi*eta*a);
drdt(2) = v1y + F1y/(6*pi*eta*a);
drdt(3) = v2x + F2x/(6*pi*eta*a);
drdt(4) = v2y + F2y/(6*pi*eta*a);
```

We need to calculate two things first: the flow velocity at the position of the ath particle, $\mathbf{v}(\mathbf{r}_a)$, and the force on the ath particle, $\mathbf{F}_a$. We will take them each in turns, first the fluid flow.

The velocity field in the fluid is determined by several points. Primarily by the Poiseuille flow that either comes from the result of a FEMlab calculation or from a parabolic approximation and the from the flow due to the companion particle,

```
v1x = Umax * postinterp(fem,'u',[sign(x1)*x1;sign(-y1)*y1]);
v1y = Umax * postinterp(fem,'v',[sign(x1)*x1;sign(-y1)*y1]) * sign(-y1);
v2x = Umax * postinterp(fem,'u',[sign(x2)*x2;sign(-y2)*y2]);
v2y = Umax * postinterp(fem,'v',[sign(x2)*x2;sign(-y2)*y2]) * sign(-y2);
```

or if we use the parabolic approximation

```
v1x = Umax * 1000 * (1-(x1/50)^2);
v1y = 0;
v2x = Umax * 1000 * (1-(x2/50)^2);
v2y = 0;
```

The flow due to neighbouring particles is found like this

$$\mathbf{u}_a = \mathbf{v}(\mathbf{r}_a) + \frac{1}{8\pi\eta}\mathbf{G}^W(\mathbf{r}, \mathbf{r}_{\not a}) \cdot \mathbf{F}_{\not a} \qquad \text{where} \qquad \text{(B.2)}$$

$$\mathbf{F}_{\not a} = 2\pi\mu_o a^3 \frac{\chi}{\chi+3} \boldsymbol{\nabla} H^2_{\text{ext}} \qquad \text{and} \qquad \text{(B.3)}$$

$$\boldsymbol{\nabla} H^2_{\text{ext}} = (\partial_y A\ \partial_{xy} A - \partial_x A\ \partial_{yy} A, -\partial_y A\ \partial_{xx} A + \partial_x A\ \partial_{yx} A) \qquad \text{in 2D} \qquad \text{(B.4)}$$

where $\not a$ is a short hand for the *other* particle, i.e. not particle a. This is translated into the following code

```
F1x = 2*pi*mu0 * a^3 * (chi/(chi+3)) * DHH(r(1), r(2), 'x', Hext);
F1y = 2*pi*mu0 * a^3 * (chi/(chi+3)) * DHH(r(1), r(2), 'y', Hext);
F2x = 2*pi*mu0 * a^3 * (chi/(chi+3)) * DHH(r(3), r(4), 'x', Hext);
F2y = 2*pi*mu0 * a^3 * (chi/(chi+3)) * DHH(r(3), r(4), 'y', Hext);

h = -50;

% Force component parallel with wall due to particle 2
v1x = v1x + Wall(x1-x2, y1-y2, y2-h,'para','x') * F2x / (8*pi*eta);
v1y = v1y + Wall(x1-x2, y1-y2, y2-h,'para','y') * F2x / (8*pi*eta);

% Force component perpendicular with wall due to particle 2
v1x = v1x + Wall(y1-y2, x1-x2, y2-h,'perp','x') * F2y / (8*pi*eta);
v1y = v1y + Wall(y1-y2, x1-x2, y2-h,'perp','y') * F2y / (8*pi*eta);

% Force component parallel with wall due to particle 1
v2x = v2x + Wall(x2-x1, y2-y1, y1-h,'para','x') * F1x / (8*pi*eta);
v2y = v2y + Wall(x2-x1, y2-y1, y1-h,'para','y') * F1x / (8*pi*eta);

% Force component perpendicular with wall due to particle 1
v2x = v2x + Wall(y2-y1, x2-x1, y1-h,'perp','x') * F1y / (8*pi*eta);
v2y = v2y + Wall(y2-y1, x2-x1, y1-h,'perp','y') * F1y / (8*pi*eta);
```

Maybe a few words on the symmetry of this problem would be in place. We have chosen to solve the hydrodynamical and the magnetostatic problem in the fourth quadrant, i.e. the values of x are positive whereas y are negative. This is because we assume that the structure is taken to be periodic in the x-direction with a period of 50μm and symmetric around the center so that we only need to model an x-domain of 25μm. We take the center of the channel to be the x-axis and this, thus, becomes a symmetry plane as well.

We can then, and indeed must, enlarge our domain by reflecting points from the greater rectangular domain defined by the corner points $(-25\mu\text{m}, -50\mu\text{m})$ and $(+25\mu\text{m}, +50\mu\text{m})$ down to the fourth quadrant. This is conveniently done by multiplying by the sign of x and $-y$.

The `drdt` is then encapsuled in a function `trajectory` that is sent to a built-in Matlab solver for ordinary differential equations `ode45`

```
track  = ode45(@trajectory,[0 t_end],[x1; y1; x2; y2],[],f,Hext,Umax,0,r_part);
```

which returns an object `track` from which we extract positions `x` at the times `t`

```
t = 0:25e-4:t_end;
x = deval(track, t);
```

The function `deval` evaluates the `track` object returning the bead positions that can subsequently be plotted together with the channel geometry and magnetic field.

Appendix C

Paper published in J. Magn. Magn. Mater.

Title
Theoretical comparison of magnetic and hydrodynamic interactions between magnetically tagged particles in microfluidic systems

Authors
Christian Mikkelsen, Mikkel Fougt Hansen and Henrik Bruus

Reference
J. Magn. Magn. Mater. **293**, 578–83, (2005)

Available online at www.sciencedirect.com
SCIENCE DIRECT®
ELSEVIER
Journal of Magnetism and Magnetic Materials 293 (2005) 578–583
Journal of magnetism and magnetic materials
www.elsevier.com/locate/jmmm

Theoretical comparison of magnetic and hydrodynamic interactions between magnetically tagged particles in microfluidic systems

Christian Mikkelsen*, Mikkel Fougt Hansen, Henrik Bruus

MIC—Department of Micro and Nanotechnology, Technical University of Denmark, DTU-Building 345 East, DK-2800 Lyngby, Denmark

Available online 7 March 2005

Abstract

Magnetic and hydrodynamic interactions between magnetic beads in microfluidic magnetic field gradient filters are compared theoretically and we find that the hydrodynamic interactions are of a longer range and dominate the magnetic ones. Hydrodynamic interactions aid the capturing of particles tagged with magnetic beads as the particles drag each other along, possibly easing requirements on magnetic parameters.

PACS: 85.70.Ay; 47.15.Pn; 47.60.+i; 47.11.+j

Keywords: Microfluidics; Capturing of magnetic beads; Magnetic interaction; Hydrodynamic interaction; Simulation; Drag; Magnetic field; FEMLAB software

1. Introduction

A promising application for magnetic carriers is in lab-on-a-chip and microfluidic systems where specifically functionalized magnetic beads can bind to and single out biomolecules or cells making up tagged composite particles. These particles can then be manipulated by means of magnetic fields. This is being done routinely in macroscopic applications (high-gradient magnetic separation) but potentially is very useful in miniaturized systems.

The technique has been pioneered by Ahn [1] in microfluidics and can be used to separate, filter, and retain species bound to magnetic beads. In laboratory procedures, separation, purification, and filtering steps are crucial and it is an important challenge for lab-on-a-chip development to find viable methods that can be incorporated into microfluidic chips.

Magnetic filtering of beads is done by magnetophoresis where forces arise due to the

*Corresponding author. Tel.: +45 4525 5788; fax: +45 4588 7762.
E-mail address: cmik@mic.dtu.dk (C. Mikkelsen).

0304-8853/$ - see front matter © 2005 Published by Elsevier B.V.
doi:10.1016/j.jmmm.2005.01.076

inhomogeneous magnetic field created by microstructures that are magnetized by either electromagnets or a permanent magnet. The structures are small so that they make large gradients and if they are made by a soft magnetic material such as permalloy [1] or nickel [2], the gradients vanish as the external field is removed. Thus, it is possible to capture and release particles, and in turn cells or biomolecules, at will. This can then be combined with washing and rinsing steps, making up a specialized laboratory on a single chip.

To design a working system that can be used to manipulate magnetic beads effectively and efficiently, it is important to understand the capturing process. Magnetic beads obviously interact magnetically but here we bring to attention the fact that the beads also influence each other through the motion of the fluid in which they are suspended. In the following, we will introduce the magnetic and hydrodynamic (fluid-mediated) interactions before discussing their relative importance.

We wish to highlight the importance of hydrodynamic interactions in connection with bead capturing. Although the importance of such interactions is acknowledged in the chemical engineering literature in connection with the settling of particle suspensions (see for example [3]), it appears to be overlooked in the context of magnetophoresis. In our opinion, this should be addressed as hydrodynamic interactions can be shown to be important on the basis of general theoretical arguments, Sections 2 and 3. A specific example of this is the illustrative simulation featured in Section 4. Hopefully, these observations can stimulate experimental work investigating the effects of hydrodynamic interactions.

2. Magnetic interaction

Magnetophoresis is the phenomenon that the gradient of a magnetic field gives rise to motion of some object due to a force on the magnetic moment induced by, for example, the same field. The induced magnetic moments also give rise to their own magnetic fields and they can thus interact.

When magnetizable objects (such as superparamagnetic beads) are immersed in an inhomogeneous external magnetic field, $\vec{H}_{\text{ext}}$, they are attracted to magnetic field extrema (maxima) as the field gradient acts with a force [4]

$$\vec{F} = \mu_0 \int (\vec{M} \cdot \vec{\nabla}) \vec{H}_{\text{ext}} \, \mathrm{d}V, \tag{1}$$

where $\vec{M}$ is the magnetization of the object and where we have assumed that the surrounding medium is non-magnetic with the permeability of vacuum.

The presence of magnetizable objects perturbs the magnetic field which in turn modifies both the local magnetic field around other magnetizable objects and changes their magnetization if, for example, they are paramagnetic. This gives rise to an effective interaction.

Restricting ourselves to the simple case of just two objects, we modify Eq. (1) to obtain the force on bead 1 at $\vec{r}_1$:

$$\vec{F}_1 = \mu_0 \int ((\vec{M}_1 + \mathrm{d}\vec{M}_1) \cdot \vec{\nabla})(\vec{H}_{\text{ext}} + \mathrm{d}\vec{H}_2) \, \mathrm{d}V, \tag{2}$$

where $\mathrm{d}\vec{H}_2$ is the modification to the magnetic field due to bead 2 (at $\vec{r}_2$) and $\mathrm{d}\vec{M}_1$ is the change in magnetization of bead 1 this causes.

The modification, $\mathrm{d}\vec{H}_2$, of the magnetic field is to leading order a dipole field and thus falls off as distance to the power -3. In the following, we assume that the magnetic beads are spherical and that the magnetic field is sufficiently homogenous over the scale of a bead diameter, $2a$, that the modified field is that of a dipole,

$$\begin{aligned} \mathrm{d}\vec{H}_2(\vec{r}) = {} & \frac{\chi}{\chi + 3} \frac{a^3}{|\vec{r}_1 - \vec{r}_2|^3} \\ & \times \left(\frac{3(\vec{H}_{\text{ext}}(\vec{r}_2) \cdot (\vec{r} - \vec{r}_2))(\vec{r} - \vec{r}_2)}{(\vec{r} - \vec{r}_2)^2} \right. \\ & \left. - \vec{H}_{\text{ext}}(\vec{r}_2) \right), \end{aligned} \tag{3}$$

where χ is the material magnetic susceptibility [5]. Furthermore, we assume that the external fields are sufficiently small so that the magnetizations of the beads depend linearly on the local

magnetic field,

$$\vec{M} = \frac{3\chi}{\chi+3}\vec{H}. \tag{4}$$

These two assumptions mean that the change in magnetization caused by the presence of a second bead is inversely proportional to the power -3 of the separation between the two beads,

$$\mathrm{d}\vec{M}_1 = 3\left(\frac{\chi}{\chi+3}\right)^2 \frac{a^3}{|\vec{r}_1-\vec{r}_2|^3} \times\left(\frac{3(\vec{H}_{\mathrm{ext}}(\vec{r}_2)\cdot(\vec{r}_1-\vec{r}_2))(\vec{r}_1-\vec{r}_2)}{(\vec{r}_1-\vec{r}_2)^2} - \vec{H}_{\mathrm{ext}}(\vec{r}_2)\right). \tag{5}$$

From Eqs. (2)–(5), we see that the leading correction to the total magnetic force on a bead is that caused by the $(\mathrm{d}\vec{M}_1\cdot\vec{\nabla})\vec{H}_{\mathrm{ext}}$ term when expanding in powers of the separation, $\vec{r}_1-\vec{r}_2$,

$$\begin{aligned}(\mathrm{d}\vec{M}_1\cdot\vec{\nabla})\vec{H}_{\mathrm{ext}}(\vec{r}_1) &= 3\left(\frac{\chi}{\chi+3}\right)^2 \frac{a^3}{|\vec{r}_1-\vec{r}_2|^3} \times\left(\frac{3(\vec{H}_{\mathrm{ext}}(\vec{r}_2)\cdot(\vec{r}_1-\vec{r}_2))((\vec{r}_1-\vec{r}_2)\cdot\nabla)\vec{H}_{\mathrm{ext}}(\vec{r}_1)}{(\vec{r}_1-\vec{r}_2)^2} -(\vec{H}_{\mathrm{ext}}(\vec{r}_2)\cdot\nabla)\vec{H}_{\mathrm{ext}}(\vec{r}_1)\right).\end{aligned} \tag{6}$$

This term is of order -3 in the separation, which is a quite rapid decay with increasing separation, though acting over a much longer range than an induced dipole–dipole interaction, for example. The demagnetization associated with a sphere limits the influence of the susceptibility; the prefactor, $3\chi^2/(\chi+3)^2$, is bounded above by 3. Lastly, the term consists of a somewhat complicated derivative taking into account the direction of the separation vector and the directions of the external magnetic field at the centre of both spherical beads and the magnitude of the magnetic field squared. The important point for the present is, however, that the interaction term is of order –3 in the separation.

Similarly, the remaining terms from the expansion of Eq. (2) are of fourth order, $(\vec{M}_1\cdot\vec{\nabla})\mathrm{d}\vec{H}_2$, and seventh order, $(\mathrm{d}\vec{M}_1\cdot\vec{\nabla})\mathrm{d}\vec{H}_2$, respectively as $\mathrm{d}\vec{H}_2$ and $\mathrm{d}\vec{M}_1$ each contribute a dependence on separation to the power -3 and differentiation contributes an additional power -1. The explicit forms of these terms are

$$\begin{aligned}(\vec{M}_1\cdot\vec{\nabla})\mathrm{d}\vec{H}_2(\vec{r}_1) &= 3\left(\frac{\chi}{\chi+3}\right)^2 \frac{a^3}{(\vec{r}_1-\vec{r}_2)^4} \times\left(-\frac{15(\vec{H}_{\mathrm{ext}}(\vec{r}_2)\cdot(\vec{r}_1-\vec{r}_2))(\vec{H}_{\mathrm{ext}}(\vec{r}_1)\cdot(\vec{r}_1-\vec{r}_2))(\vec{r}_1-\vec{r}_2)}{|\vec{r}_1-\vec{r}_2|^3} +\frac{3(\vec{H}_{\mathrm{ext}}(\vec{r}_1)\cdot\vec{H}_{\mathrm{ext}}(\vec{r}_2))(\vec{r}_1-\vec{r}_2)}{|\vec{r}_1-\vec{r}_2|} +\frac{3(\vec{H}_{\mathrm{ext}}(\vec{r}_1)\cdot(\vec{r}_1-\vec{r}_2))\vec{H}_{\mathrm{ext}}(\vec{r}_2)}{|\vec{r}_1-\vec{r}_2|}\right)\end{aligned} \tag{7}$$

and

$$\begin{aligned}(\mathrm{d}\vec{M}_1\cdot\vec{\nabla})\mathrm{d}\vec{H}_2(\vec{r}_1) &= 3\left(\frac{\chi}{\chi+3}\right)^3 \frac{a^6}{|\vec{r}_1-\vec{r}_2|^7} \times\left(-\frac{12(\vec{H}_{\mathrm{ext}}(\vec{r}_2)\cdot(\vec{r}_1-\vec{r}_2))^2(\vec{r}_1-\vec{r}_2)}{|\vec{r}_1-\vec{r}_2|^3} +\frac{3(\vec{H}_{\mathrm{ext}}(\vec{r}_2)\cdot(\vec{r}_1-\vec{r}_2))\vec{H}_{\mathrm{ext}}(\vec{r}_2)}{|\vec{r}_1-\vec{r}_2|} -\frac{3\vec{H}_{\mathrm{ext}}(\vec{r}_2)^2(\vec{r}_1-\vec{r}_2)}{|\vec{r}_1-\vec{r}_2|}\right).\end{aligned} \tag{8}$$

Again, the power dependences, -4th and -7th powers, are evident combined with involved geometric factors taking into account magnetic field orientations at the two beads and the orientation of the line of separation and the magnetic field squared. However, the point to note is that the exact form of these interaction terms is unimportant. What is always true is that the leading term is of order -3 in the separation and that this is true for any shape of bead as the modification of the magnetic field is a dipole field to leading order. We have tacitly assumed that the influence on the first bead from the change of magnetization of the second bead due to the field from first bead and any such higher order interactions are negligible as it is of even higher order in the separation than the leading term above.

3. Hydrodynamic interaction

Movement of a particle such as a magnetic bead through a viscous liquid creates a disturbance to

the fluid flow, a kind of wake, that affects nearby particles, dragging them along. The force acting on a particle is balanced by viscous forces from the fluid, transferring momentum to the fluid. Balance is attained after an acceleration phase typically much shorter than milliseconds for aqueous media and micrometre-sized particles.

As the flow in microfluidic channels almost invariably happens at very low Reynolds numbers, the motion of fluid under the action of a force distribution $\vec{f}$ is described by the linear Stokes equation for fluid velocity $\vec{v}$ and pressure p:

$$\rho \frac{\partial \vec{v}}{\partial t} = -\vec{\nabla} p + \eta \nabla^2 \vec{v} + \vec{f}, \tag{9}$$

where η is the viscosity and ρ the fluid density. Mathematically, a Green's function representing the flow due to the action of a point force can be used to describe the influence of a bead being moved through liquid. For a liquid of viscosity η, the flow due to a force $\vec{f}$ at the origin is [6]

$$\vec{v} = \frac{1}{8\pi\eta}\left(\frac{\vec{f}}{r} + \frac{(\vec{f}\cdot\vec{r})\vec{r}}{r^3}\right). \tag{10}$$

This simple expression assumes an unbounded fluid whereas the flow in a microfluidic channel, e.g. as part of a lab-on-a-chip, is always near to at least one wall. The presence of a wall modifies the flow and this can also be described by a Green's function approach [6,7]. In this approach, the wall contributes image flow singularities; a point force, a source dipole, and a force dipole, behind the wall which ensure that the flow fulfils the no-slip boundary condition. This is illustrated on Fig. 1 where a force (indicated by the dark arrow) is acting on a particle (dark disk) in the direction parallel to the wall resulting in a flow (smaller arrows) that drags fluid along with the particle. Behind the wall (shaded area) there is a virtual flow due to the singularities there (grey disk), ensuring that the flow vanishes at the boundary.

However, the observation we need to make here is that the perturbation of the flow falls off with distance to the point force to the power –1. Objects passively following the flow, such as other beads, will be moved eventhough they are far away. An effective force law with a reciprocal distance

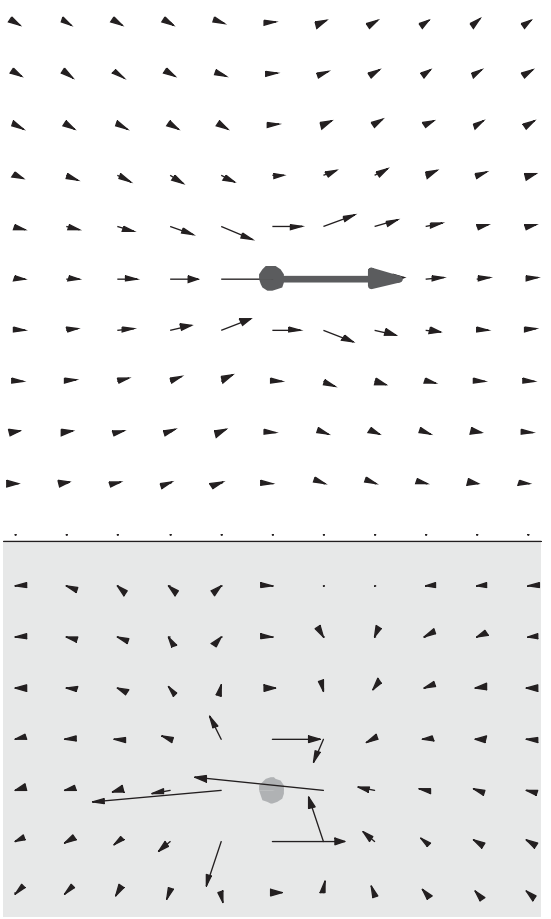

Fig. 1. Real flow (small arrows in white region) due to a point force (the large vector arrow) parallel to a wall (grey region) acting on a fluid. In order to fulfil the no-slip boundary condition at the wall, some image singularities (the grey disk) are placed behind the wall. This contributes a virtual flow in the area behind the wall (grey) that cancels the flow due to the real point force at the wall. The virtual flow is a mathematical device that does not correspond to actual fluid motion.

dependence is an unusually slow spatial decay, for example Coulomb's law from electrostatics has a one-over-distance-squared force dependence, as does gravitational attraction. At large distances, any power –1 force law will dominate any law with power –2 or lower. Furthermore, the force going into Eq. (10) is the total external, i.e. magnetic, force which means that the relative magnitude of

the hydrodynamic and the magnetic interactions cannot be changed.

4. Bead motion

It is possible to compare the importance of magnetic and hydrodynamic interactions by simulation in the simple case of just two beads moving in a two-dimensional section of an infinitely wide channel. The magnetic field and field gradient and the fluid flow are all simulated with the FEMLAB® finite element software package [8]. We then solve for the movement of the beads as their velocity relative to the surrounding fluid is determined by the sum of the external forces and viscosity. The external forces are the magnetic ones from the applied magnetic field and the field from other beads. With the aid of the Green's functions for the flow near a wall, the fluid flow due to the forces on each bead is calculated and this, in turn, describes the movement of beads relative to the fluid channel.

In the simulations, we assume 5 μm beads that move in a 100 μm wide channel under the influence of the field gradients generated by strips 10 μm wide 300 μm long of magnetizable material with permeability $1000\mu_0$, and separated by 40 μm non-magnetic patches. Applying a magnetic field, $\vec{H}_{\text{ext}} = 40000\ \text{A/m}$, along their lengths magnetizes the strips. The channel parameters are chosen so that they are representative of actual microfluidic devices. The results are insensitive to the value of the strip material permeability as long as it is much larger than that of vacuum, furthermore, the magnetic field chosen is of the order of magnitude one can realize with either small electromagnets or external permanent magnets. Finally, the important parameter for capturing is the ratio between the fluid drag and the magnetic force, i.e. the fluid velocity over the gradient of the magnetic field squared.

The motion of two beads is shown in Fig. 2 in two situations: when there is no hydrodynamic interaction between the beads, and when there is one. The beads are placed somewhat apart but near the centre of the channel where the particle flux is the highest but the magnetic field gradient vanishes due to symmetry. In the case without interactions, one of the beads is not retained against the fluid flow (1 mm/s to the right, water).

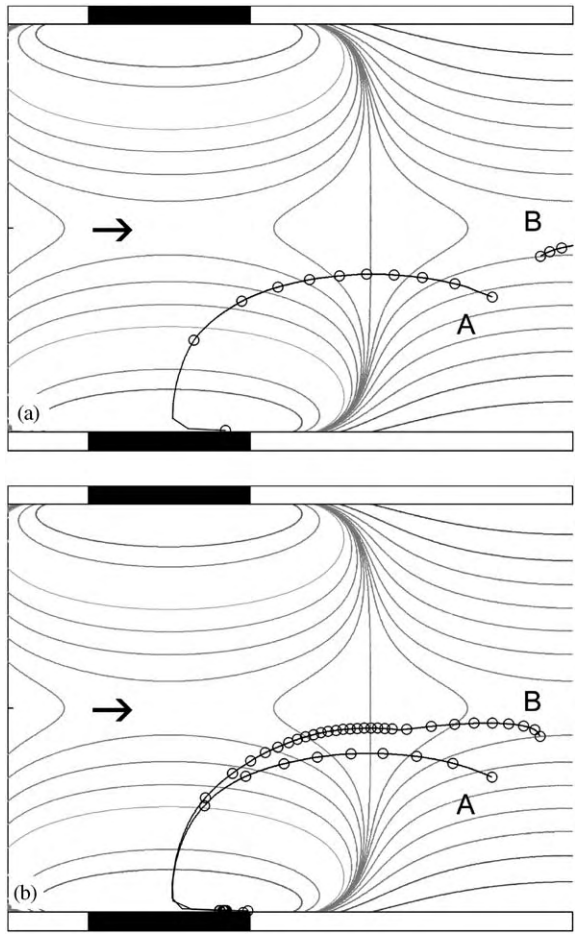

Fig. 2. (a) Motion of two beads, A and B (black lines with open circles), under the influence of a magnetic field gradient (contours, not equidistant) and a rightward-moving fluid flow (arrow) but in the absence of hydrodynamic interactions. Parts of the strips of magnetic material nearest to the channel are indicated by black rectangles and the channel walls and non-magnetic surroundings by white rectangles. Bead B is not caught as the local magnetic field gradient is small and because the fluid counter flow is too strong. The beads are placed initially at (20, 33 μm) and (23, 43 μm) in a coordinate system with origin at the channel wall by the centre of the lower magnetic strip. The figure covers an area 35 μm wide and 110 μm high. The maximum flow velocity is 1 mm/s. (b) Same simulation as (a) except that as the beads move they drag fluid along, in turn dragging each other, so both beads are caught. When the beads are close, they interact magnetically, however this is a very small effect and not visible on these figures.

In the latter case, the flow due to the one bead carries the other bead with it so that both beads are caught. This illustrates that the presence of interactions leads to qualitatively different results. Careful examination of the figure reveals that the moment the first bead is caught, the flow pattern changes and the other bead starts following a slightly different trajectory. These two observations illustrate the importance of including the effect on fluid flow due to the motion of other beads.

Magnetic interaction has been included in the simulations but it only contributes insignificantly. It is only the presence or absence of hydrodynamic interactions that gives qualitative differences.

5. Discussion

The much slower spatial decay of interactions mediated by fluid flow as compared with the direct magnetic–magnetic interactions means that the hydrodynamic interactions cannot be ignored in studies of the capturing dynamics: the -1 power law dominates the -3 power law. The fluid flow due to the motion of beads means that, for example, beads near symmetry points where gradients vanish can be driven into higher gradient regions, speeding up capturing.

We have here only studied the capturing of bead pairs but it appears reasonable that the combined effect of many is important and, in fact, crucial for reducing the requirements on magnetic parameters.

A complementary approach for studying the hydrodynamic interactions in capturing is to model the magnetic beads as a continuous concentration in the fluid [9]. The equation of motion for the fluid is then solved with a volume force density derived from magnetic parameters and the bead concentration. While we here consider few beads, the complementary approach models many. This complementary method does not include interactions between beads as such but it incorporates the fluid motion and, with it, bead convection. With that approach the author of Ref. [9] finds that fluid motion and particle convection are major mechanisms in capturing, which is consistent with our findings above.

References

[1] C.H. Ahn, M.G. Allen, W. Trimmer, et al., J. Microelectromech. Syst. 5 (1996) 151.
[2] T. Deng, M. Prentiss, G.M. Whitesides, Appl. Phys. Lett. 80 (2002) 461.
[3] J. Happel, H. Brenner, Low Reynolds Number Hydrodynamics, Noordhoff International Publishing, Leyden, 1973.
[4] A. Engel, R. Friedrichs, Am. J. Phys. 70 (2002) 428.
[5] J.D. Jackson, Classical Electrodynamics, Wiley, New Jersey, 1999.
[6] C. Pozrikidis, Boundary Integral and Singularity Methods for Linearized Viscous Flow, Cambridge University Press, Cambridge, 1992.
[7] E.R. Dufresne, T.M. Squires, M.P. Brenner, et al., Phys. Rev. Lett. 85 (2000) 3317.
[8] COMSOL AB Sweden, FEMLAB® v. 2.3, http://www.femlab.com.
[9] K.C. Warnke, IEEE Trans. Magn. 39 (2003) 1771.

Appendix D

Conference Proceedings from μTAS 2004

Title
Magnetic separation in microsystems: effects of hydrodynamic interaction

Authors
Christian Mikkelsen, Mikkel Fougt Hansen and Henrik Bruus

Reference
Micro Total Analysis Systems 2004—Proceedings of μTAS 2004, Volume 1, 587–9, (2004)

MAGNETIC SEPARATION IN MICROSYSTEMS: EFFECTS OF HYDRODYNAMIC INTERACTION

Christian Mikkelsen, Mikkel Fougt Hansen and Henrik Bruus
MIC — Department of Micro and Nanotechnology, Technical University of Denmark, Building 345 east, DK-2800 Kongens Lyngby, Denmark

Abstract

Entities such as biological macromolecules or cells can be specifically tagged with magnetic microbeads to enable simple separation, capturing and purification by means of magnetic fields. We find that interactions mediated by the fluid medium greatly help and speed up the capturing process. This hydrodynamic interaction is longer range, falling off inversely with distance, than the magnetic interaction between magnetic microbeads that falls off inversely with the distance cubed.

Keywords: magnetic separation, hydrodynamic interaction, micro fluidics

1. Introduction

Specific tagging of analytically interesting material such as biological macromolecules or cells by means of magnetic microbeads enables simple separation and purification operations in microscopic fluid handling systems. The material binds by biochemical or immunochemical means to the beads which can then be manipulated, retained and released by magnetic fields and field gradients [1,2]. The magnetic field and field gradient can either be generated by electromagnets or, for example, by external permanent magnets giving the field and the gradients being created by having submillimetre magnetizable structures in the immediate vicinity of the microscopic fluid channel.

2. Theory

Magnetic microbeads are subject to a force when immersed in magnetic field gradients, directed towards a local field maximum. The force moves the bead relative to the surrounding fluid, quickly reaching a balance with viscous forces effecting a momentum transfer from bead to fluid. This momentum transfer makes the fluid flow drag other objects along.

Viscosity and the force balance also means that speed relative to the surrounding liquid is always proportional to the applied force acting on the bead. Bead trajectories are then calculated by integrating the velocities rather than the accelerations.

For flows at the low Reynolds numbers relevant in microfluidics, the flow due to a point force can be described by a hydrodynamic Green's function [3]. The presence of a nearby wall modifies the flow due to the point force; something that can be taken into account in the Green's function approach as well [3,4].

The flow due to the motion of a bead relative to the surrounding fluid creates an effective interaction that is long range; the flow falls off as distance to the minus first power. This is much slower than the leading order (dipole-dipole) magnetic interaction that depends on the distance to the third power.

3. Simulations

A two-dimensional slice along the length of a 100-μm wide fluid channel was considered. The magnetic field was the calculated for a section of a periodic structure of strips 10 μm wide, 300 μm long of magnetic material (of relative permeability 1000) immersed in a homogeneous external magnetic field of 40000 A/m directed along the strips.

Both the magnetostatic and Poiseuille flow problems were solved with the finite element method software package FEMLAB [5]. The trajectories of up to twenty 5-μm beads were calculated from the magnetic field and from the fluid flow. The fluid flow was constantly updated

with the changes to the flow due to the motion of the other beads. This takes into account the fluid-mediated or *hydrodynamic interaction*. To identify the effects of hydrodynamic interactions, the simulations were also carried out without these.

The beads are stopped when they reach the sides of the channel, i.e. are captured, or when they go out of the simulation domain. These events are then recorded and stored.

The beads are started at random positions in the inlet half of the domain and are both flushed by the 0.5mm/s left-moving flow and pulled towards the magnets. The starting positions are chosen in this manner as to mimic random arrival of beads. If the beads are started only at the inlet and at a single time they move collectively which might not be representative of the motion in actual experiments.

4. Results and discussion

The simplest and most illuminating way of illustrating the effects of interactions is to study the trajectories of some beads as they move either *with* or *without* the hydrodynamic interactions. This is done in Figures 1 and 2. Started at random positions and looking from their trajectories, the beads are caught much faster when hydrodynamic interactions are included than when they are invisible to one another. This comes about as interacting beads move collectively; their interaction is neither attraction nor repulsion.

To get a different illustration, the capturing times in the presence and absence of interactions were simulated with random initial positions for up to 30 beads. The capturing times were then compared and it was found that interactions speed up capturing by a factor of up to 6, increasing with the number of beads. This is shown in figure 3. As is apparent, the more beads the more collective movement there is and the greater speed-up on the non-interacting case.

The results show that even having a few beads in a microfluidic channel being caught, greatly helps capturing, reducing capturing time, or easing requirements on magnetic fields and fluid flows.

5. Conclusions

Our work shows that hydrodynamic interactions influences capturing, speeding it up, and that it should be included in studies of capturing. The effect is more pronounced the more particles are being captured at the same time. The interactions are long range; falling off as inversely with distance.

References

[1] C.H. Ahn, M.G. Allen, W. Trimmer et. al, *J. Microelectromech. Syst.*, **5**, 151 (1996).

[2] T. Deng, M. Prentiss and G.M. Whitesides, *Appl. Phys. Lett.*, **80**, 461 (2002).

[3] C. Pozrikidis, *Boundary Integral and Singularity Methods for Linearized Viscous Flow*, (Cambridge University Press, Cambridge, 1992).

[4] E.R. Dufresne, T.M. Squires, M.P.Brenner et. al., *Phys. Rev. Lett.*, **85,** 3317 (2000).

[5] COMSOL AB Sweden, *FEMLAB* ® v. 2.3, http://www.femlab.com.

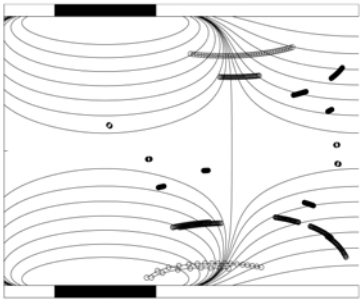

Figure 1. Non-interacting beads: catching with a magnetic field gradient. Contours (non-equidistant) indicate magnetic field. Tracks are beads being caught. The fluid flows from the right. Beads near the centre do not feel a strong gradient so they move slowly. (The circles are at equal times.)

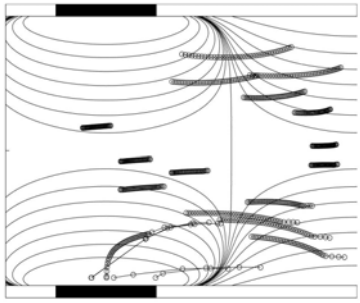

Figure 2. Interacting beads: catching beads with a magnetic field gradient in a microfluidic channel. Same parameters as Fig. 1. Here all beads are dragged along, even the ones near the centre. This greatly helps capturing. Where the field is already strong the difference is insignificant.

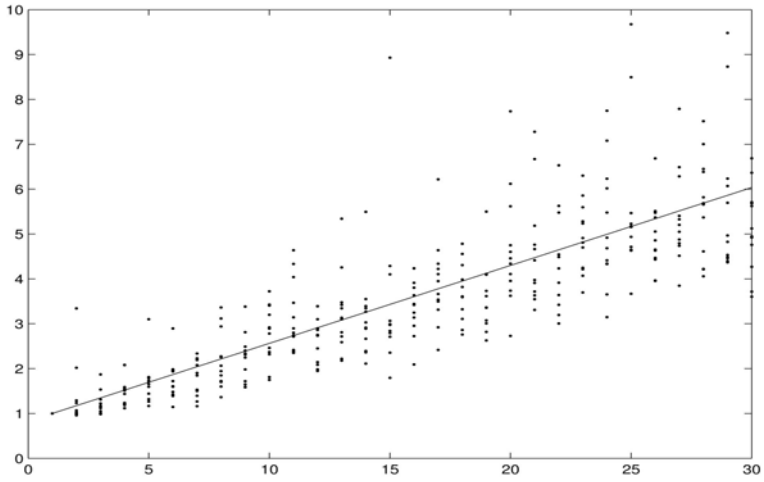

Figure 2. Having beads interact as they are caught speeds up capturing. Simulations were done with from 1 to 30 beads and the mean capturing time was calculated for 12 different runs each with and without hydrodynamic interactions. The ratio of the mean capturing times without interactions to the mean capturing times with interactions was then calculated for each of the runs (dots). The line is the best linear fit.

Appendix E

Paper submitted to Lab-on-a-Chip

Title
Microfluidic capturing-dynamics of paramagnetic bead suspension

Authors
Christian Mikkelsen and Henrik Bruus

Microfluidic capturing-dynamics of paramagnetic bead suspensions

Christian Mikkelsen and Henrik Bruus
MIC – Department of Micro and Nanotechnology,
Technical University of Denmark, DK-2800 Kongens Lyngby, Denmark
(Dated: 6 May 2005)

We study theoretically the capturing of paramagnetic beads by a magnetic field gradient in a microfluidic channel treating the beads as a continuum. Bead motion is affected by both fluidic and magnetic forces. The transfer of momentum from beads to the fluid creates an effective bead-bead interaction that greatly aids capturing. We demonstrate that for a given inlet flow speed a critical density of beads exists above which complete capturing takes place.

PACS numbers: 47.15.Pn, 47.55.Kf, 47.60.+i, 41.20.-q

I. INTRODUCTION

Recently, there has been an increasing interest in using magnetic beads in separation of, say, biochemical species in microfluidic systems [1, 2]. The principle is to have biochemically functionalized polymer beads with inclusions of superparamagnetic nanometersize particles of, for example, magnetite or maghemite. They attach to particular biochemical species and can be separated out from solution by applying external magnetic fields. As most biological material is either diamagnetic or weakly paramagnetic, this separation is specific. Paramagnetic particles in fluids are also used to measure the susceptibility of, for example, magnetically labelled cells by measuring particle capture or motion in a known field [3, 4].

In this paper we study microfluidic capturing of paramagnetic beads from suspension by modeling the beads as a continuous distribution [5]. The separation of suspended paramagnetic beads from their host fluid is an important process as it decides operating characteristics for practical microfluidic devices. It involves an interplay between forces of several kinds governing the dynamics of the process: (a) Magnetic forces from the application of strong magnetic fields and field gradients. (b) Drag forces due to the motion of the beads with respect to the host fluid. (c) The trivial effect of gravity, which we ignore in the following. We emphasize the effects of bead motion on the fluid flow as this gives rise to a hydrodynamic interaction between the beads. As we have noted in a previous few-bead study, this interaction is more important than the magnetic bead-bead interactions [6]. It is created by drag forces in two steps: First, drag transfers momentum to the fluid from the beads moving under the influence of external forces. Second, the modified flow changes the drag on and thus motion of other beads.

II. MODEL

As sketched in Fig. 1(a) we consider a viscous fluid (water) flowing in the x direction between a pair of parallel, infinite, planar walls. The walls are placed parallel to the xy plane at $z = 0$ and $z = h$, respectively. A steep magnetic field gradient is generated by a parallel pair of closely spaced, infinitely long, thin wires along the y direction separated by d and carrying opposite currents $\pm I$. The system is translation invariant in the y direction thereby reducing the simulation to a tractable problem in 2D. The simulation domain is defined by $0 < x < L$ and $0 < z < h$ with $L = 350$ μm and $h = 50$ μm. The wires intersect the xz plane near $(x, z) = (250\ \mu\text{m},\ 55\ \mu\text{m})$ just above the top plate. Paramagnetic beads in suspension are injected into the microfluidic channel by the fluid flow at $x = 0$. They are either exiting the channel at $x = L$ or getting collected at the channel wall near the wires.

When a suspension of beads is viewed on a sufficiently large scale compared to the single bead radius a but on a scale comparable to density variations, we can describe the distribution of beads in terms of a continuous, spatially varying bead number density c. We consider a suspension of beads with radius $a = 1$ μm and denote the initial number density at $x = 0$ by c_o. The four basic constituents of the model are described in the following.

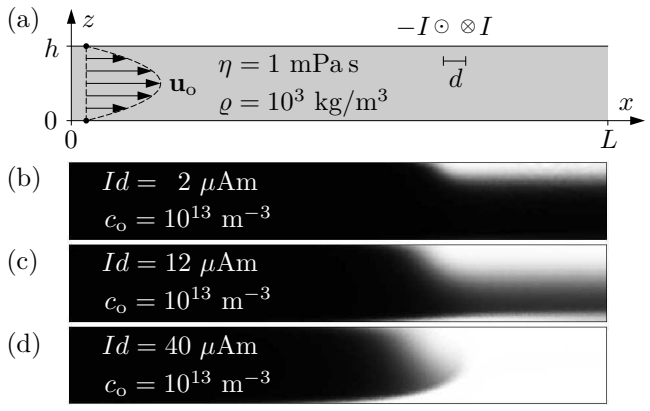

FIG. 1: (a) Sketch of the microfluidic system with $L = 350$ μm and $h = 50$ μm. A suspension of paramagnetic beads enters at $x = 0$ with a parabolic Poiseuille flow profile, $\mathbf{u}_o$, and leaves at $x = L$. Beads are caught by the pair of wires placed 100 μm from the outlet at the top and carrying currents $\pm I$. (b)–(d) Simulated stationary density of the beads ranging from zero (white) to c_o (black) for increasing values of the current-distance product Id as indicated. At $x = 0$ the concentration is $c_o = 10^{13}$ m^{-3} and the maximum flow speed is 300 μm/s.

Magnetic force. The beads are paramagnetic with a magnetic susceptibility $\chi = 1$. In an external magnetic field $\mathbf{H}_{\rm ext}(\mathbf{r})$ the force on such a bead is

$$\begin{aligned}\mathbf{F}_{\rm ext} &= \mu_{\rm o}\int_{\rm bead}(\mathbf{M}\cdot\boldsymbol{\nabla})\mathbf{H}_{\rm ext}\,dV \\ &= 4\pi\mu_{\rm o}a^3\frac{\chi}{\chi+3}(\mathbf{H}_{\rm ext}\cdot\boldsymbol{\nabla})\mathbf{H}_{\rm ext} \qquad (1)\end{aligned}$$

assuming that the bead is so small that we can take the external field $\mathbf{H}_{\rm ext}$ to be approximately constant across the bead, i.e., $a|\boldsymbol{\nabla}\mathbf{H}_{\rm ext}| \ll |\mathbf{H}_{\rm ext}|$ when determining the magnetization $\mathbf{M}$.

As mentioned, $\mathbf{H}_{\rm ext}$ in this study arises from a pair of current carrying wires. It is determined in the following manner. From Ampère's law, we readily find the magnetic field, $\mathbf{H}$, around a straight circular wire, $\mathbf{H}(\mathbf{r}) = \mathbf{J}\times\mathbf{r}/(2\pi r^2)$, where the electrical current vector $\mathbf{J}$ is along the wire orthogonal to the position vector $\mathbf{r}$ which is in the xz plane. The magnetic field from the two closely spaced anti-parallel wires is found by decreasing the separation d and increasing the current, $I = |\mathbf{J}|$, while keeping the product Id constant,

$$\mathbf{H}_{\rm ext} = \frac{1}{2\pi r^2}\left(\mathbf{J}\times\mathbf{d} - \frac{2(\mathbf{J}\times\mathbf{r})(\mathbf{d}\cdot\mathbf{r})}{r^2}\right). \qquad (2)$$

This together with Eq. (1) yields

$$\mathbf{F}_{\rm ext} = -\frac{2}{\pi}\frac{\chi}{\chi+3}\mu_{\rm o}a^3(I\,d)^2\,\frac{\mathbf{r}}{r^6}\,; \qquad (3)$$

a manifestly attractive central force (from the mid-point of the wires), independent of the direction of $\mathbf{d}$.

Fluid flow. The beads are suspended in a fluid of viscosity η and density ϱ that is launched at $x = 0$ with a parabolic velocity profile, $\mathbf{u}_{\rm o}$, and flows past the wires. In microfluidics inertial effects are unimportant compared to drag, so the small beads in suspension almost always move with constant velocity relative to the fluid. Except for acceleration phases shorter than microseconds the external forces are exactly balanced by drag [7]. The momentum transfer from beads to fluid is included by adding a bulk force term, $c\mathbf{F}_{\rm ext}(\mathbf{r})$ to the Navier–Stokes equation. This bulk force term is proportional to the number density c of beads and the magnetic external force $\mathbf{F}_{\rm ext}$ on an individual bead at position $\mathbf{r}$. The velocity $\mathbf{u}$ of the fluid is given by

$$\varrho\partial_t\mathbf{u} + \varrho(\mathbf{u}\cdot\boldsymbol{\nabla})\mathbf{u} = -\boldsymbol{\nabla}p + \eta\nabla^2\mathbf{u} + c\mathbf{F}_{\rm ext}, \qquad (4)$$

along with the incompressibility condition $\boldsymbol{\nabla}\cdot\mathbf{u} = 0$.

Bead motion. To complete the set of equations, it is necessary to have an equation of motion for the bead number density c. As the beads neither appear nor disappear in the bulk, c must obey a continuity equation

$$\partial_t c + \boldsymbol{\nabla}\cdot\mathbf{j} = 0, \qquad (5)$$

where the bead current $\mathbf{j}$ is defined by the Nernst–Planck equation [8]

$$\mathbf{j} = -D\boldsymbol{\nabla}c + c\mathbf{u} + cb\mathbf{F}_{\rm ext} \qquad (6)$$

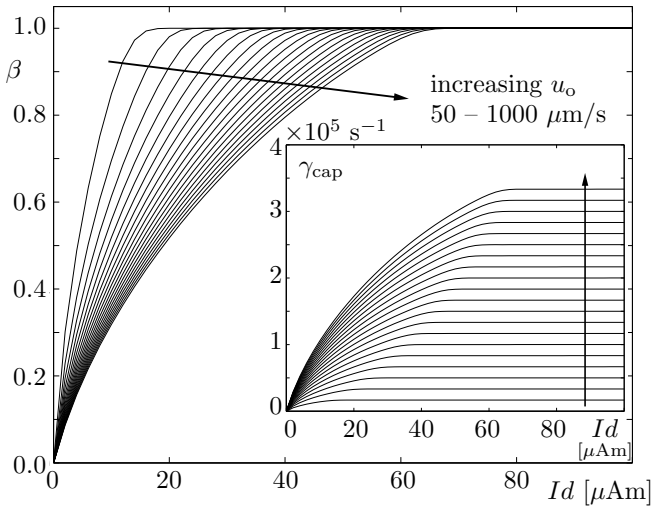

FIG. 2: The fraction β of beads caught as function of the current-distance product Id for twenty different flow speeds (50 – 1000 μm/s; indicated by the arrows). Larger current leads to higher β; faster flow to smaller β. In this simulation the initial concentration is low, $c_{\rm o} = 10^{13}$ m^{-3}. *Inset:* Rate $\gamma_{\rm cap}$ of bead capture as function of Id, for the flows above. The faster flow or the larger current, the higher $\gamma_{\rm cap}$.

with diffusivity D and bead mobility $b = 1/(6\pi\eta a)$.

For our spherical beads the diffusivity is given by the Einstein expression $D = kT/(6\pi\eta a)$ which for water at room temperature equals 2.2×10^{-13} m^2/s. In the simulations below, however, we artificially increase the magnitude of D in order to stabilize the computations and to use a coarser mesh and thus save computation time.

Boundary conditions. In addition to the bulk equations (4), (5), and (6), we need appropriate boundary conditions. As the beads move out to the walls of the domain and settle there, merely demanding that the normal component of the bead current vector $\mathbf{j}$ vanishes is not correct, rather, it must be free to take on any value as long as it is directed into the wall. As beads do not enter the bulk from the walls (by assumption once settled, beads stick) we demand that the normal current component is never directed into the liquid. For the fluid we demand the usual no-slip condition at the walls.

At the inlet $x = 0$ of the microfluidic channel we assume that the fluid comes in with the constant initial number density $c_{\rm o}$ and with a parabolic fluid velocity profile $\mathbf{u}_{\rm o}$. At the outlet $x = L$ we let the bead current take on any value, while the fluid pressure is zero.

III. RESULTS

Having set up the equations for bead and fluid motion, they are solved with the finite element method on a mesh with $\sim 10^4$ elements refined in the vicinity of the wires. To this end we employ the finite element solver software package Femlab [9]. The parameter values for the fluid

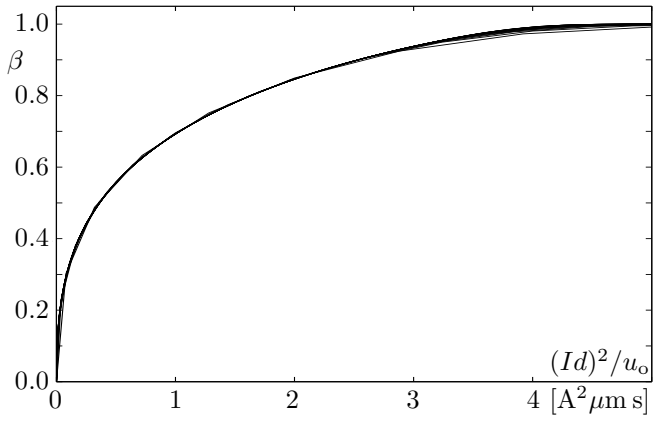

FIG. 3: The fraction β of beads caught versus $(Id)^2/u_\mathrm{o}$, the ratio of the current-distance product squared and the fluid flow velocity. This demonstrates scaling in the competition between capturing and flushing: the twenty curves from Fig. 2 approximately collapse to one single.

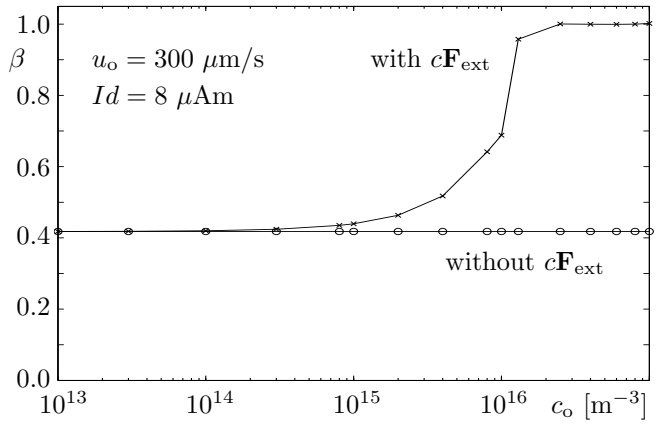

FIG. 4: Fraction β of beads caught as function of initial bead number density with and without the bulk force term $c\mathbf{F}_\mathrm{ext}$ in Eq. (4). The fixed values for the current-distance product Id and the maximum in-flow speed u_o are shown. At low densities less than 50% are caught; at high densities the collective motion of the beads leads to 100% capture.

are those of water, $\eta = 1$ mPas and $\varrho = 10^3$ kg/m^3, while for the beads $a = 1$ μm and $c_\mathrm{o} = 10^{13}$ to 10^{16} m^{-3}.

To study capturing we must keep track of which beads are captured and which are flushed through the channel with the flow. This is done by calculating the rates γ_i by which the beads are either captured or transported in/out at each of the four boundary segments i of the channel (inlet, outlet, upper wall, and lower wall). By integration of the normal components of the bead currents along each segment i, we find

$$\gamma_i = \int_i \mathbf{j}\cdot\mathbf{n}\, d\ell_i. \tag{7}$$

The rate of capture is $\gamma_\mathrm{cap} = \gamma_\mathrm{lower} + \gamma_\mathrm{upper}$. In steady state the conservation of beads enforces $\gamma_\mathrm{inlet} + \gamma_\mathrm{cap} + \gamma_\mathrm{outlet} = 0$, which provides a useful check of the simulation results. The primary control parameters are the current-wire distance product Id, the maximum fluid in-flow speed u_o, and the bead number density, c_o. The product Id decides the magnetic force which captures the beads against the fluid flow. As we are investigating effects of bead-bead interaction, our interest is properties that depend on the bead number density, in particular those that do so nonlinearly.

Electrical current and fluid flow. The effects of having electrical wires near, and thus a magnetic field gradient in, the channel is illustrated in Fig. 1(b)–(d) for three values of the current-distance product Id. At small values of Id only a narrow region is emptied but increasing the current the region expands until it covers the width of the channel.

A simple measure of the capturing is the ratio β of the bead capture rate γ_cap to the bead in-flow rate γ_inlet,

$$\beta = \frac{\text{“capture rate”}}{\text{“in-flow rate”}} = \frac{\gamma_\mathrm{cap}}{\gamma_\mathrm{inlet}}. \tag{8}$$

If capturing dominates β tends to unity, if flushing dominates β tends to zero. Fig. 2 shows this in that slow flow and strong current leads to a high β whereas fast flow and weak current leads to a small value. The rate γ_cap of bead capture as function of wire current and flow velocity is illustrated in the inset of Fig. 2.

If there is a competition between magnetic capturing and flushing, then we expect that the data can be described essentially by the ratio of the magnetic forces to the inlet fluid flow speed u_o. The force is proportional to the square of the current-distance product Id. In Fig. 3, we plot the data from Fig. 2 as function of $(Id)^2/u_\mathrm{o}$ and see that the data mostly collapses onto a single curve. The collapse is not perfect and is not expected to be as the underlying flow and bead distribution patterns (see Fig. 1) are different for different flows and magnetic fields.

Interactions and concentration. The second point we wish to make is that modification of the overall flow, and the effective bead-bead interaction this entails, is significant for bead capturing. We can study the effect by excluding momentum transfer to the fluid flow due to the bulk force term $c\mathbf{F}_\mathrm{ext}$ in the Navier–Stokes equation (4). At high bead number densities the force acting on the beads contributes a significant force on the fluid affecting fluid flow and spawning the effective interaction. The strength of this interaction must thus depend on the density of particles. This is illustrated in Fig. 4; capturing was simulated at fixed in-flow speed, $u_\mathrm{o} = 300$ μm/s, and a fixed value of the current-wire distance product, $Id = 8$ μAm, but for varying bead number densities c_o ranging from 10^{13} to 10^{16} m^{-3}. At low densities we find that capturing is roughly independent of density and the fraction β of beads captured has some intermediate value, however, for high densities all beads are caught. In contrast, leaving out the bulk force term $c\mathbf{F}_\mathrm{ext}$ in the Navier–Stokes equation, i.e., the force acting on the fluid, gives

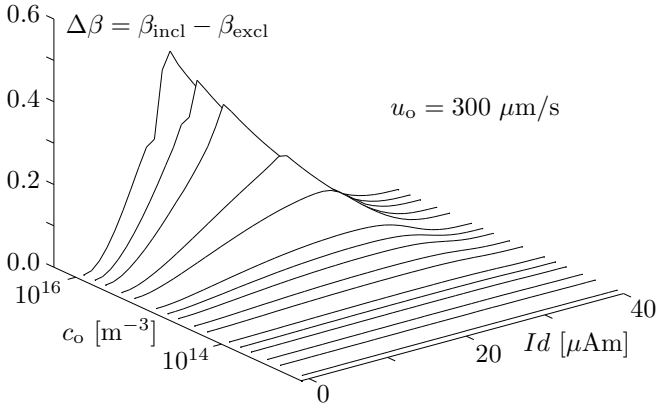

FIG. 5: The difference $\Delta\beta = \beta_{\rm incl} - \beta_{\rm excl}$ in captured bead fractions between two situations: including and excluding the bulk force term $c\mathbf{F}_{\rm ext}$ in the Navier–Stokes equation (4). At high concentrations ($c_{\rm o} > 10^{15}$ m^{-3}) there is an appreciable difference between including and excluding the bulk force term, corresponding to hydrodynamic bead-bead interactions.

concentration independence as shown in Fig. 4.

As can be seen in Fig. 5, a complementary way of exhibiting the importance of the bulk force term is to plot the difference $\Delta\beta = \beta_{\rm incl} - \beta_{\rm excl}$ between including and excluding $c\mathbf{F}_{\rm ext}$ as a function of concentration and the current-distance product. This shows that interactions makes an appreciable difference at high concentrations and intermediate magnetic fields.

Diffusion constant. Even for the small beads of radius $a = 1$ μm, the diffusion constant given by the Einstein relation is small compared to the dimensions entering the problem. The time-scale for a bead to diffuse across the channel is $\tau_{\rm diff} \sim h^2/D$. If we are to see the influence of diffusion competing with bead advection, then the relevant quantity is the Péclet number hu/D which is advection time-scale $\tau_{\rm adv} \sim h/u$ over the diffusion time-scale. When this number is larger than unity, which it is except for artificially large diffusion constants, then convection dominates. In the simulations the diffusion constant is increased artificially up to 10^{-11} m^2/s in order to help numerical convergence. But we have verified that values smaller than 10^{-10} m^2/s have no influence on the results.

IV. DISCUSSION AND CONCLUSION

We have studied microfluidic capture of paramagnetic beads in suspension. The three main findings of work are: the approximate scaling shown in Fig. 3, the existence of a critical bead density for capture shown in Fig. 4, and the qualitative difference for capturing between models with and without the hydrodynamic bead-bead interaction shown in Figs. 4 and 5.

Clearly, it is very important for the capture process to include the action of the beads on the host fluid medium. Simply leaving it out can give qualitatively wrong results for high concentrations of beads. This casts some doubt on the measurement of cell susceptibility through capturing as it depends on cell concentration [3, 4]. Deduction of susceptibilities from single bead or cell considerations together with measurements at high bead or cell concentration is suspect. Care must be taken to compare with standards of known and similar susceptibility, size, and concentration.

The effective bead-bead interaction greatly helps capturing. It should make detectable differences depending on whether there are a few or hundreds of particles in a channel at a time in actual experiments especially when the flow and magnetic field are such that the beads are barely caught one by one. This interaction should be considered when choosing operating conditions for microfluidic devices based on capturing of beads as higher bead number densities potentially eases requirements for external magnets and allows faster flushing. We hope that experimental studies will be initiated to verify this prediction of our work.

Acknowledgements. We thank Mikkel Fougt Hansen and Kristian Smistrup for valuable discussions on magnetophoresis in general and of their experiments in particular.

[1] J.-W. Choi, C. H. Ahn, S. Bhansali, H. T. Henderson, Sens. Actuators B **68**, 34–39 (2000).
[2] Q. A. Pankhurst, J. Connolly, S. K. Jones, J. Dobson, J. Phys. D **36**, R167–181 (2003).
[3] M. Zborowski, C. B. Fuh, R. Green, L. Sun, J. J. Chalmers, Anal. Chem. **67**, 3702–3712 (1995).
[4] K. E. McCloskey, J. J. Chalmers, M. Zborowski, Anal. Chem. **75**, 6868–6874 (2003).
[5] K. C. Warnke, IEEE Trans. Magn. **39**, 1771–1777 (2003).
[6] C. Mikkelsen, M. F. Hansen, H. Bruus, J. Magn. Magn. Mat. (in press, 2005).
[7] By Newton's second law and $\mathbf{F}_{\rm drag} = 6\pi\eta a\mathbf{v}$, a spherical bead with radius a approaches terminal velocity exponentially with a time constant $\tau = \frac{2}{9}\varrho_{\rm bead}a^2/\eta$, where η is the fluid viscosity. In this work $\tau = 0.2$ μs.
[8] R. F. Probstein, *Physicochemical hydrodynamics, an introduction* (John Wiley and Sons, New York, 1994).
[9] FEMLAB *version 3.1* (COMSOL AB, Stockholm, 2004).

Bibliography

[1] Femlab, www.comsol.com.

[2] MATLAB, www.mathworks.com.

[3] C. H. Ahn, M. G. Allen, W. Trimmer, Y.-N. Jun, and S. Erramilli. A fully integrated micromachined magnetic particle separator. *J. Microelectromech. Syst.*, 5:151–158, 1996.

[4] C. W. J. Beenakker and P. Mazur. Diffusion of spheres in a concentrated suspension IV. Wall-effects inside a spherical container. *Physica*, 131A:311–328, 1985.

[5] C. W. J. Beenakker, W. van Saarloos, and P. Mazur. Diffusion of spheres in a concentrated suspension III. The influence of a plane wall. *Physica*, 127A:451–472, 1984.

[6] H. Bruus. *Lecture notes, Theoretical microfluidics.* MIC, 2004.

[7] Herbert B. Callen. *Thermodynamics and an Introduction to Thermostatistics.* John Wiley & Sons, New York Chichester Brisbane Toronto Singapore, 1985.

[8] Jeffrey J. Chalmers, Yang Zhao, Masayuki Nakamura, Kristie Melnik, Larry Lasky, Lee Moore, and Maciej Zborowski. An instrument to determine the magnetophoretic mobility of labeled, biological cells and paramagnetic particles. *J. Mag. Mag. Mat.*, 194:231–241, 1999.

[9] Nan Chi, C. Mikkelsen, Lin Xu, Jianfeng Zhang, P.V. Holm-Nielsen, Haiyan Ou, J. Seoane, C. Peucheret, and P. Jeppesen. Transmission and label encoding/erasure of orthogonally labelled signal using 40 Gbit/s rz-dpsk payload and 2.5 Gbit/s im label. *Electronics Letters*, 39:1335–6, 2003.

[10] Nan Chi, Lin Xu, Jianfeng Zhang, Pablo V. Holm-Nielsen, Christophe Peucheret, Christian Mikkelsen, Haiyan Ou, Jorge Seoane, and Palle Jeppesen. Orthogonal optical labeling based on a 40 Gbit/s dpsk payload and a 2.5 Gbit/s im label. In *OFC*, page FO6, 2004.

[11] J.-W. Choi, C. H. Ahn, S. Bhansali, and H. T. Henderson. A new magnetic bead-based, filterless bio-separator with planar electromagnet surfaces for integrated bio-detection systems. *Sens. Actuators B*, 68:34–39, 2000.

[12] J.-W. Choi, T. M. Liakopoulos, and C. H. Ahn. An on-chip magnetic bead separator using spiral electromagnets with semi-encapsulated permalloy. *Biosens. Bioelectron.*, 16:409–416, 2001.

[13] Aileen Constans. Field of dreams. *The Scientist*, 14:23, 2000.

[14] T. Deng, M. Prentiss, and G. M. Whitesides. Fabrication of magnetic microfiltration systems using soft lithography. *Appl. Phys. Lett.*, 80:461–463, 2002.

[15] Bent Elbek. *Elektromagnetisme*. Niels Bohr Institutet, København, 1995.

[16] A. Engel. Comment on "Invalidation of the Kelvin force in ferrofluids". *Phys. Rev. Lett.*, 86:4978, 2001.

[17] A. Engel and R. Friedrichs. On the electromagnetic force on a polarizable body. *Am. J. Phys.*, 70:428, 2002.

[18] R.L. Eriksen, V.R. Daria, P.J. Rodrigo, and J. Glückstad. Computer-controlled orientation of multiple optically-trapped microscopic beads. *Microelectr. Eng.*, 67-68:872–878, 2003.

[19] Hilding Faxén. Der Widerstand gegen die Bewegung einer starren Kugel in einer zähen Flüssigkeit, die zwischen zwei parallelen ebenen Wänden eingeschlossen ist. *Arkiv för matematik, astronomi och fysik*, 18(29):1–52, 1924.

[20] S. Flügge, editor. *Fluid Dynamics II*, volume VIII/2 of *Encyclopedia of Physics*. Springer Verlag, Berlin, 1963.

[21] Martin A. M. Gijs. Magnetic bead handling on-chip: new opportunities for analytical applications. *Microfluid Nanofluid*, 1:22–40, 2004.

[22] John Happel and Howard Brenner. *Low Reynolds number hydrodynamics*. Noordhoff International Publishing, Leyden, 1973.

[23] Siegfried Hess and Walter Köhler. *Formeln zur Tensor-Rechnung*. Palm und Enke, Erlangen, 1980.

[24] John David Jackson. *Classical Electrodynamics*. John Wiley and & Sons. Inc., Hoboken, 3rd edition, 1999.

[25] Thomas B. Jones. *Electromechanics of Particles*. Cambridge University Press, Cambridge, 1st edition, 1995.

[26] Horace Lamb. *Hydrodynamics*. Cambridge University Press, Cambridge, 6th edition, 1932.

[27] L. D. Landau and E. M. Lifshitz. *Fluid Mechanics*, volume 6 of *Landau and Lifshitz, Course of Theoretical Physics*. Butterworth-Heinemann, Oxford, 2nd edition, 1987.

[28] L. D. Landau, E. M. Lifshitz, and L. P. Pitaevskii. *Electrodynamics of Continuous Media*, volume 8 of *Landau and Lifshitz, Course of Theoretical Physics*. Butterworth-Heinemann, Oxford, 2nd edition, 1984.

[29] Torsten Lund-Olesen. Integrated microfluidic mixer and magnetic bead trap. Master's thesis, MIC — Department of Micro and Nanotechnology, Technical University of Denmark, 2005.

[30] P. Mazur. On the motion and Brownian motion of n spheres in a viscous fluid. *Physica*, 110A:128–146, 1982.

[31] P. Mazur. Hydrodynamic interactions: a many-body problem in the theory of suspensions. *Can. J. Phys.*, 63:24–29, 1985.

[32] P. Mazur. Hydrodynamic interactions and properties of suspensions. *Helvetica Physica Acta*, 59:263–277, 1986.

[33] P. Mazur and D. Bedeaux. A generalization of Faxén's theorem to nonsteady motion of a sphere through an incompressible fluid in arbitrary flow. *Physica*, 76:235–246, 1974.

[34] P. Mazur and W. van Saarloos. Many-sphere hydrodynamic interactions and mobilities in a suspension. *Physica*, 115A:21–57, 1982.

[35] P. Mazur and A. J. Weisenborn. The oseen drag on a sphere and the method of induced forces. *Physica*, 123A:209–226, 1984.

[36] C. Mikkelsen, M.F. Hansen, and H. Bruus. Theoretical comparison of magnetic and hydrodynamic interactions between magnetically tagged particles in microfluidic systems. *J. Magn. Magn. Mater.*, 293:578–83, 2005.

[37] Christian Mikkelsen and Henrik Bruus. Microfluidic capturing-dynamics of paramagnetic bead suspensions. *(submitted to Lab Chip)*, 2005.

[38] Christian Mikkelsen, Mikkel Fougt Hansen, and Henrik Bruus. Magnetic separation in microsystems: effects of hydrodynamic interaction. In *Micro Total Analysis Systems 2004—Proceedings of μTAS 2004*, volume 1, pages 587–9, 2004.

[39] Stefan Odenbach and Mario Liu. Invalidation of the Kelvin force in ferrofluids. *Phys. Rev. Lett.*, 86:328–331, 2001.

[40] Q. A. Pankhurst, J. Connolly, S. K. Jones, and J. Dobson. Applications of magnetic nanoparticles in biomedicine. *J. Phys. D: Appl. Phys.*, 36:R167–R181, 2003.

[41] Nikola Pekas, Michael Granger, Mark Tondra, Anthony Popple, and Barc D. Porter. Magnetic particle diverter in an integrated microfluidic format. *JMMMJ. Magn. Magn. Mater.*, 293:584–8, 2005.

[42] C. Pozrikidis. *Boundary Integral and Singularity Methods for Linearized Viscous Flow.* Cambridge texts in applied mathematics. Cambridge University Press, Cambridge, 1st edition, 1992.

[43] R. F. Probstein. *PhysicoChemical Hydrodynamics, an introduction.* John Wiley and Sons, New-York, 1994.

[44] Sridhar Reddy, Lee R. Moore, Liping Sun, Maciej Zborowski, and Jeffrey J. Chalmers. Determination of the magnetic susceptibility of labeled particles by video imaging. *Chem. Eng. Sci.*, 51:947, 1996.

[45] R. E. Rosensweig. *Ferrohydrodynamics.* Dover Publication, Inc., New York, 1997.

[46] K. Smistrup. Personal communication, 2005.

[47] Kristian Smistrup, Ole Hansen, Henrik Bruus, and Mikkel F. Hansen. Magnetic separation in microfluidic systems using microfabricated electromagnets—experiments and simulations. *J. Magn. Magn. Mater.*, 293:597–604, 2005.

[48] Murray R. Spiegel. *Mathematica Handbook of Formulas and Tables*, volume 1 of *Schaum's Outline Series.* McGraw-Hill, Inc., New York, 1968.

[49] Todd M. Squires and Michael P. Brenner. Like-charge attraction and hydrodynamic interaction. *Phys. Rev. Lett.*, 85:4976, 2000.

[50] Richard D. Stoy. Solution procedure for the Laplace equation in bispherical coordinates for two spheres in a uniform external field: Parallel orientation. *J. Appl. Phys.*, 65:2611, 1989.

[51] Richard D. Stoy. Solution procedure for the Laplace equation in bispherical coordinates for two spheres in a uniform external field: Perpendicular orientation. *J. Appl. Phys.*, 66:5093, 1989.

[52] Julius Adams Stratton. *Electromagnetic Theory.* International Series in Pure and Applied Physics. McGraw-Hill Book Company, Inc., New York London, 1941.

[53] Steven H. Strogatz. *Nonlinear Dynamics and Chaos.* Addison-Wesley Publishing Company, Reading, Massachusetts, 1994.

[54] Elisabeth Verpoorte. Beads and chips: new recipes for analysis. *Lab Chip*, 3:60N–8N, 2003.

[55] Maciej Zborowski, Chwan Bor Fuh, Ralph Green, Liping Sun, and Jeffrey J. Chalmers. Analytical magnetapheresis of ferritin-labeled lymphocytes. *Anal. Chem.*, 67:3702–12, 1995.